学位論文

Primordial blackhole formation and gravitational wave production in a curvaton model

（カーバトン模型における
原始ブラックホール形成及び重力波生成）

平成２５年１２月博士（理学）申請

東京大学大学院理学系研究科

物理学専攻

北嶋　直弥

Abstract

In some high energy particle physics on which inflation models are based, many scalar fields are predicted. Some of them, which we call *curvatons*, may take a role of generating the primordial curvature perturbations and some curvatons may lead to the blue-tilted spectrum of curvature perturbation.

In this thesis, we show that a significant number of primordial blackholes can be formed in an axion-like curvaton model, in which the highly blue-tilted power spectrum of primordial curvature perturbations is achieved. It is found that the produced blackholes with masses $\sim 10^{25} - 10^{26}$ g account for the present cold dark matter. We also argue the possibility of forming the primordial blackholes with mass $\sim 10^5 M_\odot$ as seeds of the supermassive blackholes.

In addition, we also investigate the gravitational wave background induced by the first order scalar perturbations in the curvaton models. We consider the quadratic and axion-like curvaton potential which can generate the blue-tilted power spectrum of curvature perturbations on small scales and derive the maximal amount of gravitational wave background today. We find the power spectrum of the induced gravitational wave background has a characteristic peak at the frequency corresponding to the scale reentering the horizon at the curvaton decay, in the case where the curvaton does not dominate the energy density of the Universe. We also find the enhancement of the amount of the gravitational waves in the case where the curvaton dominates the energy density of the Universe. Such induced gravitational waves would be detectable by the future space-based gravitational wave detectors or pulsar timing observations.

Acknowledgement

I would like to appreciate my supervisor Masahiro Kawasaki for his kind instruction. I also would like to thank all of my colleagues in theory group of the Institute for cosmic ray research, especially, Shuichiro Yokoyama, Tomohiro Takesako. Besides, I am thankful to Tsutomu Yanagida (kavli IPMU), Kazunori Nakayama (University of Tokyo), Daisuke Yamauchi (Research Center for the Early Universe, University of Tokyo). I would like to thank the Japan Society for the Promotion of Science (JSPS) for the financial support. Finally, I am very grateful for my family.

Contents

Chapter 1

Introduction

Overview

Recent cosmological observations such as Planck [1] or Wilkinson Microwave Anisotropy probe (WMAP) [2] strongly supports the existence of an accelerated expansion era called inflation in the very early stage of the universe. In addition to solving some difficulties in the standard Big Bang cosmology such as the horizon problem, inflation can naturally generate the primordial seeds of density perturbations on superhorizon scale by expanding the quantum fluctuations of some scalar field on very small scales. This mechanism for generating the density perturbations generally predicts the almost scale-invariant spectrum of curvature perturbations obeying the Gaussian statistics,which is consistent with the observed temperature anisotropies of the cosmic microwave background (CMB) [3]. Similarly, the standard inflationary paradigm predicts the generation of the primordial tensor metric perturbations which may be detected as the gravitational wave background (GWB) by future observations.

In addition, the CMB observations have also revealed that our present universe is filled with the unknown matter called dark matter, which cannot be explained within the framework of the well-established standard model of particle physics. The observed density parameter for the cold dark matter (CDM) is found by the Planck [1] to be

$$\Omega_{\rm CDM}h^2 = 0.1196 \pm 0.0031, \tag{1.1}$$

where h is the dimensionless Hubble parameter defined via the present Hubble parameter: $H_0 = 100h$ km sec^{-1} Mpc^{-1}. In order to detect the dark matter, many experiments have been performed by now, but we have not found any meaningful signature yet. Therefore it is one of the most important problems of modern cosmology and particle physics to answer what the dark matter is.

Primordial blackhole as a component of the cold dark matter

It is often said assumed that the dark matter is the weakly-interacting massive particles (WIMPs) because the supersymmetric (SUSY) model [4], which is one of the most promising model beyond the standard model, naturally provides such WIMPs as the lightest supersymmetric particle (LSP). Another promising candidate of dark matter is the axion, which

is originally introduced to solve the strong CP problem in the standard model [5]. In addition, it is known that the primordial black holes (PBHs), the black holes formed in the early universe [6, 7], can behave like CDM. In this thesis, we argue the scenario in which the currently observed abundance of CDM is partially explained by PBHs.

PBHs are expected to be formed through the collapses of the high density regions caused by the large primordial density perturbations [8] Light PBHs with mass smaller than 10^{15} g are evaporated by now through the Hawking radiation [9], implying that only the PBHs with masses $M_{\rm BH} > 10^{15}$ g can survive and contribute to the CDM. Although, various observations have severely constrained the PBH abundance [10], it is still possible that PBHs occupy the significant fraction of the current CDM, so investigating the possibility of the PBH formation is still a meaningful research field. Although it is not easy to build the model in which a significant number of PBHs are formed, various models were proposed in the literature. Focusing on the inflation models, for examples, PBH formation was proposed in double inflation models [11–15] or running mass inflation models [16, 17].

In order for PBHs to form through the primordial density perturbations, we need the strongly blue-tilted power spectrum of the curvature perturbations, which gives the large density perturbations at small scales while the large scale density perturbations are consistent with the CMB observation. However, the observation indicates that the scale dependence of the power spectrum is slightly red-tilted at large scales. This inconsistency is solved by employing a curvaton. The curvaton was originally introduced to generate the primordial large scale curvature perturbations instead of the inflaton [18–20]. In the curvaton model, a scalar field (called curvaton) acquires fluctuations during inflation and after inflation it decays into the standard model particles producing the adiabatic perturbation in the radiation dominated universe.

In this thesis, we consider that the curvaton is responsible for generating only the small-scale curvature perturbations while the large-scale perturbations are generated by an inflaton. After the decay of the curvaton, a significant number of PBHs can be formed through large density perturbations due to the curvaton. A specific model for the PBH formation with curvaton was proposed in [21], where three scalar fields (including inflaton and curvaton) with ad hoc couplings among them evolve non-trivially during inflation and leads to large density perturbations at small scales. Our mechanism for the PBH formation is completely different from that in Ref. [21]. We consider an axion-like curvaton field whose nature is very crucial for the PBH formation. Furthermore, axion-like fields often appear in various particle physics theories. We consider that one of such axion-like (curvaton) fields may play an important role for the PBH formation as studied in this paper. Ref. [16] also discussed PBH formation in curvaton model without concrete models.

Gravitational waves as a probe of the early universe

The inflation is driven by some scalar field called inflaton whose potential is nearly flat. Although various inflation models have been proposed so far, unfortunately, there is no promising candidate for an inflaton. Moreover, the density perturbation may be produced by another scalar field like the curvaton model [18–20]. One of the difficulty to identify the model is due to lack of clues from the observations on small scales. While the CMB observation is a powerful tool for constraining the spectrum of the curvature perturbations on large scales, we know little about the one on small scales, so we have only a little information to constrain the inflation model. On the other hand, future and current detectors of

gravitational waves have a high sensitivity at higher frequency modes corresponding to the smaller scale fluctuations than that observed by CMB anisotropies. Thus, it is interesting to investigate the signal of the primordial gravitational waves on small scales, which would be a powerful tool to reveal the inflationary dynamics over a long period in combination with the CMB observations.

There are several mechanisms for generating the primordial GWBs. First, as mentioned before, they are generated by the quantum fluctuations of the tensor metric perturbations in the inflationary era, which typically has an almost scale-invariant power spectrum, and the amplitude of such gravitational waves is typically given by the inflationary Hubble scale. In addition to the direct detections, it is also expected to detect the signal of gravitational waves on cosmological scales through the observations of the B-mode polarization of the CMB anisotropy [22–25]. Second, the gravitational waves can be also induced by primordial scalar perturbations. In principle, the scalar and tensor perturbations evolve independently and are not mixed at linear order on the homogeneous isotropic FLRW universe, but at the second order these perturbations are not independent any more [26–31]. Hence the stochastic GWB can be sourced from the quadratic component of the first order scalar perturbations in the metric and energy-momentum tensor [32–34]. Actually, the blue-tilted adiabatic curvature perturbations generate a large amount of gravitational waves at high frequencies, which would be detectable by future observations [35–37] Since such curvature perturbations have the potential to form a large number of PBHs, the amount of the scalar-induced gravitational waves is also constrained by the PBH formation [38–40].

In this thesis, we also investigate the gravitational wave generation in the curvaton model. Various relevant studies have been done in the literature [41–44]. We consider two cases with the quadratic and also the axion-like potential, both where the blue-tilted adiabatic curvature perturbations can be easily realized. and we also introduce the inflaton fluctuations as a source of the adiabatic curvature perturbations on large scales so that we realize the COBE normalization and the slightly red-tilted power spectrum of the curvature perturbations. On smaller scales, the blue-tilted component sourced from the curvaton fluctuations is dominated, which is the same setup as the PBH case. In this set-up, we investigate the GWB induced from not only the scalar adiabatic perturbations but also from the transverse-traceless part of the energy momentum tensor which is due to the kinetic term of the curvaton field [41]. We also study both cases where the energy density of the curvaton field is dominant or still subdominant in the Universe at the curvaton decay [43][1].Then, we discuss the detectability of such scalar-induced GWB in the future experiments: such as the space-based gravitational wave detectors e.g., Laser Interferometer Space Antenna (LISA) [45], DECi-hertz Interferometer Gravitational wave Observer (DECIGO) [46, 47] and Big Bang Observer (BBO) [48], and also the pulsar timing observations [49] like Square Kilometre Array (SKA) [50].

Outline of this thesis

This thesis is organized as following. In chapter 2, we review the curvaton model, particularly focusing on the model with blue-tilted power spectrum of curvature perturbation. In

[1]Here, we consider the case with a single curvaton field. In [44], the authors have considered two-curvaton scenarios and have investigated the generation of the scalar-induced gravitational waves during the era when one of the curvaton is dominant.

chapter 3, we review the standard description and some observational constraints on the PBH and investigate the PBH formation in an axion-like curvaton model. In chapter 4, we review the basics on the gravitational wave and discuss the possibility for the gravitational wave generation in curvaton models. Finally, we conclude in chapter 5.

Notation

We use the units of $c = \hbar = k_B = 1$ unless noted. The signature of the Minkowski metric is adopted as $\eta_{\mu\nu} = (-, +, +, +)$. We denote the cosmic time and conformal time as respectively t and η. $M_P = (8\pi G)^{-1/2}$ and G are the reduced Planck mass and Newton's constant respectively. $M_\odot$ is the solar mass: $M_\odot = 1.99 \times 10^{33}$ g.

Chapter 2

Curvaton model

2.1 Basics of the curvaton scenario

2.1.1 Overview

In this chapter, we briefly review the curvaton model. In the curvaton scenario [18–20], one introduces an additional scalar field besides inflaton, so-called curvaton denoted as σ, which is a subdominant component and acquires quantum fluctuations during inflation. The curvaton field is required to be massless during inflation and should decay after inflation in order to convert the isocurvature perturbations from a curvaton into adiabatic ones. The curvaton model has some interesting features. One of them is that the relatively large non-Gaussianity in curvature perturbation can be predicted. Although, the CMB observation so far is consistent with the Gaussian perturbation [3], the future observation may detect the deviation from Gaussian. In addition, in the early universe scenarios based on the particle physics such as supersymmetric models, many scalar fields are predicted and some of them may take roles of curvatons. So the curvaton model is worth considering in order to figure out the physics in the very early universe.

Background dynamics In general, the curvaton is required to be massless during inflation in order to generate the superhorizon-scale curvature perturbations, so it slowly rolls down its own potential during inflation like an inflaton, and then, it starts to oscillate coherently when the Hubble parameter H becomes comparable to the curvaton mass after inflation as illustrated in Fig 2.1. Around the minimum, the curvaton potential can be generally well-approximated by the quadratic potential, and oscillating curvaton field behaves like a pressureless matter whose energy density decreases obeying $\propto a^{-3}$ where a is the scale factor of the cosmic expansion. Hence, in the radiation dominated Universe where the energy density of the Universe evolves as $\propto a^{-4}$, the ratio of the energy density of the curvaton to that of the radiation relatively increases and the isocurvature perturbations sourced from the quantum fluctuations of the curvaton contributes to the evolution of the adiabatic curvature perturbations on superhorizon scales. After the curvaton decays into the radiation, which occurs when the Hubble parameter becomes equal to the decay rate of the curvaton written as Γ_σ, the resultant adiabatic curvature perturbations stay constant in time. These history of the background energy density of the Universe in a curvaton scenario is illustrated by Fig. 2.2.

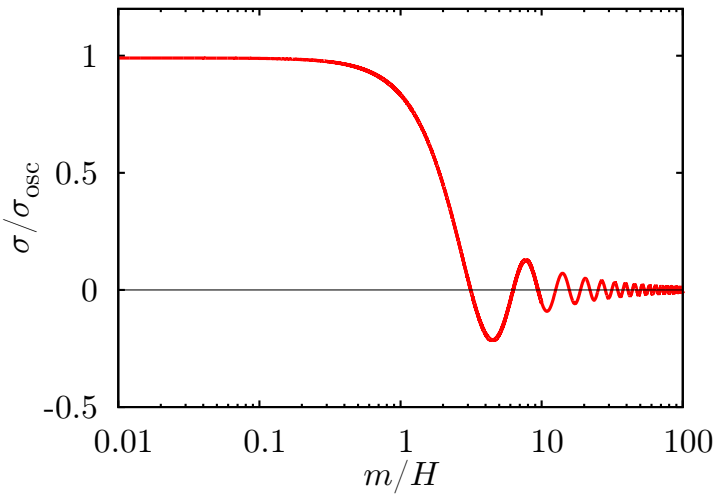

Figure 2.1: This figure shows the background dynamics of the curvaton field. We can see that the curvaton field remains unchanged as long as the Hubble parameter (H) is larger than the curvaton mass (m), and starts to oscillate when $H = m$.

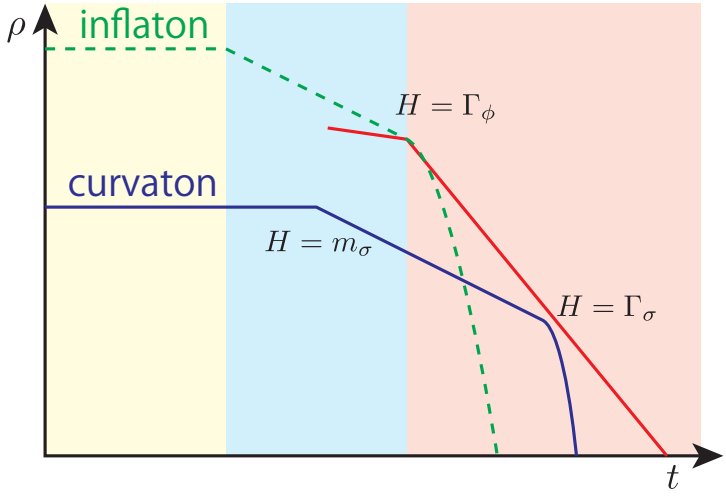

Figure 2.2: A schematic view of the time evolution of the energy density of the inflaton (dashed green), the curvaton (solid blue) and the radiation (solid red) is shown. m_σ, Γ_σ and Γ_ϕ are respectively the curvaton mass, the curvaton decay rate and the inflaton decay rate.

2.1.2 Curvature perturbation in a curvaton model

Based on the δN formalism [51–54], the curvature perturbations on uniform total energy density hypersurface on super-horizon scales are given by the perturbation of the local e-folding number and can be expanded in terms of the fluctuations of an inflaton field and a curvaton field as

$$\zeta = \delta N = N_\phi \delta\phi_* + N_\sigma \delta\sigma_* + \cdots , \tag{2.1}$$

where ϕ and σ denote the inflaton and curvaton respectively, $N_\phi = \partial N/\partial\phi_*$ and $N_\sigma = \partial N/\partial\sigma_*$ with $N = \int_{t_*}^{t} H dt$. Here, an subscript $*$ denotes the value at an initial flat hypersurface and we take $t = t_*$ to be the time when the scale of interest exits the Hubble horizon during inflation.

The inflaton contribution to the total curvature perturbation can be easily derived as following. Under the slow-roll approximation, $3H\dot{\phi} + V'(\phi) \simeq 0$, we can rewrite the formula for the e-folding number:

$$N = \frac{1}{M_P^2}\int_{\phi_f}^{\phi_i} \frac{V}{V'} d\phi, \tag{2.2}$$

where the subscripts i and f denote an initial and a final value of the inflaton during inflation. Thus, from the definition of the first slow-roll parameter, $\epsilon = -\dot{H}/H^2$ (overdot denotes the time derivative), we obtain the perturbation of the e-folding number and coefficient N_ϕ is derived as

$$N_\phi = \frac{1}{\sqrt{2\epsilon M_P^2}}. \tag{2.3}$$

The curvaton contribution to the curvature perturbation comes from the isocurvature perturbation originated from the curvaton field fluctuation during inflation. The nonlinear curvature perturbation on uniform i-component density hypersurface is given by

$$\zeta_i = \delta N + \frac{1}{3}\int_{\bar{\rho}_i}^{\rho_i} \frac{d\tilde{\rho}_i}{(1+w_i)\tilde{\rho}_i}, \tag{2.4}$$

where w_i is an equation of state parameter for i-component, that is 1/3 (0) for radiation (matter) and barred quantities ($\bar{\rho}_i$) here denote the background values. Then, the curvature perturbations on uniform radiation- and curvaton-density hypersurface are given by

$$\zeta_r = \delta N + \frac{1}{4}\ln\left(\frac{\rho_r}{\bar{\rho}_r}\right), \tag{2.5}$$

and

$$\zeta_\sigma = \delta N + \frac{1}{3}\ln\left(\frac{\rho_\sigma}{\bar{\rho}_\sigma}\right). \tag{2.6}$$

From this formula, the energy conservation on uniform density hypersurface at an arbitrary time after the beginning of the curvaton oscillation before the curvaton decay yields

$$\Omega_r e^{4(\zeta_r - \delta N)} + \Omega_\sigma e^{3(\zeta_\sigma - \delta N)} = 1, \tag{2.7}$$

where Ω_r and Ω_σ are density parameters of the radiation and the curvaton respectively defined as $\Omega_i = \bar{\rho}_i/\bar{\rho}_{\rm tot}$ with $i = r,\ \sigma$. Keeping only the first order quantities, we obtain δN as

$$\delta N = \frac{4\Omega_r}{4\Omega_r + 3\Omega_\sigma}\zeta_r + \frac{3\Omega_\sigma}{4\Omega_r + 3\Omega_\sigma}\zeta_\sigma. \tag{2.8}$$

On the other hand, the curvaton isocurvature perturbation is defined as

$$\mathcal{S}_\sigma = 3(\zeta_\sigma - \zeta_r), \tag{2.9}$$

so we can rewrite δN in terms of ζ_r and $\mathcal{S}_\sigma$ as

$$\delta N = \zeta_r + \frac{r(\eta)}{4+3r(\eta)}\mathcal{S}_\sigma, \tag{2.10}$$

where $r(\eta)$ is the time-dependent ratio of the background energy density of the curvaton $\bar{\rho}_\sigma$ to that of radiation $\bar{\rho}_r$ given by

$$r(\eta) = \begin{cases} \dfrac{\bar{\rho}_\sigma(\eta)}{\bar{\rho}_r(\eta)} & \text{(before the curvaton decay)} \\ r_D \equiv \left.\dfrac{\bar{\rho}_\sigma}{\bar{\rho}_r}\right|_{t=t_D} & \text{(after the curvaton decay),} \end{cases} \tag{2.11}$$

where a subscript "D" denotes the value at the curvaton decay. Because of $r(\eta) \propto a$ before the curvaton decay, in the case where the *first* reheating induced by the inflaton decay occurs before the beginning of the curvaton oscillation, r_D is calculated as

$$r_D = \frac{1}{6}\left(\frac{\bar{\sigma}_{\rm osc}}{M_P}\right)^2\left(\frac{m_\sigma}{\Gamma_\sigma}\right)^{1/2} \quad \text{for} \quad m_\sigma < \Gamma_\phi, \tag{2.12}$$

where m_σ is the curvaton mass and Γ_ϕ and Γ_σ are respectively the decay rate of the inflaton and curvaton. A subscript "osc" denotes the value at the beginning of the curvaton oscillation. In another case where $m_\sigma > \Gamma_\phi$, that is, the curvaton starts to oscillate before the inflaton decays into radiation, we obtain

$$r_D = \frac{1}{6}\left(\frac{\bar{\sigma}_{\rm osc}}{M_P}\right)^2\left(\frac{\Gamma_\phi}{\Gamma_\sigma}\right)^{1/2} \quad \text{for} \quad m_\sigma > \Gamma_\phi. \tag{2.13}$$

Because the curvaton is a subdominant component at the beginning of the curvaton oscillation, the total background energy density at that time can be well approximated by the radiation energy density, $\bar{\rho} \simeq \bar{\rho}_r$, which implies that the uniform total energy density slicing coincides with the uniform radiation density slicing, $\delta N = \zeta \simeq \zeta_r$. Therefore we obtain the energy density of the curvaton as

$$\rho_\sigma = \bar{\rho}_\sigma e^{3(\zeta_\sigma - \zeta)} \simeq \bar{\rho}_\sigma e^{\mathcal{S}_\sigma}. \tag{2.14}$$

On the other hand, the energy density of the curvaton can be expressed in terms of the curvaton field fluctuation on spatially flat slicing as $\rho_\sigma = m_\sigma^2(\bar{\sigma}_{\rm osc} + \delta\sigma_{\rm osc})^2/2$. Because an isocurvature perturbation from the curvaton is the gauge-invariant quantity, we obtain the relation between the curvaton isocurvature perturbation and the curvaton field fluctuation up to first order as

$$\mathcal{S}_\sigma \simeq \frac{2\delta\sigma_{\rm osc}}{\bar{\sigma}_{\rm osc}} = \frac{2d\ln\sigma_{\rm osc}}{d\sigma_*}\delta\sigma_*, \tag{2.15}$$

and then, we obtain the coefficient N_σ as

$$N_\sigma = \frac{2r(\eta)}{4+3r(\eta)}\frac{d\ln\sigma_{\rm osc}}{d\sigma_*}. \tag{2.16}$$

In the curvaton model, the power spectrum of the curvature perturbations is obtained as

$$\langle \zeta(\mathbf{k},\eta)\zeta(\mathbf{k}',\eta)\rangle = \delta^{(3)}(\mathbf{k}+\mathbf{k}')\frac{2\pi^2}{k^3}\mathcal{P}_\zeta(k,\eta), \tag{2.17}$$

$$\mathcal{P}_\zeta(k,\eta) = \mathcal{P}_{\zeta,\mathrm{inf}}(k) + \mathcal{P}_{\zeta,\mathrm{curv}}(k), \tag{2.18}$$

where $\mathcal{P}_{\zeta,\mathrm{inf}}(k)$ and $\mathcal{P}_{\zeta,\mathrm{curv}}(k)$ are contributions from the inflaton and the curvaton respectively and they are given by

$$\mathcal{P}_{\zeta,\mathrm{inf}}(k) = \frac{1}{2\epsilon}\left(\frac{H_{\mathrm{inf}}}{2\pi M_P}\right)^2, \tag{2.19}$$

$$\begin{aligned}\mathcal{P}_{\zeta,\mathrm{curv}}(k) &= \left(\frac{r(\eta)}{4+3r(\eta)}\right)^2\left(\frac{2d\ln\sigma_{\mathrm{osc}}}{d\sigma_*}\right)^2\left(\frac{H_{\mathrm{inf}}}{2\pi}\right)^2 \\ &\equiv \left(\frac{r(\eta)}{4+3r(\eta)}\right)^2\mathcal{P}_{S,\mathrm{curv}}(k),\end{aligned} \tag{2.20}$$

where $\mathcal{P}_{S,\mathrm{curv}}$ is the power spectrum of the isocurvature perturbations induced by the curvaton and we have used the formula: (see Appendix A)

$$\langle \delta\phi(\mathbf{k})_*\delta\phi(\mathbf{k}')_*\rangle = \langle \delta\sigma(\mathbf{k})_*\delta\sigma(\mathbf{k}')_*\rangle = \delta(\mathbf{k}+\mathbf{k}')\left(\frac{2\pi^2}{k^3}\right)\left(\frac{H_{\mathrm{inf}}}{2\pi}\right)^2. \tag{2.21}$$

2.2 Curvaton model with blue spectrum

Recent cosmological observations have indicated that the power spectrum of the primordial curvature perturbations is almost scale-invariant and $\mathcal{P}_\zeta \simeq 10^{-9}$ in large scales: $k \lesssim 1\ \mathrm{Mpc}^{-1}$. On the other hand, due to the difficulty of the direct observation, the primordial fluctuations on smaller scales are almost free from the tight observational bounds except for the constraints from the abundance of PBHs [10, 55], ultra-compact minihalos (UCMHs) [56, 57] or CMB μ-distortion [58] and GWBs [38].

On the other hand, large density perturbation on small scales is required for the formation of PBHs as seeds for the SMBHs. So, we want the model realising the blue-tilted power spectrum of curvature perturbation. Generically, it is very difficult in single field inflation models which are rigorously constrained by the Planck observation. Then, we are motivated to consider the multi-field model during inflation. In particular, the curvaton model can easily realize the blue-tilted spectrum as shown later. Therefore, we consider the case in which the inflaton is responsible for generating the large scale perturbations, which are constrained by observations, and the curvaton is responsible for the small scale ones, which are schematically illustrated in Fig 2.3.

We parametrize the power spectrum of the curvature perturbations induced from the curvaton fluctuations as

$$\mathcal{P}_{\zeta,\mathrm{curv}}(k) = \mathcal{P}_{\zeta,\mathrm{curv}}(k_c)\left(\frac{k}{k_c}\right)^{n_\sigma-1} \tag{2.22}$$

where n_σ is the spectral index, k_c is some reference value of wave number which are here taken to be $k_c = 1\ \mathrm{Mpc}^{-1}$ and

$$\mathcal{P}_{\zeta,\mathrm{curv}}(k_c) = \mathcal{P}_{\zeta,\mathrm{inf}} = 2\times 10^{-9}. \tag{2.23}$$

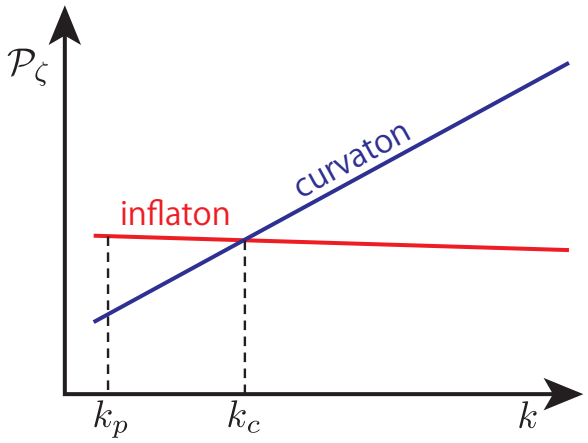

Figure 2.3: This figure illustrates the power spectrum of curvature perturbation in our situation. The red and blue lines correspond to the contributions from a inflaton and curvaton respectively. k_p is the pivot scale taken to be 0.002 Mpc^{-1} and we have taken $k_c = 1$ Mpc^{-1} throughout the thesis.

Here, we would like to note the non-Gaussianity of the primordial curvature perturbations, characterized by the nonlinearity parameter $f_{\rm NL}$. The curvaton model has been well-known as a model which can predict the large non-Gaussianity: $f_{\rm NL} \sim 1/r_D \gtrsim 10$. Recently, Planck observation placed a stringent constraint on $f_{\rm NL}$, giving $-8.9 < f_{\rm NL} < 14.3$ at two sigma level [1,3] However, even if we take small r_D in the later discussion, our model does not conflict with the Planck constraint. Because we rely on the inflaton to generate the large scale curvature perturbations, $f_{\rm NL}$ is suppressed by roughly $(\mathcal{P}_{\zeta,\rm curv}/\mathcal{P}_{\zeta,\rm inf})^2 \times 1/r_D$.

2.2.1 Quadratic curvaton model

Let us consider a simple curvaton model with quadratic potential as a representative model which realizes the blue-tilted spectrum, whose potential is given by

$$V(\sigma) = \frac{1}{2} m_\sigma^2 \sigma^2. \tag{2.24}$$

Under the slow-roll approximation, $3H_{\rm inf}\dot{\sigma} + V'(\sigma) \approx 0$, the field value of σ when the mode k exits the horizon is obtained as

$$\sigma_*(k) = \sigma_f \exp\left(-\frac{m_\sigma^2}{3H_{\rm inf}^2} N \right) \left(\frac{k}{k_p} \right)^{-\frac{m_\sigma^2}{3H_{\rm inf}^2}}, \tag{2.25}$$

where σ_f is the field value at the end of the inflation and $k_p = 0.002$ Mpc^{-1} is the pivot scale. Here we set $N = 50$ from the time when the pivot scale k_p leave the horizon to the end of the inflation. Note that since the field fluctuation on superhorizon scale is given by (see Appendix A)

$$\delta\sigma = \left(\frac{H_{\rm inf}}{2\pi} \right) \left(\frac{k}{aH_{\rm inf}} \right)^{m_\sigma^2/3H_{\rm inf}} \propto \exp\left(-\frac{m_\sigma^2}{3H_{\rm inf}^2} N \right), \tag{2.26}$$

the isocurvature perturbation, $\mathcal{S}_\sigma = 2\delta\sigma/\sigma$ remains constant on superhorizon scales, so it can be well-approximated by the value at the horizon exiting. Because of $m_\sigma \sim H_{\rm inf}$ in the present setup, the curvaton starts to oscillate soon after the inflation, which leads to $\sigma_f = \sigma_{\rm osc}$. Therefore, we have

$$\frac{d\ln\sigma_{\rm osc}}{d\sigma_*} = \frac{1}{\sigma_*(k)} \propto \left(\frac{k}{k_p}\right)^{\frac{m_\sigma^2}{3H_{\rm inf}^2}}, \tag{2.27}$$

and hence the spectral index of the power spectrum of the curvature perturbations is derived as

$$n_\sigma \simeq 1 + \frac{2m_\sigma^2}{3H_{\rm inf}^2}, \tag{2.28}$$

where we have neglected the contribution from the time-derivative of Hubble parameter, which is $\mathcal{O}(\epsilon)$ and much smaller than $2m_\sigma^2/3H_{\rm inf}^2$, because we set $m_\sigma \sim H_{\rm inf}$ to realize the strongly blue-tilted power spectrum as illustrated in Fig. 2.3.

2.2.2 Axion-like curvaton model

In this subsection, we review an axion-like curvaton model which was originally introduced in [59] (see also [60]) as an axion model with extremely blue-tilted spectrum of the axion isocurvature perturbations. The model is built in the framework of supersymmetry and has the following superpotential:

$$W = hS(\Phi\bar{\Phi} - f^2), \tag{2.29}$$

where Φ, $\bar{\Phi}$ and S are chiral superfields whose R-charges are $+1$, -1 and $+2$ respectively, f is some energy scale and h is a dimensionless coupling constant. This model has also an additional global $U(1)$ symmetry and Φ, $\bar{\Phi}$ and S have charges $+1$, -1 and 0, respectively. In the limit of the global SUSY, the scalar potential is derived from (2.29) as

$$V = h^2|\Phi\bar{\Phi} - f^2|^2 + h^2|S|^2(|\Phi|^2 + |\bar{\Phi}|^2), \tag{2.30}$$

where, the scalar components are denoted by the same symbols as the superfields. Provided that $|S| < f$ is satisfied, S tends to the origin and Φ and $\bar{\Phi}$ are settled on the flat direction satisfying

$$\Phi\bar{\Phi} = f^2 \quad \text{with} \quad S = 0, \tag{2.31}$$

which makes the scalar potential (2.30) vanish. In the very early universe whose energy scale is nearly the Planck scale, most of the scalar fields has field value comparable to the Planck scale. So, we can say that Φ has initially the Planck scale field value and S is stabilized at the origin. Thus, hereafter, we can reasonanbly assume that the flat condition (2.31) is always satisfied. Including the supergravity effects, the Hubble-induced mass terms are added to the scalar potential [61] as

$$V_H = c_1H^2|\Phi|^2 + c_2H^2|\bar{\Phi}|^2 + c_SH^2|S|^2, \tag{2.32}$$

where c_1, c_2 and c_S are numerical constants assumed to be real, positive and of order unity. In addition, there also exist the low energy SUSY breaking terms,

$$V_m = m_1^2|\Phi|^2 + m_2^2|\bar{\Phi}|^2 + m_S^2|S|^2, \tag{2.33}$$

where m_1, m_2 and m_S are soft masses of order of the gravitino mass. Because we are interested in the inflationary epoch, we neglect the low energy SUSY breaking mass terms and the flat direction is lifted by only the Hubble-induced mass terms (2.32) and the minimums of Φ and $\bar{\Phi}$ are determined as

$$|\Phi|_{\rm min} \simeq \left(\frac{c_2}{c_1}\right)^{1/4} f, \quad |\bar{\Phi}|_{\rm min} \simeq \left(\frac{c_1}{c_2}\right)^{1/4} f. \tag{2.34}$$

Now, we decompose the complex scalar fields into the radial and the phase components as

$$\Phi = \frac{1}{\sqrt{2}}\varphi \exp(i\theta_+), \quad \bar{\Phi} = \frac{1}{\sqrt{2}}\bar{\varphi} \exp(i\theta_-). \tag{2.35}$$

Then, along the flat direction, the massless direction is found as a linear combination of the phases, $\theta = (\theta_+ - \theta_-)/2$. Without loss of generality, we can take $\varphi \gg \bar{\varphi}$ as the initial condition and neglect the dynamics of $\bar{\varphi}$ in the early epoch [60], so we follow the dynamics of only the complex scalar field $\Phi = \varphi e^{i\theta}/\sqrt{2}$ whose potential is given by

$$V_\varphi = \frac{1}{2} c H^2 (\varphi - \varphi_{\rm min})^2, \tag{2.36}$$

where $\varphi_{\rm min}$ is the potential minimum of φ given by (2.34) which is taken to be $\varphi_{\rm min} = f$ hereafter. Note that since the mass is comparable to the Hubble parameter, φ rolls down the potential somewhat rapidly during inflation.

In our model, the curvaton is defined as the phase component of Φ. Note that since the curvaton is well-defined canonically-normalized field only after φ reaches the minimum, we denote it as $\sigma = f\theta$. In order for the curvaton to have a mass, the $U(1)$ symmetry should be broken by some non-perturbative effect. Because the curvaton has a shift symmetry: $\sigma + 2\pi f = \sigma$, the potential should be periodic, so we choose a cosine form for it like an axion illustrated in Fig 2.4:

$$V(\sigma) = \Lambda^4 \left[1 - \cos\left(\frac{\sigma}{f}\right)\right] \simeq \frac{1}{2} m_\sigma^2 \sigma^2, \tag{2.37}$$

where the second equality holds near the minimum $\sigma_{\rm min} = 0$ and the curvaton mass is defined as $m_\sigma = \Lambda^2/f$. After the Hubble parameter becomes smaller than the curvaton mass, the curvaton field starts to oscillate coherently with the initial amplitude $\sigma_i = f\theta$ and behaves as matter.

The curvaton decays when the Hubble parameter becomes equal to the decay rate of the curvaton and the decay temperature of the curvaton is determined from the decay rate. The interaction of the curvaton with its decay product is suppressed by f like an axion, so the decay rate of the curvaton is characterized by the dimensionless numerical constant κ which should be smaller than unity:

$$\Gamma_\sigma = \frac{\kappa^2}{16\pi} \frac{m_\sigma^3}{f^2}. \tag{2.38}$$

Then, the decay temperature of the curvaton is derived as

$$T_{\rm dec} = 0.5 \left(\frac{g_*}{100}\right)^{-1/4} (\Gamma_\sigma M_P)^{1/2}, \tag{2.39}$$

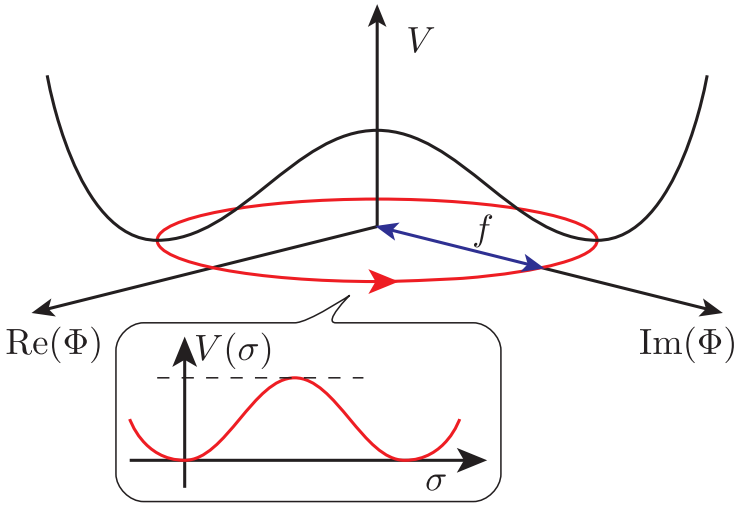

Figure 2.4: This figure illustrates the curvaton potential in an axion-like curvaton model.

where g_* is the relativistic degrees of freedom.

Let us consider the generation of the fluctuations of the curvaton in this model which is illustrated schematically in Fig. 2.5. During inflation, the fluctuation of the angular direction θ is roughly given by $\delta\theta_* \sim H_{\rm inf}/\varphi_*$ at the horizon exit and it stays constant on superhorizon scales. After φ reaches the minimum, the field value of the curvaton is unchanged because the mass of the curvaton is much smaller than $H_{\rm inf}$ and the fluctuation of θ can be identified with that of the curvaton as (see Appendix A) [1]

$$\frac{d\ln\sigma_{\rm osc}}{d\sigma_*}\delta\sigma_* = \left.\frac{\delta\sigma}{\sigma}\right|_{\varphi=f} = \left.\frac{\delta\theta}{\theta_i}\right|_{\varphi=f} = \frac{\delta\theta_*}{\theta_i} = \frac{1}{\varphi_*(k)\theta_i}\left(\frac{H_{\rm inf}}{2\pi}\right), \tag{2.40}$$

where θ_i is the initial misalignment angle assumed to be $\theta_i > H_{\rm inf}/(2\pi f)$ in order for the quantum fluctuations not to dominate over the classical value. $\varphi_*(k)$ indicates the value of φ just when the scale k exit the horizon. From the above expression, the scale dependence of the curvature perturbations sourced from the fluctuations of the curvaton is determined by solving the equation of motion for φ during inflation. For the potential (2.36), it is given by

$$\ddot{\varphi} + 3H_{\rm inf}\dot{\varphi} + cH_{\rm inf}^2(\varphi - f) = 0, \tag{2.41}$$

and we obtain the following solution:

$$\varphi \propto e^{-\lambda N} \quad \text{with} \quad \lambda = \frac{3}{2} - \frac{3}{2}\sqrt{1 - \frac{4}{9}c}. \tag{2.42}$$

In order to realize the blue-tilted spectrum, the initial value of φ is required to be far displaced from the minimum, so the solution (2.42) leads to $\varphi_*(k) \propto k^{-\lambda}$ for $\varphi \gg f$. This yields the spectral index:

$$n_\sigma = 4 - 3\sqrt{1 - \frac{4}{9}c}, \tag{2.43}$$

[1] The fluctuations of φ also give a contribution to $\delta\theta$. However, it is small (suppressed by θ) and hence can be neglected.

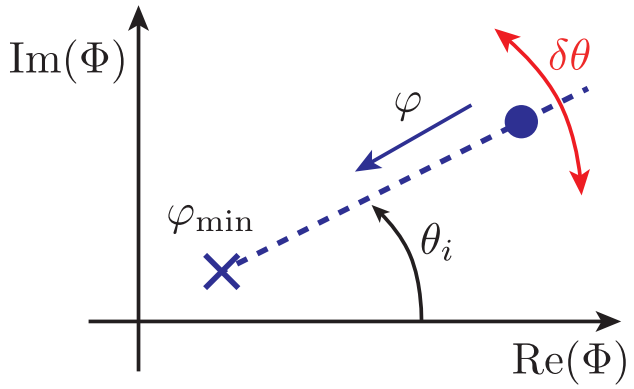

Figure 2.5: This figure illustrates the angular fluctuation of the complex scalar field in an axion-like curvaton model is illustrated. As the radial component approaches the minimum, the angular fluctuation becomes large because the background value of the phase component (which is the displacement from the global minimum) is unchanged.

which implies the extremely blue-tilted spectrum up to $n_\sigma = 4$ for $c \sim 9/4$. Note that the fluctuations of the curvaton which exit the horizon after φ reaches the minimum is scale-invariant.

As a summary, we can express the power spectrum as

$$\mathcal{P}_{\zeta,\mathrm{curv}}(k) = \begin{cases} \mathcal{P}_{\zeta,\mathrm{curv}}(k_c)\left(\dfrac{k}{k_c}\right)^{n_\sigma - 1} & \text{for} \quad k < k_f \\ \mathcal{P}_{\zeta,\mathrm{curv}}(k_f) & \text{for} \quad k > k_f, \end{cases} \tag{2.44}$$

where k_f corresponds to the scale exiting the horizon just when φ reaches the minimum f and $\mathcal{P}_{\zeta,\mathrm{curv}}(k_f)$ is calculated as

$$\mathcal{P}_{\zeta,\mathrm{curv}}(k_f) = \mathcal{P}_{\zeta,\mathrm{curv}}(k_c)\left(\frac{k_f}{k_c}\right)^{n_\sigma - 1} = \left(\frac{2r(\eta)}{4+3r(\eta)}\right)^2 \left(\frac{H_{\mathrm{inf}}}{2\pi f \theta_i}\right)^2. \tag{2.45}$$

Note that, from the φ_* dependence of $\mathcal{P}_{\zeta,\mathrm{curv}}(k)$;

$$\mathcal{P}_{\zeta,\mathrm{curv}}(k) = \mathcal{P}_{\zeta,\mathrm{curv}}(k_c)\left(\frac{\varphi_*(k_c)}{\varphi_*(k)}\right)^2 \quad \text{for} \quad k \leq k_f, \tag{2.46}$$

one obtain the relation

$$k = k_c \left(\frac{\varphi_*(k_c)}{\varphi_*(k)}\right)^{2/(n_\sigma - 1)} \quad \text{for} \quad k \leq k_f. \tag{2.47}$$

Domain wall problem Because we adopt the curvaton potential as a cosine function, there are two minima, $\theta = 0, 2\pi$. If the quantum fluctuation of the curvaton field is large enough to get over the maximum of the potential, domain walls are formed after the curvaton

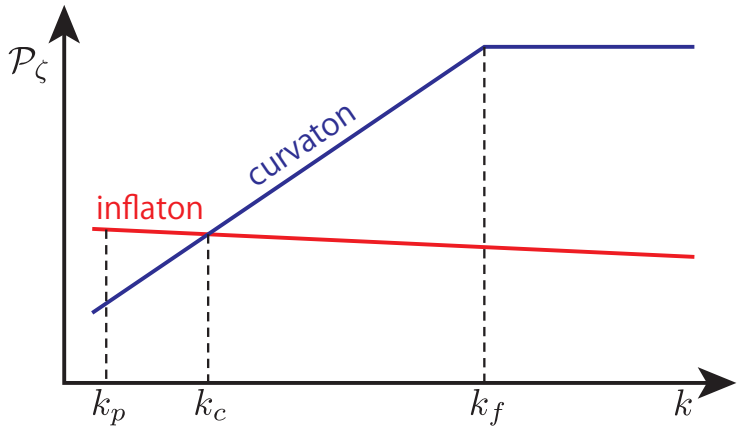

Figure 2.6: This figure schematically illustrates the power spectrum of curvature perturbation in an axion-like curvaton model. k_f is defined as the wave number corresponding to the scale which exits the horizon just when φ reaches the minimum.

starts to oscillate and they induce the cosmological disaster. So, we must impose the condition $|\pi - \theta_i| > \delta\theta$ to avoid the domain wall formation. Because the maximal angular fluctuation is given by $\delta\theta_{\rm max} = H_{\rm inf}/2\pi f$, we obtain the condition to avoid the domain wall formation as

$$\theta_i < \pi - \frac{H_{\rm inf}}{2\pi f} \quad \text{or} \quad \theta_i > \pi + \frac{H_{\rm inf}}{2\pi f}, \tag{2.48}$$

which is shown in Fig 2.7.

Here we have derived the scalar potential in the frame work of supergravity. However, we can build the model without supersymmetry if we start with the potential (2.30). The Hubble induced mass terms (2.32) which are necessary for generating the blue-tilted power spectrum can be obtained through couplings with the inflaton field. For example, suppose that a scalar φ causes chaotic inflation and its potential is given by $V(\varphi) = \lambda\varphi^4$. Then the term like $g\varphi^2|\Phi|^2$ (g: small coupling) lead to the Hubble induced mass term for Φ if we take appropriate g.

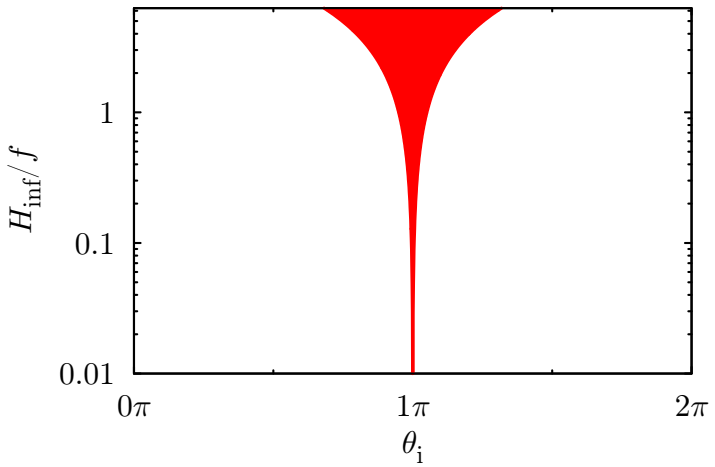

Figure 2.7: This figure shows the constraint on the initial angle to avoid the domain wall formation. The red region is ruled out.

Chapter 3

Primordial blackholes from a curvaton model

3.1 The standard description of the PBH

Primordial blackholes (PBHs) are expected to be formed through the collapse of highly overdensity regions which are usually seeded by the primordial fluctuation. If the density contrast smoothed over the horizon scale is larger than some critical value, δ_c, this region collapses into the PBH. Fig. 3.1 illustrates the criterion for the PBH formation. δ_c is given by w which is determined from the relation between the pressure and the energy density of the cosmic fluid $P = w\rho$ and it takes $1/3$ in radiation dominated universe. This criterion for the PBH formation is well confirmed by the numerical calculations [62–64].

According to the above PBH formation process, the mass of PBHs is as large as the horizon mass at the formation time, which is given by

$$\begin{aligned} M_{\rm BH} = \frac{4\pi}{3}\rho_r H^{-3} &\simeq 0.05 M_\odot \left(\frac{g_*}{100}\right)^{-1/2}\left(\frac{T_{\rm form}}{\rm GeV}\right)^{-2} \\ &\simeq 1\times 10^{13} M_\odot \left(\frac{g_*}{100}\right)^{-1/6}\left(\frac{k_{\rm form}}{\rm Mpc^{-1}}\right)^{-2}, \end{aligned} \tag{3.1}$$

where the subscript "form" represents the value at the PBH formation. (For example, $T_{\rm form}$ is the PBH formation temperature and $k_{\rm form}$ is the wave number corresponding to the scale reentering the horizon at the PBH formation) It is also well known that light PBHs evaporate into particles in thermal equilibrium with the Hawking temperature given by

$$T_H = \frac{\hbar c^3}{8\pi G M_{\rm BH} k_B} \approx 10^{-7}\left(\frac{M_{\rm BH}}{M_\odot}\right)^{-1} \ {\rm K}, \tag{3.2}$$

and the lifetime of such PBHs is estimated as

$$\tau(M) \approx \frac{\hbar c^4}{G^2 M_{\rm BH}^3} \approx 10^{64}\left(\frac{M_{\rm BH}}{M_\odot}\right)^3 \ {\rm yr}. \tag{3.3}$$

This means that the lifetime of those PBHs with mass $M_{\rm BH} \lesssim 10^{15}$ g is shorter than the age of the present Universe and such PBHs have completely evaporated by now. Here, we

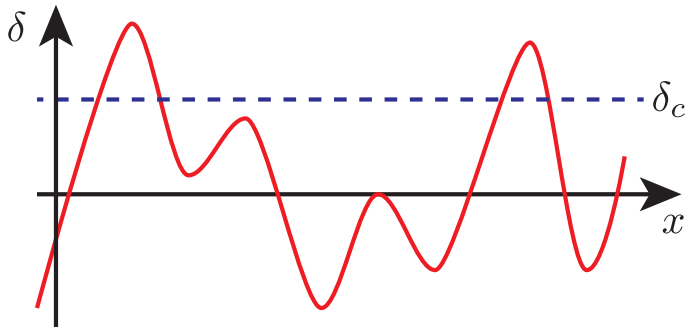

Figure 3.1: This figure schematically illustrates the criterion for the PBH formation. The horizontal axis and the vertical axis represent the spatial coordinate and the local density contrast smoothed over the horizon scale. Those regions where the density contrast exceeds the threshold value shown as a dashed line collapses into the PBH.

are interested in PBHs which can account for the present CDM or seeds for SMBHs, so we focus only on non-evaporating PBHs.

According to the PBH formation criterion in radiation dominated universe, PBHs can be formed in those horizon-volume region satisfying $\delta(R) > \delta_c$, where $\delta(R)$ is the density contrast smoothed over the horizon scale R which is expressed as

$$\delta(R) = \int_R d^3x \delta(\mathbf{x}) W(\mathbf{x}), \tag{3.4}$$

where $\delta(\mathbf{x})$ is the density contrast, $\delta\rho/\bar{\rho}$, at a given spatial point $\mathbf{x}$, $W(\mathbf{x})$ is the window function and we set $\delta_c = 1/3$. So the probability for the PBH formation is expressed as

$$\beta = \frac{\rho_{\rm PBH}(t_{\rm form})}{\rho_{\rm tot}(t_{\rm form})} = \int_{\delta_c}^{\infty} p(\delta(R)) d\delta(R), \tag{3.5}$$

where $p(\delta(R))$ is the probability distribution function for $\delta(R)$. Normally, the probability distribution obeys the Gaussian statistics;

$$p(\delta) d\delta(R) = \frac{1}{\sqrt{2\pi}\sigma(R)} \exp\left(- \frac{\delta^2(R)}{2\sigma^2(R)} \right) d\delta(R), \tag{3.6}$$

where $\sigma(R)$ is the smoothed variance over the horizon scale evaluated at the horizon reentering (do not confuse it with the curvaton field value) defined as

$$\sigma(R) = \int_0^{\infty} \frac{k^3 P(k)}{2\pi^2} \tilde{W}^2(kR) \frac{dk}{k}, \tag{3.7}$$

where $P(k)$ is the power spectrum of density contrast and $\tilde{W}(kR)$ is the Fourier transformation of the window function. Considering the top hat window function for example, which is given by

$$W(\mathbf{x}) = \frac{1}{V} \Theta(R - |\mathbf{x}|) \quad \text{with} \quad V = \frac{4\pi}{3} R^3, \tag{3.8}$$

we obtain

$$\tilde{W}(kR) = \frac{3}{(kR)^3}\big[-kR\cos(kR) + \sin(kR)\big], \tag{3.9}$$

and for the Gaussian window function given by

$$W(\mathbf{x}) = \frac{1}{\sqrt{2\pi}}\exp\left(-\frac{|\mathbf{x}|^2}{2}\right), \tag{3.10}$$

we obtain

$$\tilde{W}(kR) = \exp\left(-\frac{k^2R^2}{2}\right). \tag{3.11}$$

Assuming that the density contrast obeys the Gaussian distribution, the PBH formation probability or initial energy fraction of PBH is approximated as

$$\beta \approx \sigma(M)\exp\left[-\frac{1}{18\sigma^2(M)}\right], \tag{3.12}$$

where M is the mass contained in the smoothing scale given by $M = (4\pi/3)\rho R^3$. Once the initial abundance of PBH are determined, we can obtain the current density parameter of PBH which has not evaporated by now;

$$\Omega_{\rm PBH}h^2 = \frac{\rho_{\rm PBH,eq}}{\rho_{\rm tot,eq}}\Omega_{\rm m}h^2 \simeq 5\times10^7\beta\left(\frac{M_\odot}{M_{\rm BH}}\right)^{1/2}, \tag{3.13}$$

where the subscript "eq" indicates the time of the matter-radiation equality and $\Omega_{\rm m} \simeq 0.13h^{-2}$ is the density parameter of matter component today.

Here, we show the relation between the density perturbation and the curvature perturbation. In the comoving gauge in which the curvature perturbation is expressed as $\mathcal{R}$, which coincides with ζ well outside the horizon, the following relation is derived (see (B.36) in Appendix B);

$$\mathcal{P}_\delta(k) = \frac{6(1+w)^2}{(5+3w)^2}\mathcal{P}_\mathcal{R}(k), \tag{3.14}$$

at the time the scale k leaves the horizon [65]. Assuming the Gaussian window function $\tilde{W}(kR) = \exp(-k^2R^2/2)$ and taking into account $\mathcal{P}_\zeta \approx \mathcal{P}_\mathcal{R}$ on superhorizon scales, (2.44) and (2.45), we can approximate the variance as

$$\sigma^2(R) = \frac{8}{81}\mathcal{P}_{\zeta,\rm curv}(k_f)\big[(k_fR)^{-(n_\sigma-1)}\gamma((n_\sigma-1)/2, k_f^2R^2) + E_1(k_f^2R^2)\big], \tag{3.15}$$

where $\gamma(a,x)$ and E_1 are respectively the incomplete gamma function and exponential integral function defined as

$$\gamma(a,x) = \int_0^x t^{a-1}e^{-t}dt, \quad \text{and} \quad E_1(x) = \int_x^\infty \frac{e^{-t}}{t}dt. \tag{3.16}$$

Then, if we write

$$\sigma^2(k^{-1}) = \alpha\mathcal{P}_{\zeta,\rm curv}(k), \tag{3.17}$$

the numerical coefficient α is taken to be 0.1-4 as shown in Fig. 3.2.

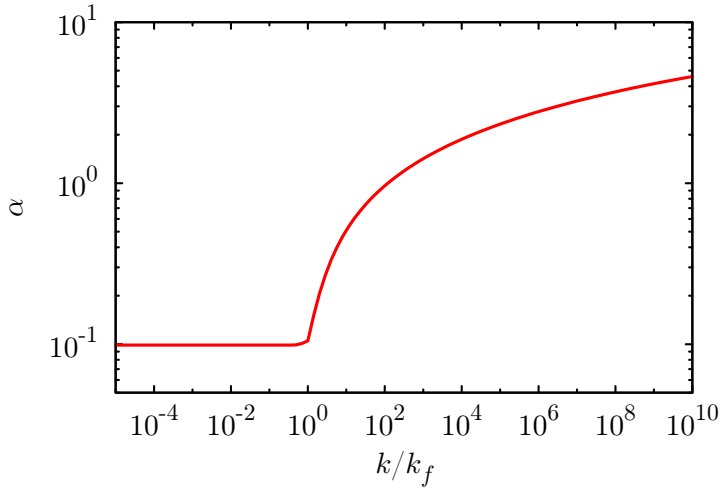

Figure 3.2: The ratio of the smoothed variance of density perturbation to the power spectrum of curvature perturbation are shown. The horizontal axis is the wave number corresponding to the smoothing scale as $k = R^{-1}$ divided by k_f. This curve is independent of n_σ.

3.2 Constraints on the abundance of PBH

3.2.1 Constraints from CDM density parameters

Here we briefly review the constraints on the abundance of PBHs, which is summarized in [10]. Since we are interested in the PBHs which can contribute to the CDM, we focus on the constraints on the non-evaporating PBH with mass $M_{\rm BH} > 10^{15}$ g. First of all, such PBHs must not overclose the universe, that is $\Omega_{\rm PBH} < \Omega_{\rm CDM}$, which yields

$$\beta < 3 \times 10^{-11} \left(\frac{M_{\rm BH}}{M_\odot} \right)^{1/2} \quad \text{for} \quad M_{\rm BH} \gtrsim 10^{15}\ \text{g}. \tag{3.18}$$

This is the most conservative constraint and a number of observations have further constrained the PBH abundance as briefly summarized below.

3.2.2 Constraints from microlensing

If the dark matter is made of massive compact objects, it induces the gravitational lensing with an optical depth of order 10^{-6}, which is called microlensing [66]. In particular, as the massive compact halo objects (MACHOs), including PBHs, move through the Milky Way halo, they may pass near the line of sight to a star from us, causing the magnification of the observed flux. So, the microlensing is a powerful tool to search for the dark matter existing in the Milky Way haloes. Actually, the microlensing surveys of stars in the Large and Small Magellanic Cloud (LMC and SMC) such as MACHO and EROS survey have been performed for many years and ruled out the MACHO CDM including the PBH CDM as dominant component of the CDM in the mass range 6×10^{25} g – 6×10^{34} g ($3 \times 10^{-8} M_\odot$ – $30 M_\odot$) [67–71]. In addition, the recent microlensing survey by the Kepler satellite, which is

mainly aimed to finding the extra-solar planets [72,73], have also succeeded to constrain the PBH CDM [74–76]. Thanks to the high precision photometry of the Kepler telescope, we have obtained the more stringent constraint than previous microlensing observations. As a result, it have found that PBHs in the mass range 4×10^{24} g – 2×10^{26} g ($2 \times 10^{-9} M_\odot$ – $10^{-7} M_\odot$) cannot be the dominant component of the present CDM.

3.2.3 Constraints from accretion

After matter-radiation equality, sufficiently massive PBHs begins to capture the surrounding gas and injects some energy into CMB by producing X-rays, which results in changing the recombination history affecting the CMB temperature anisotropy observed today and inducing the y-type spectral distortion of the CMB spectrum from the Planck distribution [77]. For example, the Thomson scattering optical depth may possibly become $\tau \sim 1$ due to the X-ray ionization from PBH accretion, which is inconsistent with the Planck result, so the PBH abundance is severely constrained in some mass range. In addition, the FIRAS spectrometer on the COBE satellite have set the upper limit on the comptonization y parameter which is defined in terms of the energy density injection ΔU and background energy density of CMB U as $\Delta U/U = 4y$, that is $y \leq 1.5 \times 10^{-5}$ at 95% confidence level [78,79]. Combining the above two constraints, we are able to constrain the abundance of the PBHs with 2×10^{32} g – 2×10^{41} g ($0.1 M_\odot < M_{\rm BH} < 10^8 M_\odot$).

3.2.4 Constraints from stars

At the time of star formation, i.e. $z \lesssim 10$, PBHs may be captured by the gravitational potential created by stars and may continue to live there even after the stars evolve into the compact remnants like the neutron stars (NSs) or the white dwarfs (WDs). Since baryons can contract by non-gravitational force, which develops the very steep gravitational potential, surrounding PBHs are pulled into a center of the potential and eventually trapped near the core of the NS or WD. The recent work [80] suggests that, in such a situation, PBHs may destroy such NSs or WDs by accretion, so we can constrain the abundance of PBHs since we actually have observed NSs and WDs. They have shown that the observations of NSs and WDs in globular clusters constrain the PBHs with mass 10^{16} g $\gtrsim M_{\rm BH} \gtrsim 10^{21}$ g and 10^{21} g $\gtrsim M_{\rm BH} \gtrsim 3 \times 10^{22}$ g respectively. In these mass range, PBHs cannot be the dominant component of the dark matter.

The direct capture of surrounding PBHs by NSs can also be possible and NSs can also be destroyed, which can put more stringent limits on the PBH abundance [81,82] Considering a close encounter of a PBH and a NS, the PBH loses its initial energy, which becomes the gravitationally bound energy. Following ref. [82], the energy loss is estimated as

$$\Delta E = \frac{M_{\rm BH}}{R_{\rm NS}} \frac{2\gamma}{1-n} \left(\frac{\pi}{4}\right)^{1-n} \left(\frac{R_{\rm NS}}{M_{\rm BH}}\right)^{1-n} \tag{3.19}$$

where $R_{\rm NS}$ is the radius of the neutron star which we take 12 km as a typical value, n is a parameter of the polytropic equation of state of stars defined via $p \propto \rho^{1+1/n}$, which we take $n = 1/2$ and γ is order unity constant taken here to be $\gamma = 1$. From this, an upper bound on the dark matter fraction in PBHs can be calculated as

$$\frac{\Omega_{\rm PBH}}{\Omega_{\rm CDM}} < \frac{M_{\rm BH}\sigma_v(1 - 2GM_{\rm NS}/R_{\rm NS})}{2\sqrt{6\pi} t_{\rm NS} M_{\rm NS} R_{\rm NS} \rho_{\rm DM}} \left(1 - \exp\left(-\frac{3\Delta E}{M_{\rm BH}\sigma_v^2}\right)\right)^{-1}, \tag{3.20}$$

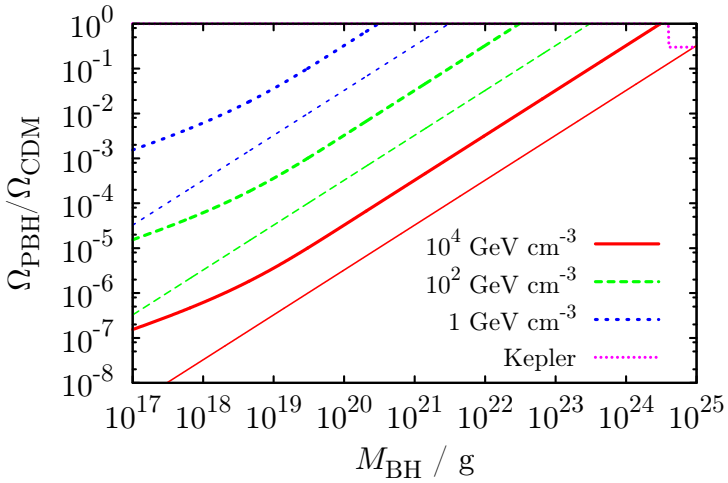

Figure 3.3: An upper bound on the dark matter fraction in PBHs from the neutron star. We have taken $\rho_{\rm DM} = 10^4$ GeV cm^{-3} (solid red), 10^2 GeV cm^{-3} (dashed green) and 1 GeV cm^{-3} (dotted blue) and $\sigma_v = 100$ km s^{-1} (thick lines) and 10 km s^{-1} (thin lines). The small-dotted magenta line show the upper bound from the Kepler satellite.

where $M_{\rm NS}$ and $t_{\rm NS}$ are respectively the mass and the lifetime of the neutron star which are taken to be $1.4M_\odot$ and 10^{10} yr and $\rho_{\rm DM}$ and σ_v are the energy density and velocity dispersion of dark matter. Fig. 3.3 shows an upper bound on dark matter fraction in PBHs. We can see that, if we take $\rho_{\rm DM} \sim 10^4$ GeV cm^{-3} and $\sigma_v \sim 10$ km s^{-1}, there are no allowed region in which the PBH is the dominant dark matter component. However, the constraint is sensitive to the dark matter density and the velocity dispersion which are quite uncertain, so the PBH can be still a viable candidate for the dark matter.

3.3 PBHs as seeds of supermassive blackhole

Another motivation to consider the PBH is the existence of supermassive blackholes (SMBHs) at the center of galaxies [83,84]. The observation of quasars (QSO) reveals that the SMBHs with mass $M_{\rm BH} \approx 10^9\ M_\odot$ exist at the redshift $z \approx 6$ [85]. Because the mass of the SMBH is roughly 9 orders magnitude larger than the stellar mass object, it is very difficult to explain these blackholes within the purely astrophysical mechanism, so we should rely on the primordial origin. However, it is also very difficult to provide such heavy PBHs because we need the PBH formation temperature to be $T_{\rm form} \lesssim 1$ MeV and large density perturbation on scales $k_{\rm form} \lesssim 10$ Mpc^{-1}. Actually, such a situation is ruled out from the constraint on the CMB spectral distortions due to photon diffusion [86] by the COBE/FIRAS observation. It is known that the energy of the small scale density perturbation is dissipated into CMB photons via diffusion damping and diffusion damping scale is given by

$$k_d^{-1} \simeq 2.5 \times 10^5 (1+z)^{-3/2}\ {\rm Mpc}. \tag{3.21}$$

After the double Compton scattering become ineffective at $z_{\rm DC} \sim 2 \times 10^6$, then, CMB photons with $k < k_d(z_{\rm DC}) \simeq 10^4$ Mpc^{-1} receive the energy injection from the small scale fluc-

tuations, which results in the μ-type CMB spectral distortion parametrized by the chemical potential μ and constrained by the COBE/FIRAS observation to be $|\mu| < 9 \times 10^{-5}$ [78,79]. In this situation, the calculation for μ contains the integral of the power spectrum of the photon energy density, $\int d^3k P_\gamma(k)$ where $P_\gamma(k)$ is decomposed into the power spectrum of the primordial perturbation and diffusion damping factor, $e^{-(k/k_d)^2}$. Because very large primordial perturbations on scale $k_{\rm form}$ are necessary to form PBHs, $k_{\rm form} > k_d$ should be satisfied not to yield too large μ. Thus, from the relation (3.1), $M_{\rm BH} \lesssim 10^5 M_\odot$ must be satisfied from $k_{\rm form} > k_d(z_{\rm DC})$, which seems to be too light to explain the supermassive blackholes. However, PBHs can accrete and grow in the universe filled with the dark energy fluid or quintessence field with equation of state $p < -1/3\rho$ [87,88] and PBHs with mass 10^4 – $10^5 M_\odot$ can be seeds for the supermassive blackholes [89].

3.4 PBH formation from an axion-like curvaton model

Here, we consider the PBH formation from an axion-like curvaton model introduced in the previous chapter based on the paper [90]. First of all, we show the energy density fraction of PBH in terms of $\mathcal{P}_{\zeta,\rm curv}$ in Fig. 3.4(a) in the case of $\alpha = 1$ (solid red line) and $\alpha = 0.1$ (dashed green line). The dotted blue line (the small-dotted magenta line) corresponds to the upper limit in the case of $M_{\rm BH} = 10^{27}$ (10^{17}) g, which comes from the current observation of the CDM density. In order for PBHs to be the dominant component of dark matter as an imaginary situation, the required value of curvature perturbation is $\mathcal{P}_{\zeta,\rm curv} \sim 2 \times 10^{-3}$ (2×10^{-2}) for $\alpha = 1$ (0.1). Substituting (2.22) and (3.17) into (3.12) and taking $\varphi(k) \sim f$, the constraint (3.18) is rewritten in terms of $H_{\rm inf}/(f\theta)$ shown in Fig. 3.4(b). In this figure, the thick (thin) solid red line corresponds to $r_D = 1$ and $\alpha = 1$ (0.1) and the thick dashed green line corresponds to $r_D = 0.1$ and $\alpha = 1$. The breaking point of each line corresponds to the point at which the quantum fluctuation of the curvaton, $\delta\sigma = H_{\rm inf}/2\pi$, becomes f. If $H_{\rm inf}/2\pi > f$, the amplitude of the quantum fluctuations of S overtakes the critical value f, which invalidates our underlying assumption (2.31). From Fig. 3.4(b) we need $r_D \sim 1$ and $f\theta \sim H_{\rm inf}$ to account for the present dark matter abundance.

For $r_D > 1$, PBHs can be formed after the curvaton starts to dominate the universe. The PBH formation in matter dominated universe is discussed in [91,92] and the initial energy fraction of PBH is estimated as $\beta \simeq 2 \times 10^{-2} \sigma^{13/2}(M)$. We have found $\mathcal{P}_\zeta \sim 2 \times 10^{-4}$ and $f\theta \sim 10 H_{\rm inf}$ to explain the present dark matter abundance as shown in Fig 3.5. We also note that there is a non-negligible effect from the non-Gaussianity in the case of $r_D \gg 1$. In such a case, the non-Gaussianity parameter $f_{\rm NL}$ becomes negative and the resultant PBH abundance becomes too small to be the dominant component of the CDM [93].

Now let us estimate the mass spectrum of PBHs in the present model. This is especially impotent for SMBHs since, taking into account the merging and accretion events prior to the formation of SMBHs and constraint from the CMB distortion, the mass spectrum of primordial seeds of SMBHs is required to have a sharply peaked shape [89]. With $R = k^{-1}$ and Eq.(3.1) we rewrite the smoothed variance (3.15) in terms of PBH masses as

$$\sigma^2(M_{\rm BH}) = \frac{8}{81}\mathcal{P}_{\zeta,\rm curv}(k_f)\left[\left(\frac{M_f}{M_{\rm BH}}\right)^{(n_\sigma-1)/2}\gamma\left(\frac{n_\sigma-1}{2}, \frac{M_{\rm BH}}{M_f}\right) + E_1\left(\frac{M_{\rm BH}}{M_f}\right)\right], \tag{3.22}$$

where M_f is the mass of PBH formed when the scale k_f enters the horizon. Using (3.22), we can calculate the mass function, which is defined as the number of PBHs per comoving

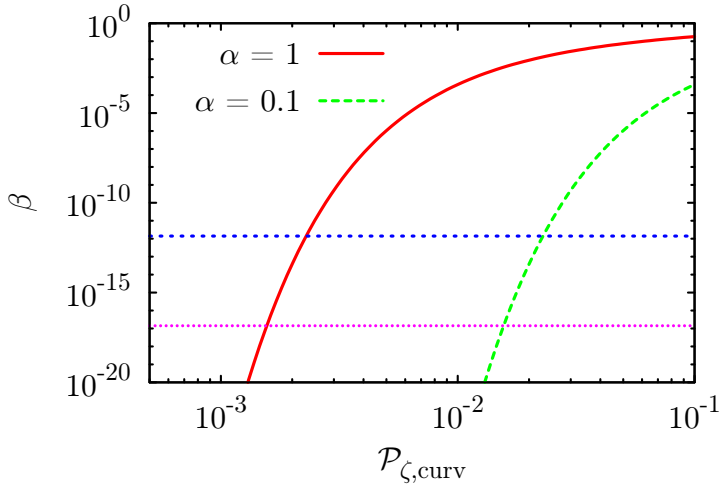

(a)

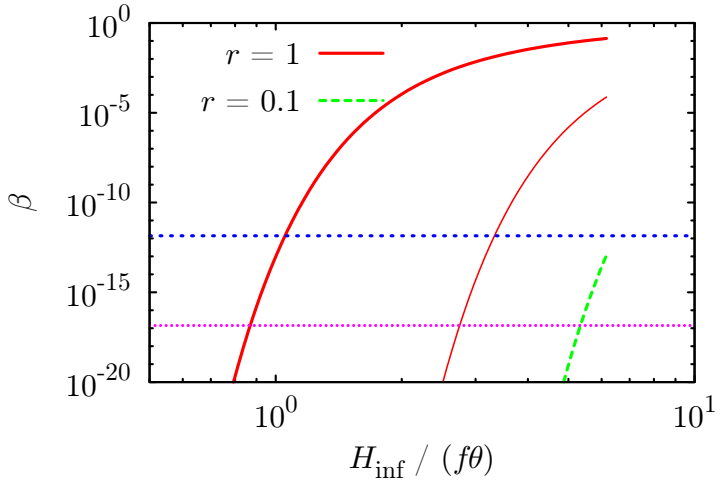

(b)

Figure 3.4: The energy density fraction of the PBH at the formation is shown. The horizontal axis correspond to $\mathcal{P}_{\zeta,\mathrm{curv}}$ in Fig. 3.4(a) and $H_{\mathrm{inf}}/f\theta$ in Fig. 3.4(b). In Fig. 3.4(a), the solid red line and the dashed green line correspond to $\alpha = 1$ and $\alpha = 0.1$ respectively. In Fig. 3.4(b), the thick (thin) solid red line corresponds to $r_D = 1$ and $\alpha = 1$ (0.1) and the thick dashed green line corresponds to $r_D = 0.1$ and $\alpha = 1$. Breaking point of each line in Fig. 3.4(b) corresponds to $\delta\sigma/\sigma = 1$. The dotted blue line (the small-dotted magenta line) corresponds to the upper limit in the case of $M_{\mathrm{BH}} = 10^{27}$ (10^{17}) g, which comes from the current observational value of the CDM density parameter : $\Omega_{\mathrm{CDM}} = 0.23$.

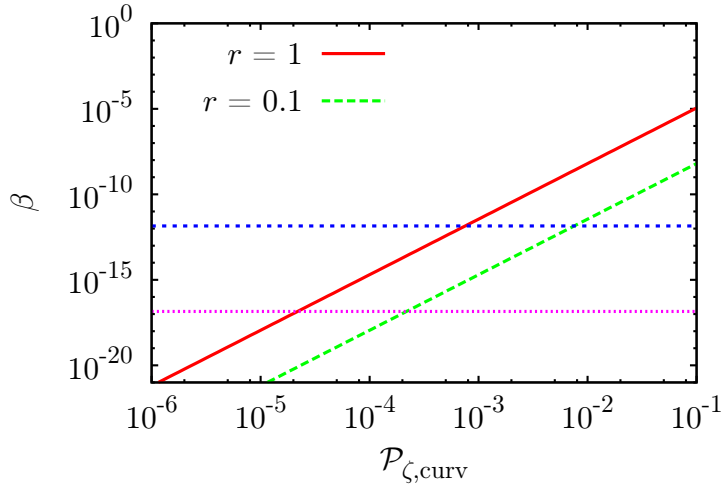

(a)

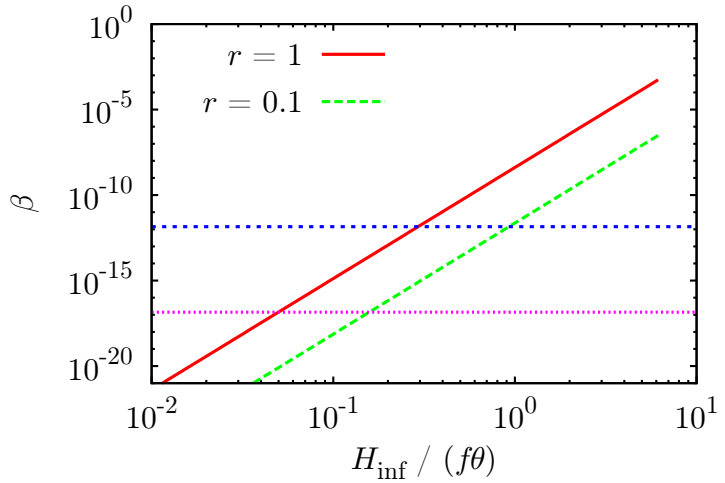

(b)

Figure 3.5: The energy density fraction of the PBH at the formation is shown. The horizontal axis correspond to $\mathcal{P}_{\zeta,\mathrm{curv}}$ in Fig. 3.5(a) and $H_{\mathrm{inf}}/f\theta$ in Fig. 3.5(b). In Fig. 3.5(a), the solid red line and the dashed green line correspond to $\alpha = 1$ and $\alpha = 0.1$ respectively. We have taken $r_D = 10$ for both figures. Breaking point of each line in Fig. 3.5(b) corresponds to $\delta\sigma/\sigma = 1$. The dotted blue line (the small-dotted magenta line) corresponds to the upper limit in the case of $M_{\mathrm{BH}} = 10^{27}$ (10^{17}) g, which comes from the current observational value of the CDM density parameter : $\Omega_{\mathrm{CDM}} = 0.23$.

volume whose mass range is $M_{\rm BH} \sim M_{\rm BH} + dM_{\rm BH}$, as [94] : (see appendix C)

$$\frac{dn_{\rm PBH}}{dM_{\rm BH}} = \sqrt{\frac{1}{18\pi}}\frac{\bar{\rho}_r^{\rm com}(t_f)}{M_{\rm BH}^2}\left(\frac{M_f}{M_{\rm BH}}\right)^{1/2}\left|\frac{d\ln\sigma^2(M_{\rm BH})}{d\ln M_{\rm BH}}\right|\frac{\beta(M_{\rm BH})}{\sigma^2(M_{\rm BH})}, \tag{3.23}$$

where $\bar{\rho}_r^{\rm com}(t_f)$ is the radiation energy per comoving volume when the scale k_f enters the horizon and $\beta(M_{\rm BH})$ is the density fraction of PBH whose mass is $M_{\rm BH}$. Since we assume that PBHs are formed after the curvaton decays, the mass spectrum has the lower cutoff $M_{\rm min}$, which corresponds to the mass of PBH formed just after the curvaton decays.[1]The mass spectrum of PBHs is shown in Fig. 3.6(a). The solid red and dashed green lines correspond to $M_{\rm min}/M_f = 10^{-8}$ and $M_{\rm min}/M_f = 10^{-3}$ respectively and they are normalized by the their own peak values. The mass spectrum depends only on $M_{\rm min}$ and it is independent of n_σ. It is clear that the dominant contribution to the energy density of PBHs comes from the smaller mass PBHs, so the constraint on the initial PBH abundance should be applied to the PBHs with $M_{\rm min}$. In particular, for $M_{\rm min}/M_f = 10^{-8}$, it is seen that the number of PBHs with mass larger than $\sim 10^{-4}M_f$ decreases drastically. This is due to the sudden decreasing of α, which implies the sudden decreasing of $\sigma^2(M)$, for $k \lesssim 10^2 k_f$ (see Fig. 3.2). Thus we can obtain a very narrow mass spectrum by tuning $M_{\rm min}/M_f$ as 10^{-3}–10^{-2}, which is required to explain SMBHs.

Critical collapse So far, we have considered that the PBH mass is equal to the horizon mass at formation. It may be true only if the smoothed variance of density perturbation is much lager than the critical density, δ_c. However, in most cases, the PBH formation occurs near the critical value, so we should consider the critical phenomena in gravitational collapse [62,63,95]. Here let us consider the effect of critical collapse. Numerical simulations show that the mass of PBH obeys the scaling relation [62]:

$$M_{\rm BH} = KM_H(\delta - \delta_c)^\gamma, \tag{3.24}$$

where M_H is the horizon mass and γ, K and δ_c are numerical constants which are in the range $0.34 < \gamma < 0.37$, $2.4 < K < 11.9$ and $0.67 < \delta_c < 0.71$ respectively. Assuming the Gaussian probability distribution function for density perturbation smoothed over the horizon scale at reentering, the probability of PBH formation with mass $M_{\rm BH}$ is given by

$$p(\delta(M_{\rm BH}))d\delta(M_{\rm BH}) = \frac{1}{\sqrt{2\pi}\sigma(M_H)}\exp\left[-\frac{(\delta_c + (M_{\rm BH}/KM_H)^{1/\gamma})^2}{2\sigma^2(M_H)}\right]d\delta(M_{\rm BH}). \tag{3.25}$$

Then, PBH mass spectrum is calculated as

$$\frac{dn_{\rm PBH}}{dM_{\rm BH}} = \sqrt{\frac{2}{\pi}}\frac{\bar{\rho}_{\rm com}}{M_{\rm BH}^2}\frac{1}{\sigma(M_H)\gamma}\left(\frac{M_{\rm BH}}{KM_H}\right)^{1/\gamma}\exp\left[-\frac{(\delta_c + (M_{\rm BH}/KM_H)^{1/\gamma})^2}{2\sigma^2(M_H)}\right], \tag{3.26}$$

which is shown in Fig 3.6(b). This figure shows that the mass spectrum is slightly broadened but they do not conflict with the requirement for the SMBH formation.

[1] PBH formation before the curvaton decays in radiation dominated universe may also be possible. In such a case, however, $\mathcal{P}_\delta$ is suppressed through the factor $(\rho_\sigma/\rho_r)^2$ at the formation. Since the number of produced PBHs is very sensitive to $\mathcal{P}_\delta$ and exponentially suppressed for small $\mathcal{P}_\delta$, the number of those PBHs produced before the curvaton decay may be negligibly small. Thus, even if we include the above effect, the mass spectrum (Fig. 3.6) may slightly spread around the cutoff and nothing is affected in our discussion.

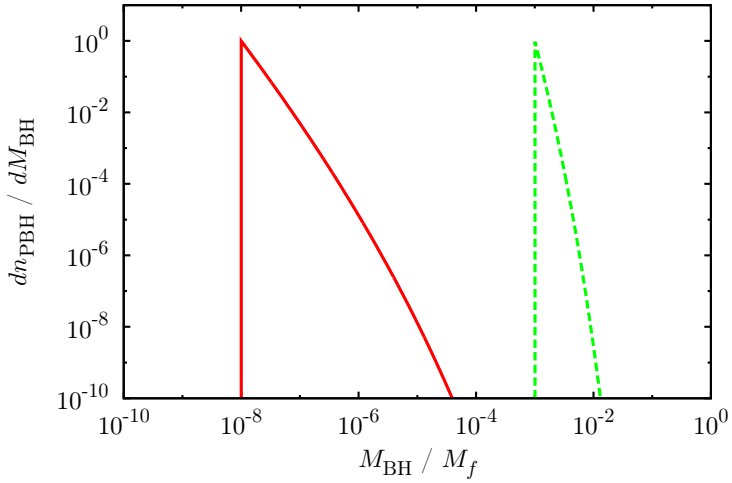

(a)

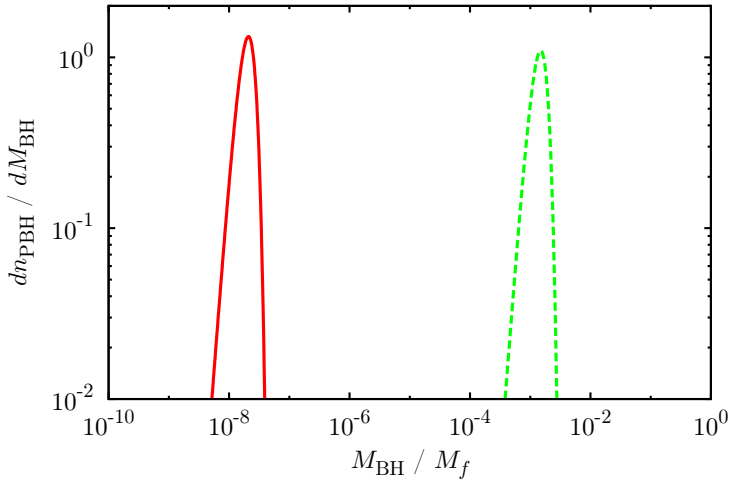

(b)

Figure 3.6: The mass spectrum of PBH, $dn_{\rm PBH}/dM_{\rm BH}$, is shown. In Fig 3.6(a), PBH mass is assumed to be horizon mass at formation and the solid red line and dashed green line correspond to $M_{\rm min}/M_f = 10^{-8}$ and $M_{\rm min}/M_f = 10^{-3}$ respectively and they are normalized by the their own peak values. They are independent of n_σ. In Fig 3.6(b), the critical phenomena is taken into account and we fix the horizon mass to be $10^{-8}M_f$ (solid red) and $10^{-3}M_f$ (dashed green). We have taken $\gamma = 0.37$, $K = 11.9$ and $\delta_c = 0.7$ and each line is normalized by the value at $M_{\rm BH} = 0.6M_H$ in Fig 3.6(b).

Now, we investigate the parameters allowing the formation of PBHs which eventually contribute significantly to the CDM. We also impose several conditions to build the viable scenario, which are listed below.

- Going back to the time when the pivot scale $k_p = 0.002$ Mpc^{-1} leaves the horizon, φ should be smaller than the Planck scale. The value of φ at that time ($\varphi(k_p) = \varphi_p$) is easily calculated as

$$\varphi_p = \left(\frac{k_f}{k_p}\right)^{(n_\sigma-1)/2} f. \tag{3.27}$$

  Combining this with the second equality of (2.45), we obtain

$$\varphi_p = \left(\frac{k_c}{k_p}\right)\left(\frac{2r(\eta)}{4+3r(\eta)}\right)\frac{H_{\rm inf}}{2\pi\theta_i\mathcal{P}_\zeta^{1/2}}. \tag{3.28}$$

  which is shown in Fig 3.7. Imposing $\varphi < M_P$, we obtain an upper bound on the Hubble parameter during inflation:

$$H_{\rm inf} < 2^{(n_\sigma-1)/2}10^{-3(n_\sigma+1)/2}\theta_i M_P\left(\frac{k_{\rm c}}{\rm Mpc^{-1}}\right)^{-(n_\sigma-1)/2}. \tag{3.29}$$

  Combining this with the constraint from the tensor-to-scalar ratio [96], $H_{\rm inf} < 5\times 10^{-5}M_P$, we get

$$H_{\rm inf} < \min\left[\ 2^{(n_\sigma-1)/2}10^{-3(n_\sigma+1)/2}\theta_i M_P,\ 5\times 10^{-5}M_P\ \right], \tag{3.30}$$

  where we set $k_{\rm c} = 1$ Mpc^{-1}.

- The mass of PBHs formed when the scale k_f reenter the horizon, M_f, is calculated with use of (2.23),(2.44) and (3.1). Since M_f is larger than the minimum mass of PBHs, we obtain the following condition:

$$M_{\rm min} < M_f = 2\times 10^{46-12/(n_\sigma-1)}\ {\rm g}\left(\frac{g_*}{100}\right)^{-1/6}\left(\frac{k_{\rm c}}{\rm Mpc^{-1}}\right)^{-2}\left(\frac{\mathcal{P}_{\zeta,{\rm curv}}(k_f)}{2\times 10^{-3}}\right)^{-2/(n_\sigma-1)} \tag{3.31}$$

- The curvaton should decay before the Big Bang nucleosynthesis (BBN), that is $T_{\rm dec} > 1$ MeV. From (3.1), the minimum mass of PBHs is related to $T_{\rm dec}$ as

$$T_{\rm dec} \simeq 1\times 10^3\ {\rm GeV}\left(\frac{g_*}{100}\right)^{-1/4}\left(\frac{10^{26}\ {\rm g}}{M_{\rm min}}\right)^{1/2}. \tag{3.32}$$

  Hence the minimum mass of PBHs is constrained as

$$M_{\rm min} \lesssim 1\times 10^{38}\ {\rm g}\left(\frac{g_*}{100}\right)^{-1/2}, \tag{3.33}$$

  which is combined with (3.31) and we get

$$M_{\rm min} \lesssim \min\left[\ 2\times 10^{46-12/(n_\sigma-1)}\ {\rm g},\ 1\times 10^{38}\ {\rm g}\ \right], \tag{3.34}$$

  where we set $g_* \approx 100$, $k_c = 1$ Mpc^{-1} and $\mathcal{P}_{\zeta,{\rm curv}}(k_f) = 2\times 10^{-3}$.

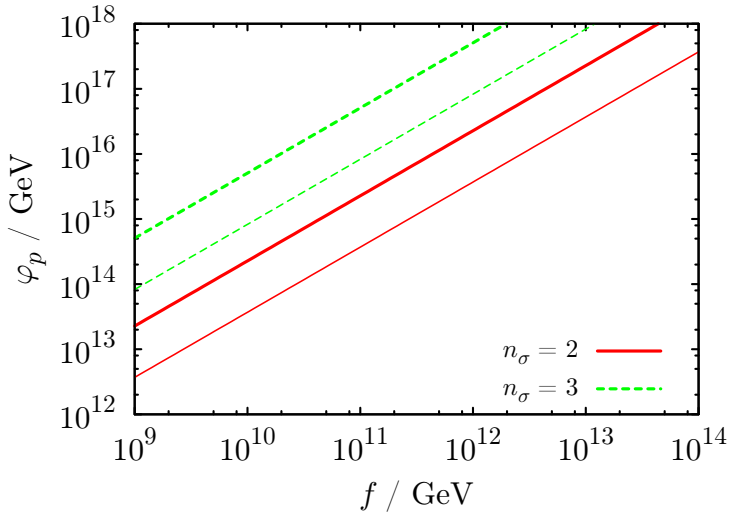

Figure 3.7: This figure shows the value of φ when the pivot scale leaves the horizon ($\varphi(k_p) = \varphi_p$). Solid red (dashed green) line corresponds to $n_\sigma = 2$ (3) and thick (thin) line corresponds to $r_D = 1$ (0.1).

- The reheating temperature is also constrained. In the case of $\Gamma_\phi < m_\sigma$, from (2.13) and (3.32) we obtain

$$T_R \approx 6 \times 10^3 \text{ GeV} \left(\frac{10^{26} \text{ g}}{M_{\rm min}}\right)^{1/2} \left(\frac{M_P}{H_{\rm inf}}\right)^2, \tag{3.35}$$

  where we take $f\theta \approx H_{\rm inf}$, $r_D \approx 1$ and $g_* \approx 100$. In the case of $\Gamma_\phi > m_\sigma$, on the other hand, we get the similar relation by simply replacing T_R with $T_{\rm osc}$. The reheating temperature or the curvaton oscillation temperature is constrained from the inequality (3.30).

We show the parameter space allowing for the PBH to take a role of the dominant component of the CDM in Fig. 3.8 in the case of $\Gamma_\phi < m_\sigma$ and $k_{\rm c} = 1$ Mpc^{-1}. The allowed region is inside the respective contours. The dashed-and-dotted-cyan line is the lower limit on the PBH mass, which comes from the current upper limit on the tensor-to-scalar ratio. For the PBH to take a role of the dominant component of the CDM, we need the somewhat high reheating temperature $T_R \gtrsim 10^{12}$ GeV.

Then, we investigate the allowed region of our model parameters, f and m_σ, in which the current dark matter density can be explained by the PBH. The allowed parameter region becomes much narrower than Fig. 3.8 if we take into account the decay rate formula (2.38). The relation between the decay temperature of the curvaton and PBH mass given by (3.32) is rewritten as

$$f \simeq 1 \times 10^{14} \text{ GeV } \kappa \left(\frac{M_{\rm min}}{10^{26} \text{ g}}\right)^{1/2} \left(\frac{m_\sigma}{10^6 \text{ GeV}}\right)^{3/2}, \tag{3.36}$$

which constrains the interesting region in $f - m_\sigma$ plane when 10^{25} g $< M_{\rm min} < 10^{27}$ g is

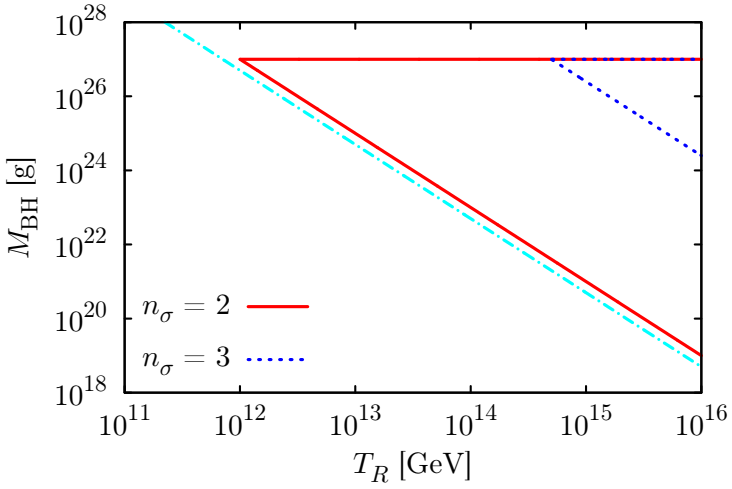

Figure 3.8: The allowed parameter region in which PBHs can contribute to the CDM in our model is shown. The allowed region is inside the respective contours. The dotted-blue line and the solid-red line correspond to the boundary in the case of $n_\sigma = 3$ and 2 respectively. The dashed-and-dotted-cyan line is the lower limit on the PBH mass coming from the upper limit on the tensor-to-scalar ratio. We have taken $r = 1$ and $\theta = 1$.

imposed. In the case of $m_\sigma > \Gamma_\phi$, (2.13) is translated into the following inequality :

$$f \gtrsim 1 \times 10^{14}\ \text{GeV}\ \kappa^{1/3}\left(\frac{m_\sigma}{10^6\ \text{GeV}}\right)^{1/3}, \tag{3.37}$$

where we set $\theta = 1$ and $g_* \approx 100$. In the case of $m_\sigma < \Gamma_\phi$, on the other hand, the relation from (2.12) becomes approximately same as (3.37) but replacing $\gtrsim$ with $\simeq$. Moreover, the constraints (3.30) is trivially translated into upper bound on f by simply replacing $H_{\rm inf}$ with $f\theta$. The constraint (3.34) is rewritten as

$$f \lesssim 1 \times 10^{18}\ \text{GeV}\ \kappa\left(\frac{M_{\rm c}}{10^{34}\ \text{g}}\right)^{1/2}\left(\frac{m_\sigma}{10^6\ \text{GeV}}\right)^{3/2}, \tag{3.38}$$

where $M_{\rm c}$ is defined as the right-hand-side of (3.34).

We summarize the above constraints in Fig. 3.9(a) and Fig. 3.9(b) for$r_D = 1$ and $n_\sigma = 2$. In the case of $m_\sigma > \Gamma_\phi$, the conditions (3.37) and (3.38) correspond to the region inside the thick solid-red (dashed-green) lines for $\kappa = 1$ (0.01). In addition, it must be below the thick (thin) dashed-and-dotted-cyan lines corresponding to the upper bound of the PBH mass, 10^{27} g for $\kappa = 1$ (0.01). Thus, the allowed parameters are inside the yellow shaded regions. In the opposite case, $m_\sigma < \Gamma_\phi$, allowed parameters are on the lower boundary of these regions. From these, it is found that f and m_σ must be $f \sim 5 \times 10^{13}$ – 10^{14} GeV, $m_\sigma \sim 5 \times 10^5$ – 10^8 GeV and $\Lambda \sim 10^{10}$ – 10^{11} GeV to explain the current CDM abundance. Similar results were found when we considered the PBH formation in the matter (curvaton) dominated era. For example, setting $r_D = 10$ and same parameters as those we have taken in Fig. 3.9, we found the parameter space shown in Fig. 3.10.

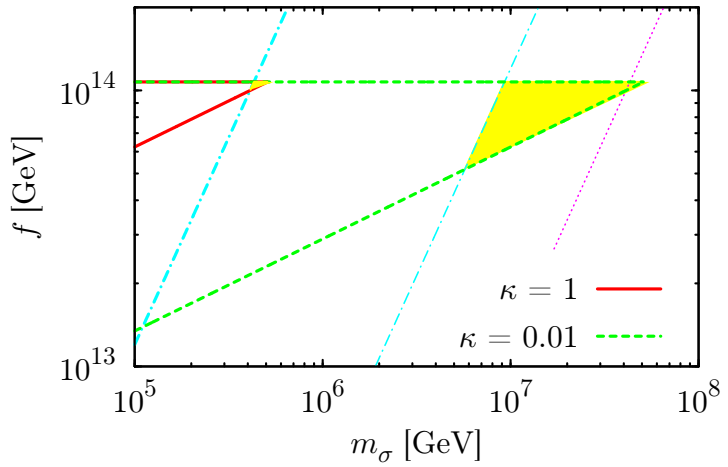

(a)

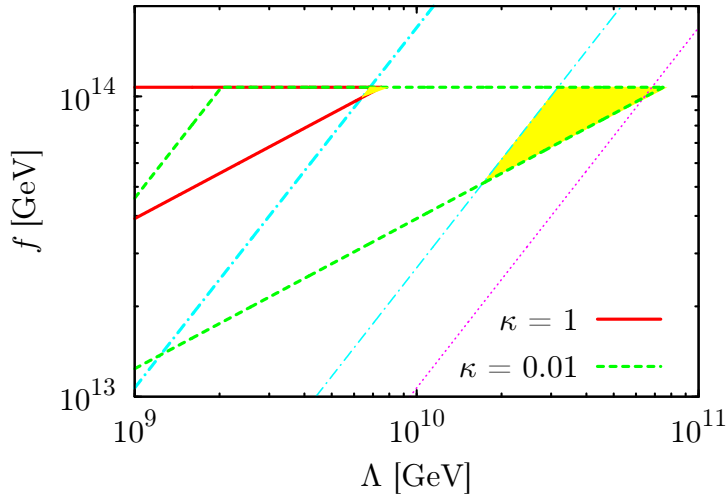

(b)

Figure 3.9: The allowed regions for the PBH to contribute to the CDM in $f - m_\sigma$ plane and $f - \Lambda$ plane are shown. Inside the thick solid-red (dashed-green) lines, the conditions (3.37) and (3.38) are satisfied for $\kappa = 1$ (0.01). The thick (thin) dashed-and-dotted-cyan lines corresponds to the upper limit which comes from the maximum mass of PBH dark matter: $M_{\rm BH} = 10^{27}$ g for $\kappa = 1$ (0.01), so the allowed parameters are inside the yellow shaded regions. The thin small-dotted magenta lines correspond to $M_{\rm BH} = 10^{25}$ g for $\kappa = 0.01$. We have taken $r_D = 1$, $n_\sigma = 2$ and $\theta = 1$ and assumed $m_\sigma > \Gamma_I$ in both figures.

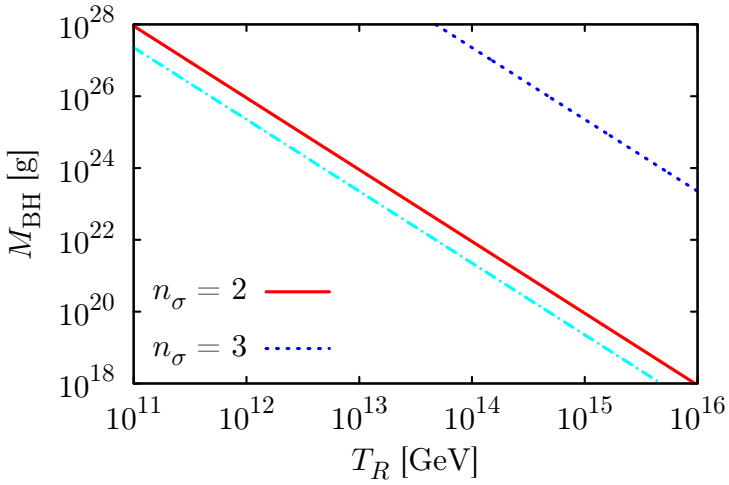

(a)

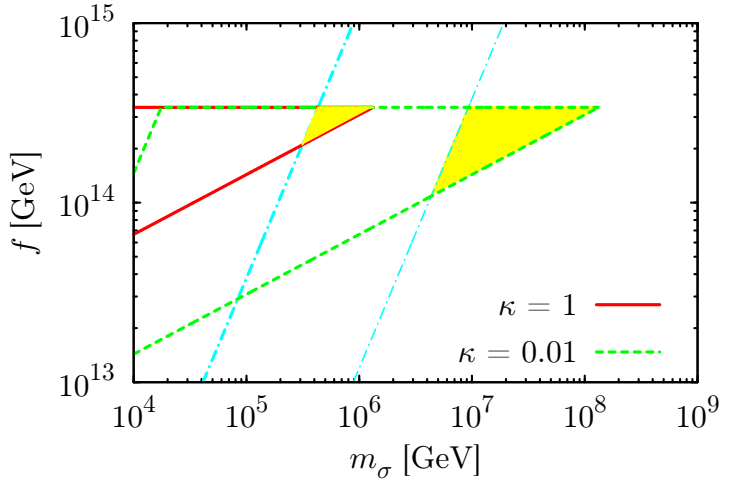

(b)

Figure 3.10: The allowed regions for the PBH to account for the CDM in $M_{\rm BH} - T_R$ plane and $f - m_\sigma$ plane are shown in Fig. 3.10(a) and Fig. 3.10(b) respectively. In Fig. 3.10(a), the allowed region is inside the solid-red line (the dotted-blue line) for $n_\sigma = 2$ ($n_\sigma = 3$) and the dashed-and-dotted-cyan line (small-dotted-magenta line) corresponds to $M_{\rm BH} = 10^5 M_\odot$ ($10^4 M_\odot$). In Fig. 3.10(b), inside the thick solid-red (dashed-green) lines, the conditions (3.37) and (3.38) are satisfied for $\kappa = 1$ (0.01). The thick (thin) dashed-and-dotted-cyan lines corresponds to the upper limit which comes from the maximum mass of PBH dark matter: $M_{\rm BH} = 10^{27}$ g for $\kappa = 1$ (0.01), so the allowed parameters are inside the yellow shaded regions. We have taken $r_D = 10$ and $\theta = 1$ in both figures and $n_\sigma = 2$ in Fig. 3.10(b).

Another outcome of our model is the possibility of explaining the seeds of SMBHs. The initial mass fraction of PBHs as seeds of SMBHs is constrained by the observed comoving number density of QSOs: $a^3 n_{\rm QSO} \simeq (6 \pm 2) \times 10^{-10}$ Mpc^{-3} [85]. The comoving number density of PBHs is given by

$$a^3 n_{\rm PBH} \simeq 6 \times 10^{18} \beta \ {\rm Mpc}^{-3} \left(\frac{g_*}{10}\right)^{-1/4} \left(\frac{M_\odot}{M_{\rm BH}}\right)^{3/2}, \tag{3.39}$$

so, compared with $a^3 n_{\rm QSO}$, β is estimated as

$$\beta \sim 2 \times 10^{-21} \left(\frac{g_*}{10}\right)^{1/4} \left(\frac{M_{\rm BH}}{10^5 \ M_\odot}\right)^{3/2}. \tag{3.40}$$

Since a quite large mass and a narrow mass spectrum of the PBH are needed to explain the SMBH, we set $M_{\rm min} \sim M_f$ which leads $\alpha \simeq 0.1$, $H_{\rm inf}/f\theta \sim 2$ and $\mathcal{P}_{\zeta,{\rm curv}}(k_f) \sim 1 \times 10^{-2}$. Then the parameter space is constrained by the same way as those of the PBH dark matter case and we summarize it in Fig. 3.11 and Fig 3.12 for $r_D = 1$ and $r_D = 10$ respectively.

In Fig. 3.11(a) and Fig 3.12(a), the allowed region is inside the solid-red line (the dotted-blue line) for $n_\sigma = 2.5$ ($n_\sigma = 2.75$). The dashed-and-dotted-cyan line (the small-dotted-magenta line) corresponds to $M_{\rm BH} = 10^5 M_\odot$ ($10^4 M_\odot$), on which the SMBH is explained by the PBH. In Fig. 3.11(b) and Fig. 3.12(b), the allowed region is inside the solid-red line (the dashed-green line) for $\kappa = 1$ (0.01). The thick (thin) dashed-and-dotted-cyan line and small-dotted-magenta line correspond to $M_{\rm BH} = 10^5 M_\odot$ and $M_{\rm BH} = 10^4 M_\odot$ respectively for $\kappa = 1$ (0.01). We found that our model can provide the seeds of SMBHs for $T_R \gtrsim 10^9$ GeV, $f \sim 10^{12}$ GeV, $m_\sigma \sim 0.5$ – 100 GeV and $\Lambda \sim 10^6$ – 10^7 GeV.

It is clear that the dark matter and SMBHs cannot be explained by *single* curvaton because the mass spectrum of PBH has peaked shape, so we need multiple curvaton field to explain them. Fortunately, various axion-like particles often appears in particle physics theories. One of them may be the curvaton which is responsible for SMBHs and another may explain the present dark matter. In addition, another axion field can play a role of the usual QCD axion which solves the strong CP problem. If the Peccei-Quinn scale f_a is $\sim 10^{12}$ GeV, the QCD axion can account for the dark matter of the universe. The coincidence of two independent scales $f \simeq f_a \sim 10^{12}$ GeV may be very interesting. Furthermore, it is pointed out that the axion dark matter is a good candidate consistent with the presence of the primordial SMBHs [57]. The required scale $\Lambda \sim 10^6$ – 10^7 GeV is coincide with the SUSY breaking scale when it is mediated by gauge interactions, which suggests that the dynamics generates the curvaton mass may be related to physics of SUSY breaking.

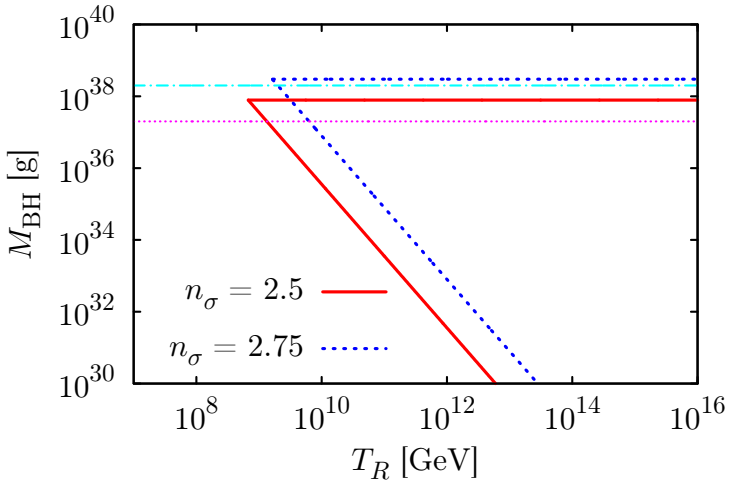

(a)

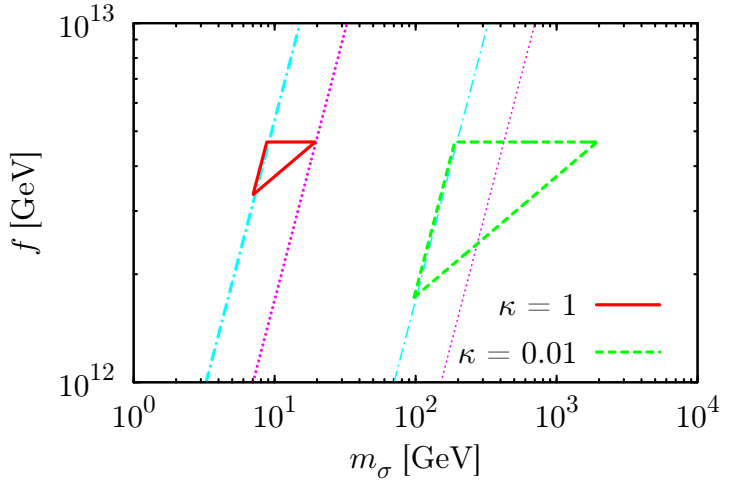

(b)

Figure 3.11: The allowed regions for the PBH to be the seed of the SMBHs in $M_{\rm BH}$ – T_R plane and f – m_σ plane are shown in Fig. 3.11(a) and Fig. 3.11(b) respectively. In Fig. 3.11(a), the allowed region is inside the solid-red line (the dotted-blue line) for $n_\sigma = 2.5$ ($n_\sigma = 2.75$) and the dashed-and-dotted-cyan line (small-dotted-magenta line) corresponds to $M_{\rm BH} = 10^5 M_\odot$ ($10^4 M_\odot$). In Fig. 3.11(b), the allowed region is inside the solid-red line (the dashed-green) and the thick (thin) dashed-and-dotted-cyan line and small-dotted-magenta line correspond to $M_{\rm BH} = 10^5 M_\odot$ and $M_{\rm BH} = 10^4 M_\odot$ respectively for $\kappa = 1$ (0.01). We have taken $r_D = 1$ and $\theta = 1$ in both figures and $n_\sigma = 2.75$ in Fig. 3.11(b).

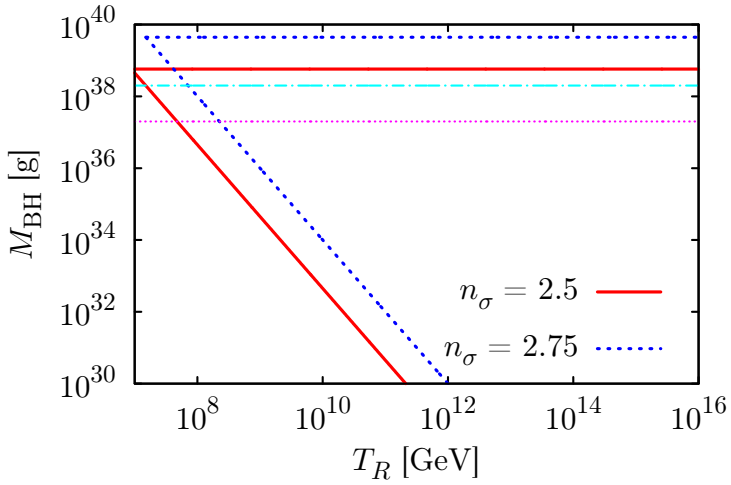

(a)

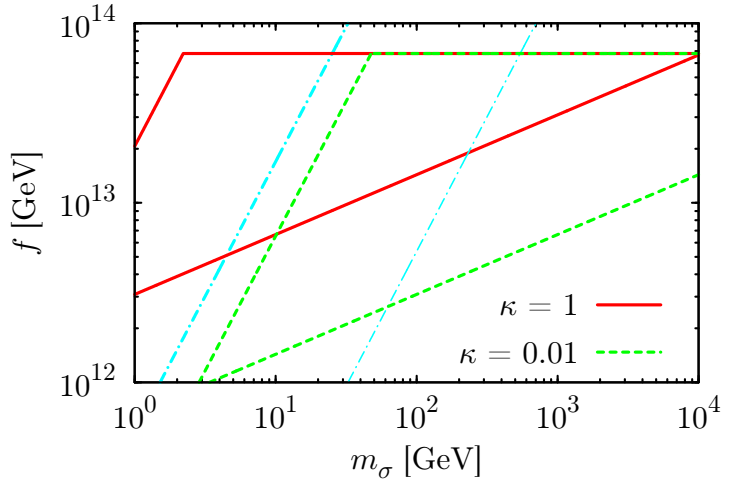

(b)

Figure 3.12: The allowed regions for the PBH to be the seed for SMBHs in $M_{\rm BH} - T_R$ plane and $f - m_\sigma$ plane are shown in Fig. 3.12(a) and Fig. 3.12(b) respectively. In Fig. 3.12(a), the allowed region is inside the solid-red line (the dotted-blue line) for $n_\sigma = 2.5$ ($n_\sigma = 2.75$) and the dashed-and-dotted-cyan line (small-dotted-magenta line) corresponds to $M_{\rm BH} = 10^5 M_\odot$ ($10^4 M_\odot$). In Fig. 3.12(b), the allowed region is inside the solid-red line (the dashed-green) and the thick (thin) dashed-and-dotted-cyan line corresponds to $M_{\rm BH} = 10^5 M_\odot$ for $\kappa = 1$ (0.01). We have taken $r_D = 10$ and $\theta = 1$ in both figures and $n_\sigma = 2$ in Fig. 3.10(b).

Chapter 4

Gravitational waves from a curvaton model

In this chapter, we consider the scalar induced gravitational waves in curvaton models with blue-tilted power spectrum of the curvature perturbation. We begin by the basics on gravitational waves, and then we briefly explain the scalar induced gravitational waves. Finally we show the resultant spectrum of the gravitational waves in our models and discuss the detectability by future detectors.

4.1 Basics on gravitational waves

4.1.1 Power spectrum of the gravitational waves

The stochastic background of the gravitational waves are described by the tensor metric perturbation, $h_{ij}(\mathbf{x}, \eta)$, satisfying trace-free ($h^i_i = 0$) and transverse ($\partial^i h_{ij} = 0$) on the spatially flat FRW metric, which is given by

$$ds^2 = a^2(\eta)\big[-d\eta^2 + (\delta_{ij} + h_{ij})dx^i dx^j\big]. \tag{4.1}$$

Conventionally, the Fourier transformation of the tensor metric perturbation is defined as

$$h_{ij}(\mathbf{x}, \eta) = \int \frac{d^3k}{(2\pi)^{3/2}} e^{i\mathbf{kx}}\big[h^+_{\mathbf{k}}(\eta)e^+_{ij}(\mathbf{k}) + h^\times_{\mathbf{k}}(\eta)e^\times_{ij}(\mathbf{k})\big], \tag{4.2}$$

where $e^+_{ij}(\mathbf{k})$ and $e^\times_{ij}(\mathbf{k})$ are two polarization tensors defined in terms of two orthonormal basis vectors, $e_i(\mathbf{k})$ and $\bar{e}_i(\mathbf{k})$, orthogonal to $\mathbf{k}$ as

$$e^+_{ij}(\mathbf{k}) = \frac{1}{\sqrt{2}}\big[e_i(\mathbf{k})e_j(\mathbf{k}) - \bar{e}_i(\mathbf{k})\bar{e}_j(\mathbf{k})\big], \tag{4.3}$$

$$e^\times_{ij}(\mathbf{k}) = \frac{1}{\sqrt{2}}\big[e_i(\mathbf{k})\bar{e}_j(\mathbf{k}) + \bar{e}_i(\mathbf{k})e_j(\mathbf{k})\big]. \tag{4.4}$$

Then, the power spectrum of the tensor metric perturbation is defined through

$$\langle h^r_{\mathbf{k}}(\eta)h^s_{\mathbf{p}}(\eta)\rangle \equiv \frac{2\pi^2}{k^3}\delta^{rs}\delta^3(\mathbf{k}+\mathbf{p})\mathcal{P}^r_h(k,\eta), \tag{4.5}$$

where r and s are either $+$ or $\times$ and we obtain the total power spectrum as $\mathcal{P}_h = \mathcal{P}^+_h + \mathcal{P}^\times_h$.

4.1.2 The power spectrum of primordial tensor metric perturbations

The dynamics of the spacetime is governed by the Einstein-Hilbert action given by

$$S = \frac{1}{16\pi G}\int d\eta d^3x\sqrt{-g}R. \tag{4.6}$$

Substituting our metric with tensor metric perturbations into the Ricci scalar and keeping up to the second order, we obtain the action for the tensor metric perturbations without source terms,

$$S = \frac{1}{64\pi G}\int d\eta d^3x\sqrt{-\bar{g}}\big[-\bar{g}^{\mu\nu}\partial_\mu h_{ij}\partial_\nu h^{ij}\big], \tag{4.7}$$

where $\bar{g}_{\mu\nu}$ is the background FRW metric and $\bar{g}$ is its determinant. By varying h_{ij}, the evolution equation for GW is derived as

$$h''_{ij} + 2\mathcal{H}h'_{ij} - \nabla^2 h_{ij} = 0. \tag{4.8}$$

Further, by substituting (4.2) into (4.7), we obtain

$$S = \sum_r \int d\eta d^3k \frac{a^2}{32\pi G}[(h^r_{\mathbf{k}})'(h^r_{-\mathbf{k}})' - k^2 h^r_{\mathbf{k}} h^r_{-\mathbf{k}}]. \tag{4.9}$$

If we redefine h_{k} as

$$\tilde{h}^r_{\mathbf{k}} = \frac{a}{\sqrt{16\pi G}}h^r_{\mathbf{k}}, \tag{4.10}$$

and after integration by parts, the action (4.9) yields the so called Mukhanov action form,

$$S = \sum_r \int d\eta d^3k \frac{1}{2}\left[(\tilde{h}^r_{\mathbf{k}})'(\tilde{h}^r_{-\mathbf{k}})' - \left(k^2 + \frac{a''}{a}\right)\tilde{h}^r_{\mathbf{k}}\tilde{h}^r_{-\mathbf{k}}\right], \tag{4.11}$$

which implies that $\tilde{h}_{\mathbf{k}}$ is a canonically normalized field. Hereafter we regard $\tilde{h}_{\mathbf{k}}$ as quantum fields, $\hat{\tilde{h}}_{ij}$. The conjugate momentum is given by

$$\hat{\tilde{\pi}}^r_{\mathbf{k}}(\eta) = (\hat{\tilde{h}}^r_{-\mathbf{k}}(\eta))', \tag{4.12}$$

which is assumed to be satisfied the equal-time commutation relations,

$$[\hat{\tilde{h}}^r_{\mathbf{k}}(\eta), \hat{\tilde{\pi}}^s_{\mathbf{k}'}(\eta)] = i\delta^{rs}\delta^{(3)}(\mathbf{k}-\mathbf{k}') \tag{4.13}$$

$$[\hat{\tilde{h}}^r_{\mathbf{k}}(\eta), \hat{\tilde{h}}^s_{\mathbf{k}'}(\eta)] = [\hat{\tilde{\pi}}^r_{\mathbf{k}}(\eta), \hat{\tilde{\pi}}^s_{\mathbf{k}'}(\eta)] = 0. \tag{4.14}$$

Since $\hat{\tilde{h}}^r_{\mathbf{k}}$ is Hermitian, we can express it in terms of the c-number mode functions $\tilde{h}_k(\eta)$;

$$\hat{\tilde{h}}^r_{\mathbf{k}}(\eta) = \tilde{h}_k(\eta)\hat{a}^r_{\mathbf{k}} + \tilde{h}^*_k(\eta)\hat{a}^{r\dagger}_{-\mathbf{k}} \tag{4.15}$$

where $\hat{a}^r_{\mathbf{k}}$ and $\hat{a}^{r\dagger}_{\mathbf{k}}$ are creation and annihilation operator respectively satisfying the commutation relations

$$[\hat{a}^r_{\mathbf{k}}, \hat{a}^{s\dagger}_{\mathbf{k}'}] = \delta^{rs}\delta^{(3)}(\mathbf{k}-\mathbf{k}'), \tag{4.16}$$

$$[\hat{a}^r_{\mathbf{k}}, \hat{a}^s_{\mathbf{k}'}] = [\hat{a}^{r\dagger}_{\mathbf{k}}, \hat{a}^{s\dagger}_{\mathbf{k}'}] = 0. \tag{4.17}$$

The equation of motion for the mode function is derived as

$$\tilde{h}_k'' + \left(k^2 - \frac{2}{\eta^2}\right)\tilde{h}_k = 0. \tag{4.18}$$

Imposing the initial condition as

$$\lim_{\eta\to-\infty} \tilde{h}_k = \frac{e^{-ik\eta}}{\sqrt{2k}}, \tag{4.19}$$

and the subhorizon ($|k\eta| \gg 1$) solution is given by

$$\tilde{h}_k(\eta) = \frac{e^{-ik\eta}}{\sqrt{2k}}\left(1 - \frac{i}{k\eta}\right) \tag{4.20}$$

To compute the power spectrum, we consider the following vacuum expectation value,

$$\langle 0|\hat{\tilde{h}}_{\mathbf{k}}\hat{\tilde{h}}_{\mathbf{k}'}|0\rangle = \frac{1}{2k}\left(1 + \frac{1}{k^2\eta^2}\right) \tag{4.21}$$

and connecting it with the definition of the power spectrum (4.5), we obtain

$$\mathcal{P}_h^+ = \mathcal{P}_h^\times = \frac{4}{M_P^2}\left(\frac{H_{\rm inf}}{2\pi}\right)_*^2 \tag{4.22}$$

where $*$ denote the value at the horizon exit.

Adding the contributions from two polarization modes, the power spectrum of total tensor metric perturbation is given by

$$\mathcal{P}_t = \mathcal{P}_h^+(k) + \mathcal{P}_h^\times(k) = \frac{2}{\pi^2}\frac{H_{\rm inf}^2}{M_P^2}, \tag{4.23}$$

and the tensor-to-scalar ratio is

$$r = \frac{\mathcal{P}_t(k)}{\mathcal{P}_\zeta(k)} = \frac{2}{\pi^2}\frac{H_{\rm inf}^2}{M_P^2}\frac{1}{\mathcal{P}_\zeta} = 16\epsilon. \tag{4.24}$$

Rewriting this as

$$H_{\rm inf} \simeq 3.4\times10^{-5} M_P\left(\frac{r}{0.1}\right)^{1/2}\left(\frac{\mathcal{P}_\zeta}{2.4\times10^{-9}}\right)^{1/2}, \tag{4.25}$$

we obtain the upper bound on the Hubble parameter during inflation as $H_{\rm inf} \lesssim 3\times10^{-5}M_P$ from the observational constraint on the tensor-to-scalar ratio, $r \lesssim 0.1$.

4.1.3 The energy spectrum of gravitational waves

Next, we derive the energy density and energy spectrum of GW. The energy momentum tensor is given by

$$T_{\mu\nu} = -2\frac{\delta\mathcal{L}}{\delta\bar{g}^{\mu\nu}} + \bar{g}_{\mu\nu}\mathcal{L} \tag{4.26}$$

where $\mathcal{L}$ is the Lagrangian density. Substituting the Lagrangian density of the tensor metric perturbation, we obtain the energy density of the GW which is defined as the $(0,0)$ component of the energy momentum tensor,

$$\rho_{\rm GW} = -T^0_0 = \frac{1}{64\pi G a^2}\left[(h'_{ij})^2 + (\nabla h_{ij})^2\right] \tag{4.27}$$

which has vacuum expectation value,

$$\langle 0|\rho_{\rm GW}|0\rangle = \int_0^\infty \frac{k^3}{2\pi^2}\frac{|h'_k(\eta)|^2 + k^2|h_k(\eta)|^2}{a^2(\eta)}\frac{dk}{k}. \tag{4.28}$$

In order to discuss the amount of the present gravitational wave background at the present, it is useful to introduce a density parameter of gravitational waves within the logarithmic interval of wavenumber which is given by

$$\Omega_{\rm GW}(k,\eta) = \frac{1}{\rho_{\rm cr}(\eta)}\frac{d\langle 0|\rho_{\rm GW}|0\rangle}{d\ln k}, \tag{4.29}$$

where $\rho_{\rm cr}$ is the critical density and it leads to

$$\Omega_{\rm GW}(k,\eta) = \frac{8\pi G}{3H^2(\eta)}\frac{k^3}{2\pi^2}\frac{|h'_k(\eta)|^2 + k^2|h_k(\eta)|^2}{a^2(\eta)}. \tag{4.30}$$

Taking into account both $+$-mode and $\times$-mode, this is related to the power spectrum of the tensor mode as

$$\Omega_{\rm GW}(k,\eta) = \frac{k^2}{6\mathcal{H}^2}\mathcal{P}_h(k,\eta). \tag{4.31}$$

In particular, focusing only on those gravitational waves generated before the matter radiation equality, $\Omega_{\rm GW}$ today is calculated via

$$\Omega_{\rm GW}(k) = \frac{k^2\Omega_\gamma}{6\mathcal{H}^2(\eta_\star)}\mathcal{P}_h(k,\eta_\star), \tag{4.32}$$

where $\Omega_\gamma \simeq 4.8\times10^{-5}$ is the density parameter of radiation today, and a subscript $\star$ denotes a certain time after the amplitude of the gravitational wave, $|h_{\mathbf{k}}|$, starts monotonically to decrease as $1/a$ on sub-horizon scales during radiation dominated era.

4.2 Scalar-induced gravitational waves

4.2.1 Power spectrum of the gravitational waves with a source term

Here, we formulate the gravitational waves induced by the scalar metric perturbations and anisotropic stress at second order. The time evolution for the metric perturbations is described by the Einstein equation and that for h_{ij} is given by

$$h''_{ij} + 2\mathcal{H}h'_{ij} - \nabla^2 h_{ij} = -4\hat{\mathcal{T}}_{ij}{}^{lm}\mathcal{S}_{lm}, \tag{4.33}$$

where $\hat{\mathcal{T}}_{ij}{}^{lm}$ is the projection tensor which projects any tensor into the transverse trace-free one and $\mathcal{S}_{ij}$ is the scalar induced source term which is given later. Using the polarization tensors, (4.16) and (4.17), the projection tensor $\hat{\mathcal{T}}_{ij}{}^{lm}$ is defined via

$$\hat{\mathcal{T}}_{ij}{}^{lm}\mathcal{S}_{lm} = \int \frac{d^3k}{(2\pi)^{3/2}}e^{i\mathbf{kx}}\left[e^+_{ij}(\mathbf{k})e^{+lm}(\mathbf{k}) + e^\times_{ij}(\mathbf{k})e^{\times lm}(\mathbf{k})\right]\mathcal{S}_{lm}(\mathbf{k},\eta) \tag{4.34}$$

where $\mathcal{S}_{ij}(\mathbf{k},\eta)$ is the Fourier transformed component of $\mathcal{S}_{ij}(\mathbf{x},\eta)$. Thus the evolution equation for the Fourier transformed component of h_{ij} is derived as

$$h_{\mathbf{k}}'' + 2\mathcal{H}h_{\mathbf{k}}' + k^2 h_{\mathbf{k}} = \mathcal{S}(\mathbf{k},\eta), \tag{4.35}$$

where $\mathcal{S}(\mathbf{k},\eta) = -4e^{lm}\mathcal{S}_{lm}(\mathbf{k},\eta)$. Note that, here and hereafter, we omit the polarization indices $+$ or $\times$ on $h_{\mathbf{k}}$ and $\mathcal{S}(\mathbf{k},\eta)$. Now we solve Eq. (4.35) by using the Green's function method. The solution is found to be

$$h_{\mathbf{k}}(\eta) = \frac{1}{a(\eta)}\int_{\eta_0}^{\eta} d\tilde{\eta} a(\tilde{\eta}) g_{\mathbf{k}}(\eta;\tilde{\eta})\mathcal{S}(\mathbf{k},\tilde{\eta}), \tag{4.36}$$

where $g_{\mathbf{k}}(\eta,\tilde{\eta})$ is the Green's function which is defined through

$$g_{\mathbf{k}}''(\eta;\tilde{\eta}) + \left(k^2 - \frac{a''(\eta)}{a(\eta)}\right) g_{\mathbf{k}}(\eta;\tilde{\eta}) = \delta(\eta-\tilde{\eta}). \tag{4.37}$$

In particular, the Green's function is given by

$$g_{\mathbf{k}}(\eta;\tilde{\eta}) = \frac{\sin[k(\eta-\tilde{\eta})]}{k}\theta(\eta-\tilde{\eta}) \tag{4.38}$$

in radiation dominated era and

$$g_{\mathbf{k}}(\eta;\tilde{\eta}) = \frac{(k^2\eta\tilde{\eta}+1)\sin[k(\eta-\tilde{\eta})] - k(\eta-\tilde{\eta})\cos[k(\eta-\tilde{\eta})]}{k^3\eta\tilde{\eta}}\theta(\eta-\tilde{\eta}) \tag{4.39}$$

in matter dominated era. Then, the power spectrum is formally calculated through

$$\begin{aligned}\langle h_{\mathbf{k}}(\eta)h_{\mathbf{p}}(\eta)\rangle &= \frac{1}{a(\eta)^2}\int_{\eta_0}^{\eta} d\tilde{\eta}_1 a(\tilde{\eta}_1) g_{\mathbf{k}}(\eta;\tilde{\eta}_1)\int_{\eta_0}^{\eta} d\tilde{\eta}_2 a(\tilde{\eta}_2) g_{\mathbf{p}}(\eta;\tilde{\eta}_2)\langle \mathcal{S}(\mathbf{k},\tilde{\eta}_1)\mathcal{S}(\mathbf{p},\tilde{\eta}_2)\rangle \\ &\equiv \frac{2\pi^2}{k^3}\delta^3(\mathbf{k}+\mathbf{p})\mathcal{P}_h(k,\eta).\end{aligned} \tag{4.40}$$

In the following, we calculate the power spectrum with two kind of source terms; scalar metric perturbations and anisotropic stresses, and then, we will apply these formalism to the curvaton models and discuss the detectability by the future gravitational wave detectors.

4.2.2 Source terms for gravitational waves

In the first order perturbation theory, the right hand side of (4.33), $\mathcal{S}_{ij}$, is zero when the anisotropic stress does not appear in that order. However, once the second order contributions are included, it induces non-zero $\mathcal{S}_{ij}$. In the curvaton scenario considered here, we have two contributions to the source term at the second order; one is coming from the scalar adiabatic curvature perturbations and another is the anisotropic stress due to the kinetic term of the curvaton before the curvaton decay. In this subsection, we discuss these two sources separately.

Second order adiabatic curvature perturbations

Following the literature, let us consider the scalar metric perturbations in conformal-Newtonian gauge which is described as

$$ds^2 = a^2(\eta)\Big[-(1+2\Phi)d\eta^2 + (1-2\Psi)\delta_{ij}dx^i dx^j\Big]. \tag{4.41}$$

At the second order, the source term induced from the above scalar metric perturbations can be written as [97] (see also appendix D)

$$\mathcal{S}^{\Phi}_{ij} = -2\partial_i\Phi\partial_j\Phi - \mathcal{H}^{-2}\partial_i(\Phi' + \mathcal{H}\Phi)\partial_j(\Phi' + \mathcal{H}\Phi), \tag{4.42}$$

where we have assumed that the first order anisotropic stress is zero and it leads to $\Phi = \Psi$. Then, $\mathcal{S}^{\Phi}(\mathbf{k})$, which appears in the right hand side of the evolution equation for the Fourier transformed component of h_{ij}, is calculated through the convolution of two Fourier modes as

$$\begin{aligned}\mathcal{S}^{\Phi}(\mathbf{k},\eta) &= -4e^{lm}(\mathbf{k})\mathcal{S}^{\Phi}_{lm}(\mathbf{k},\eta)\\ &= 4\int\frac{d^3\tilde{k}}{(2\pi)^{3/2}}e^{lm}(\mathbf{k})\tilde{k}_l\tilde{k}_m\Big[3\Phi_{\tilde{\mathbf{k}}}(\eta)\Phi_{\mathbf{k}-\tilde{\mathbf{k}}}(\eta)\\ &\qquad + \frac{2}{\mathcal{H}}\Phi'_{\tilde{\mathbf{k}}}(\eta)\Phi_{\mathbf{k}-\tilde{\mathbf{k}}}(\eta) + \frac{1}{\mathcal{H}^2}\Phi'_{\tilde{\mathbf{k}}}(\eta)\Phi'_{\mathbf{k}-\tilde{\mathbf{k}}}(\eta)\Big].\end{aligned} \tag{4.43}$$

Let us consider the evolution of Φ. The gravitational potential in conformal-Newtonian gauge, Φ, is related to the curvature perturbation on uniform density slicing as [98,99] (see also appendix B)

$$-\zeta = \Psi + \frac{H}{\dot{\rho}}\delta\rho = \frac{6+5r}{4+3r}\Phi + \frac{2+2r}{4+3r}\frac{\Phi'}{\mathcal{H}}, \tag{4.44}$$

where r is the ratio of the energy density of the curvaton to that of radiation defined in the previous chapter. Note that in the curvaton mechanism $\Phi' \neq 0$ before the curvaton decay even on the superhorizon scales. Denoting $\zeta = \zeta_{\rm inf} + (r(\eta)/(4+3r(\eta)))S_\sigma$ and following the above relation, we obtain the evolution equation for Φ on superhorizon scales as

$$\frac{\Phi'(\eta)}{\mathcal{H}(\eta)} + \frac{6+5r(\eta)}{2+2r(\eta)}\Phi(\eta) + \frac{4+3r(\eta)}{2+2r(\eta)}\zeta_{\rm inf} + \frac{r(\eta)}{2+2r(\eta)}S_\sigma = 0, \tag{4.45}$$

which is rewritten by adopting the e-folding number N as a time derivative as

$$\frac{d\Phi}{dN} + \frac{6+5r}{2+2r}\Phi + \frac{4+3r}{2+2r}\zeta_{\rm inf} + \frac{r}{2+2r}S_\sigma = 0. \tag{4.46}$$

Denoting $r = r_D e^N$ and choosing the initial condition $\Phi(N\to-\infty) = -2\zeta_{\rm inf}/3$ which is consistent with the standard (non-curvaton) scenario, we obtain the analytic solution for the above first order differential equation:

$$\begin{aligned}\Phi = &\left(\frac{1}{r^3} - \frac{16\sqrt{1+r}}{15r^3} + \frac{1+r}{15r^3} + \frac{7(1+r)}{15r^2} - \frac{3(1+r)}{5r}\right)\zeta_{\rm inf}\\ &+\left(-\frac{1}{r^3} + \frac{16\sqrt{1+r}}{5r^3} - \frac{11(1+r)}{5r^3} + \frac{3(1+r)}{5r^2} - \frac{1+r}{5r}\right)S_\sigma.\end{aligned} \tag{4.47}$$

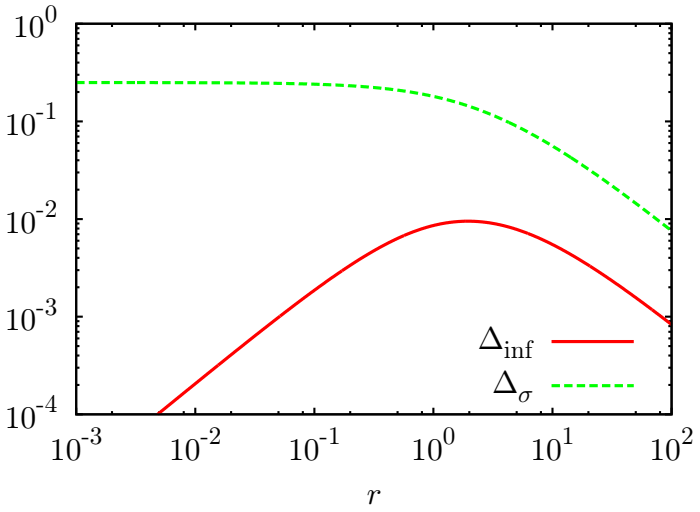

Figure 4.1: The deviation from $\Phi' = 0$ defined via (4.48) is shown. The horizontal axis shows $r(\eta)$. The solid red line and dashed green line correspond to the inflaton and the curvaton contributions respectively.

If we express the solution as

$$\Phi = -\frac{4+3r}{6+5r}\left(1+\Delta_{\rm inf}\right)\zeta_{\rm inf} - \frac{r}{6+5r}\left(1-\Delta_\sigma\right)S_\sigma, \quad \text{(superhorizon)} \tag{4.48}$$

where $\Delta_{\rm inf}$ and Δ_σ represent the deviations from $\Phi' = 0$, $\Delta_{\rm inf}$ and Δ_σ is expressed explicitly as

$$\Delta_{\rm inf} = -1 - \frac{6+5r}{4+3r}\left(\frac{1}{r^3} - \frac{16\sqrt{1+r}}{15r^3} + \frac{1+r}{15r^3} + \frac{7(1+r)}{15r^2} - \frac{3(1+r)}{5r}\right), \tag{4.49}$$

$$\Delta_\sigma = 1 + \frac{6+5r}{r}\left(-\frac{1}{r^3} + \frac{16\sqrt{1+r}}{5r^3} - \frac{11(1+r)}{5r^3} + \frac{3(1+r)}{5r^2} - \frac{1+r}{5r}\right), \tag{4.50}$$

and they are shown in Fig. 4.1. This figure shows that Φ deviates from the value with $\Phi' = 0$ at most 25%. Although the deviations are not so large, in the following numerical calculation of the scalar-induced gravitational wave background, we properly include the contribution from Φ' on super-horizon scales.

For subhorizon modes, Φ is constrained by the Poisson equation and we obtain

$$\Phi(\eta) = -\frac{3}{2}\left(\frac{\mathcal{H}(\eta)}{k}\right)^2\left(\frac{1}{1+r(\eta)}\frac{\delta\rho_r}{\rho_r} + \frac{r(\eta)}{1+r(\eta)}\frac{\delta\rho_\sigma}{\rho_\sigma}\right). \quad \text{(subhorizon)} \tag{4.51}$$

Note that Φ is frozen after the curvaton starts to dominate the universe until its decay if $r_D > 1$. Focusing only on the curvaton contribution, we unify (4.48) and (4.51), which can be expressed as

$$\Phi(\eta(<\eta_{\rm dec})) \approx \begin{cases} T_S(k,\eta)S_\sigma & \text{for} \quad \eta < \eta_{\rm dom} \\ T_S(k,\eta_{\rm dom})S_\sigma & \text{for} \quad \eta > \eta_{\rm dom}, \end{cases} \tag{4.52}$$

where $\eta_{\rm dec}$ and $\eta_{\rm dom}$ are the conformal time at the decay and at the beginning of curvaton domination respectively and we define

$$T_S(k,\eta) = -\frac{r(\eta)}{6+5r(\eta)}(1-\Delta_\sigma)S_\sigma\left[1+\frac{2(1+r(\eta))}{3(6+5r(\eta))}(1-\Delta_\sigma)(k\eta)^2\right]^{-1}. \tag{4.53}$$

The transfer function of Φ after the curvaton decay in radiation dominated era is given by a decaying-oscillation solution as [100]

$$T_\Phi(k,\eta) = \frac{3}{(k\eta/\sqrt{3})^3}\left[\sin\left(\frac{k\eta}{\sqrt{3}}\right) - \frac{k\eta}{\sqrt{3}}\cos\left(\frac{k\eta}{\sqrt{3}}\right)\right], \tag{4.54}$$

and we obtain the time evolution of Φ after the curvaton decay as

$$\Phi(k,\eta(>\eta_{\rm dec})) \approx \begin{cases} T_\Phi(k,\eta)T_S(k,\eta_{\rm dec})S_\sigma & \text{for} \quad k < 1/\eta_{\rm dec} \\ T_\Phi(1/\eta_{\rm dec},\eta)T_S(k,\eta_X)S_\sigma & \text{for} \quad k > 1/\eta_{\rm dec}, \end{cases} \tag{4.55}$$

where we define $\eta_X = \eta_{\rm dec}$ for $r_D < 1$ and $\eta_X = \eta_{\rm dom}$ otherwise.

Assuming that there exists the curvaton dominated epoch, $r_D > 1$, the resultant density parameter of gravitational waves is enhanced on scales which are inside the horizon in curvaton dominated era because Φ remains constant at that time. This leads to $h_{\mathbf{k}} \simeq$ const. on subhorizon scales [37, 43]. On the other hand, gravitational waves emitted before the curvaton domination, the energy density of gravitational waves suffers an additional suppression because of $\rho_{\rm GW}/\rho_\sigma \propto a^{-1}$. Thus, the present energy density spectrum of gravitational waves (4.32) is expressed as

$$\Omega_{\rm GW}(k) = \frac{k^2\Omega_\gamma}{6\mathcal{H}^2(\eta_k)}F^2\mathcal{P}_h(k,\eta_k), \tag{4.56}$$

where η_k denotes the conformal time when mode k reentering reenter the horizon and F^2 denotes the enhancement and suppression due to the early matter (curvaton) domination, which is given by

$$F^2 \approx \begin{cases} (k\eta_{\rm dec})^2 & \text{for} \quad 1/\eta_{\rm dec} < k < 1/\eta_{\rm dom}, \\ (k\eta_{\rm dom})^{-4}(\eta_{\rm dec}/\eta_{\rm dom})^2 + (\eta_{\rm dom}/\eta_{\rm dec})^2 & \text{for} \quad 1/\eta_{\rm dom} < k \\ 1 & \text{otherwise.} \end{cases} \tag{4.57}$$

Here we assume the density perturbation on subhorizon scales, which grows proportional to the scale factor in matter dominated universe, does not reach $\mathcal{O}(1)$. Otherwise, the enhancement ends at the cut off scale $k_{\rm NL} \sim \mathcal{P}_{\zeta,\rm curv}^{-1/4}(1/\eta_{\rm dec})/\eta_{\rm dec}$ corresponding to the scale which becomes nonlinear at the curvaton decay and $1/\eta_{\rm dom}$ in (4.57) must be replaced with $k_{\rm NL}$.

Anisotropic stress sourced from the kinetic term of the curvaton

Next, in the curvaton scenario, there is another source induced from the kinetic term of the curvaton as

$$\mathcal{S}_{ij}^{\rm kin} = M_P^{-2}\partial_i\delta\sigma\partial_j\delta\sigma, \tag{4.58}$$

and the source term of the evolution equation for $h_{\rm k}$ is given by

$$\begin{aligned}\mathcal{S}^{\rm kin}(\mathbf{k},\eta) &= -4e^{lm}(\mathbf{k})\mathcal{S}^{\rm kin}_{lm}(\mathbf{k},\eta)\\ &= -4M_P^{-2}\int\frac{d^3\tilde{k}}{(2\pi)^{3/2}}e^{lm}(\mathbf{k})\tilde{k}_l\tilde{k}_m\delta\sigma_{\tilde{\mathbf{k}}}(\eta)\delta\sigma_{\mathbf{k}-\tilde{\mathbf{k}}}(\eta).\end{aligned} \tag{4.59}$$

By decomposing $\delta\sigma$ into the transfer function and the initial value evaluated on super-horizon scales at a certain time before the curvaton starts to oscillate as

$$\delta\sigma_{\mathbf{k}}(\eta) = T_\sigma(k,\eta)\delta\sigma_{\mathbf{k}}, \tag{4.60}$$

the transfer function, $T_\sigma(k,\eta)$, is derived from the evolution equation for $\delta\sigma$ for each Fourier mode,

$$\ddot{\delta\sigma}_{\mathbf{k}} + 3H\dot{\delta\sigma} + \left(m_\sigma^2 + \frac{k^2}{a^2}\right)\delta\sigma_{\mathbf{k}} = 0. \tag{4.61}$$

For $H > m_\sigma, k/a$, $\delta\sigma_{\mathbf{k}}$ remains unchanged because of the Hubble overdamping and otherwise, the behavior of the solution is found to be

$$\delta\sigma_{\mathbf{k}} \propto \begin{cases} a^{-1} & \text{for} \quad k/a > m_\sigma, H, \\ a^{-3/2} & \text{for} \quad m_\sigma > k/a, H. \end{cases} \tag{4.62}$$

Taking into account it, we can derive the transfer function for $\delta\sigma$ which is summarized below.

- For Fourier modes reentering the horizon after the curvaton starts to oscillate at $\eta_{\rm osc}$, $\delta\sigma$ remains frozen for $\eta < \eta_{\rm osc}$ on super-horizon scales and evolves like $a^{-3/2}$ for $\eta > \eta_{\rm osc}$ both on super-horizon and sub-horizon scales. Hence we obtain the transfer function for $k\eta_{\rm osc} < 1$ as

$$T_\sigma\left(k(<1/\eta_{\rm osc}),\eta\right) = \begin{cases} 1 & \text{for} \quad \eta < \eta_{\rm osc} \\ \left(\frac{\eta_{\rm osc}}{\eta}\right)^{3/2} & \text{for} \quad \eta > \eta_{\rm osc}. \end{cases} \tag{4.63}$$

- Oppositely, for modes reentering the horizon before the curvaton oscillation, $\delta\sigma$ remains constant for $\eta < 1/k$, evolves like $\propto a^{-1}$ for $1/k < \eta < \eta_m$ and $\propto a^{-3/2}$ for $\eta > \eta_m$, where η_m is defined via $k/a(\eta_m) = m_\sigma$ and given by $\eta_m = k\eta_{\rm osc}^2$ [41]. Thus we obtain the transfer function for $k\eta_{\rm osc} > 1$ as

$$T_\sigma\left(k(>1/\eta_{\rm osc}),\eta\right) = \begin{cases} 1 & \text{for} \quad \eta < 1/k \\ \frac{1}{k\eta} & \text{for} \quad 1/k < \eta < \eta_m \\ \frac{1}{k\eta_m}\left(\frac{\eta_m}{\eta}\right)^{3/2} & \text{for} \quad \eta > \eta_m. \end{cases} \tag{4.64}$$

Power spectrum

Substituting the superhorizon evolution for Φ, given by (4.48), and the transfer function, given by (4.54), (4.63) and (4.64), into (4.43) and (4.59), we obtain the following expression for the contribution from curvaton:

$$\mathcal{S}^i(\mathbf{k},\eta) = \int\frac{d^3k}{(2\pi)^{3/2}}e(\mathbf{k},\tilde{\mathbf{k}})f_i(\mathbf{k},\tilde{\mathbf{k}},\eta)S_\sigma(\tilde{\mathbf{k}})S_\sigma(\mathbf{k}-\tilde{\mathbf{k}}) \quad \text{with} \quad i = \Phi,\ \text{kin}, \tag{4.65}$$

where we define

$$e(\mathbf{k},\tilde{\mathbf{k}}) = e^{lm}(\mathbf{k})\tilde{k}_l\tilde{k}_m = \sqrt{2}\tilde{k}^2\sin^2\theta \tag{4.66}$$

and

$$\begin{aligned} f_\Phi(\mathbf{k},\tilde{\mathbf{k}},\eta) = 4\left(\frac{r(1-\Delta_\sigma)}{6+5r}\right)^2\Bigg[&\left(3+\frac{2\Delta_\sigma}{(1-\Delta_\sigma)^2}\left(\frac{6+5r}{2+2r}\right)\right.\\ &\left.+\left(\frac{6+5r}{2+2r}\right)^2\left(\frac{\Delta_\sigma}{1-\Delta_\sigma}\right)^2\right)T_\Phi(\tilde{k},\eta)T_\Phi(|\mathbf{k}-\tilde{\mathbf{k}}|,\eta)\\ &+\frac{2}{\mathcal{H}}\left(1+\frac{\Delta_\sigma}{1-\Delta_\sigma}\left(\frac{6+5r}{2+2r}\right)\right)T'_\Phi(\tilde{k},\eta)T_\Phi(|\mathbf{k}-\tilde{\mathbf{k}}|,\eta)\\ &+\frac{1}{\mathcal{H}^2}T'_\Phi(\tilde{k},\eta)T'_\Phi(|\mathbf{k}-\tilde{\mathbf{k}}|,\eta)\Bigg], \end{aligned} \tag{4.67}$$

$$f_{\rm kin}(\mathbf{k},\tilde{\mathbf{k}},\eta) = -\left(\frac{\sigma_{\rm osc}}{M_P}\right)^2 T_{\delta\sigma}(\tilde{k},\eta)T_{\delta\sigma}(|\mathbf{k}-\tilde{\mathbf{k}}|,\eta)\theta(1-k_{\rm dec}\eta). \tag{4.68}$$

Then, substituting these source terms into (4.40), and assuming that the primordial isocurvature perturbation, $S_\sigma(\mathbf{k})$, obeys the Gaussian statisctics, we obtain

$$\begin{aligned} \langle h_{\mathbf{k}}(\eta)h_{\mathbf{p}}(\eta)\rangle = &\frac{2\pi^2}{k^3}\delta^3(\mathbf{k}+\mathbf{p})\int_0^\infty dy\int_{|1-y|}^{1+y}dx\\ &\times\frac{2y^2}{x^2}\left(1-\frac{(1+y^2-x^2)^2}{4y^2}\right)^2\mathcal{P}_{S,\rm curv}(kx)\mathcal{P}_{S,\rm curv}(ky)\\ &\times\left[\frac{k^2}{a(\eta)}\int_{\eta_0}^{\eta}d\tilde{\eta}a(\tilde{\eta})g_{\mathbf{k}}(\eta;\tilde{\eta})f_i(kx,ky,\tilde{\eta})\right]^2, \end{aligned} \tag{4.69}$$

where we define $x = |\mathbf{k}-\tilde{\mathbf{k}}|/k$ and $y = \tilde{k}/k$. This leads the power spectrum of gravitational waves through (4.40). We calculate this integral numerically to yield the resultant spectrum.

4.3 Results

Based on the above formulation, let us evaluate the amount of the gravitational waves induced from the scalar fluctuations in the curvaton scenario [101].

4.3.1 Contribution from $\mathcal{S}_{ij}^\Phi$

Let us consider the contribution from $\mathcal{S}_{ij}^\Phi$ given by Eq. (4.42). This has been well investigated in the literature and the resultant density parameter for gravitational waves can be approximated as [33, 34]

$$\Omega_{\rm GW} \sim 10^{-19}\left(\frac{\mathcal{P}_{\zeta,\rm curv}(k)}{\mathcal{P}_\zeta(k_c)}\right)^2, \tag{4.70}$$

which is also confirmed by our full numerical integration. This result is quite reasonable since the gravitational waves are sourced by the quadratic of the curvature perturbation.

In the curvaton model with blue spectrum, $\Omega_{\rm GW}$ has a peak at the wave number $k_{\rm dec}$ given by

$$k_{\rm dec} \simeq 1.7 \times 10^{15}\ {\rm Mpc}^{-1} \left(\frac{\Gamma_\sigma}{1\ {\rm GeV}} \right)^{1/2}, \tag{4.71}$$

for $r_D < 1$ because the power spectrum of curvature perturbations from the curvaton is suppressed proportional to $r = \rho_\sigma/\rho_r \propto a$ before the curvaton decay. For $r_D > 1$, the peak wave number is either $k_{\rm dom} = 1/\eta_{\rm dom}$ or $k_{\rm NL}$ given by

$$k_{\rm peak} = \min(k_{\rm dom}, k_{\rm NL}) \sim \min(r_D^{1/2} k_{\rm dec}, \mathcal{P}_{\zeta,{\rm curv}}(k_{\rm dec})^{-1/4} k_{\rm dec}). \tag{4.72}$$

Taking into account the above, we show the resultant spectrum of the gravitational waves in the quadratic curvaton model and the axion-like curvaton model below.

Quadratic curvaton model

First, we consider the induced gravitational waves in the quadratic curvaton model. Here we assume $m_\sigma \simeq \Gamma_\phi$ which means that the reheating occurs soon after inflation, because this gives the maximal amount of gravitational waves once we fix r_D, $H_{\rm inf}$ and n_σ. We show the peak value of $\Omega_{\rm GW}$ written as $\Omega_{\rm GW}(k_{\rm peak})$ in terms of the spectral index n_σ in Fig. 4.2 and the wave number at the peak $k_{\rm peak}$ or corresponding frequency in Fig. 4.3. In these figures, we have used the approximation (4.70) and taken $H_{\rm inf} = 3 \times 10^{-5} M_P$ (red solid), $10^{-5} M_P$ (dashed green) and $10^{-6} M_P$ (dotted blue), $r_D = 1$ (thick lines) and $r_D = 0.1$ (thin lines) in the top panels and $H_{\rm inf} = 3 \times 10^{-5} M_P$, $r_D = 10$ (solid red), $r_D = 100$ (dashed green) and $r_D = 1000$ (dotted blue) in the bottom panels. Upper limit of these lines correspond to the breakdown of $\sigma > H_{\rm inf}/2\pi$. We have found that the maximal amount of gravitational waves is about $\Omega_{\rm GW} \sim 10^{-10}$ for $r_D < 1$ and $\Omega_{\rm GW} \sim 10^{-8}$ for $r_D > 1$ with a peak frequency $\sim 10^{-4}$ Hz. Note that the decay rate of the curvaton is proportional to r_D^{-2} from (2.12), so the decay of the curvaton is delayed for large r_D, which implies the smaller $k_{\rm NL}$ and the amount of gravitational waves decreases. We have found that $r_D \sim 100$ maximizes the amount of gravitational waves in this model. Fig. 4.4 shows the numerical resultant power spectrum of $\Omega_{\rm GW}$ (solid thick red). In this figure, we have taken $H_{\rm inf} = 3 \times 10^{-5} M_P$, $n_\sigma = 1.3$, $r_D = 1$ (top panel) and $r_D = 10$ (bottom panel). The thin line corresponds to the contribution from the primordial tensor metric perturbations and sensitivity curves[1] of LISA (dashed green), DECIGO/BBO (dotted blue), ultimate-DECIGO (small dotted magenta) and the pulsar timing observation by SKA (dash dotted cyan) are also shown. The region above the dash double-dotted orange line is already ruled out by pulsar timing observations. We have found that the amount of induced gravitational waves can overcome that of the primordial ones. Note that the shape of the spectrum varies depending on whether the universe experience the curvaton dominated epoch or not, so we can distinguish the model with $r_D < 1$ and that with $r_D > 1$.

Axion-like curvaton model

Next we discuss the axion-like curvaton model. Fig. 4.5 and Fig. 4.6 show the peak of $\Omega_{\rm GW}$ in terms of n_σ and $k_{\rm dec}$ respectively. We have used the approximated formula (4.70) and

[1] We have used the online sensitivity curve generator. http://www.srl.caltech.edu/~shane/sensitivity/

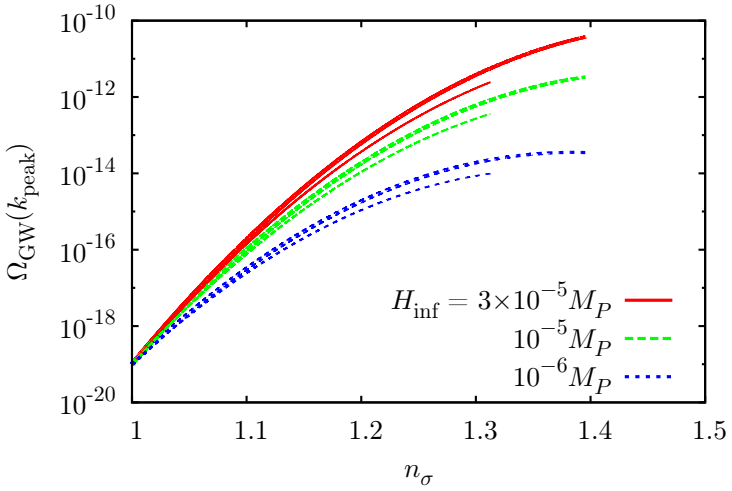

(a)

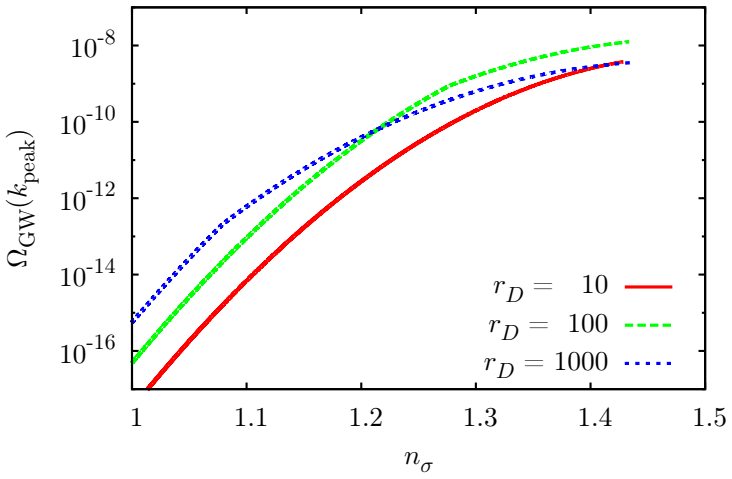

(b)

Figure 4.2: The peak values of $\Omega_{\rm GW}$ in quadratic curvaton model are shown. The horizontal axises is the spectral index n_σ. We have taken $H_{\rm inf} = 3 \times 10^{-5} M_P$ (solid red), $10^{-5} M_P$ (dashed green) and $10^{-6} M_P$ (dotted blue), $r_D = 1$ (thick lines) and $r_D = 0.1$ (thin lines) in the top panel and $H_{\rm inf} = 3 \times 10^{-5} M_P$, $r_D = 10$ (solid red), $r_D = 100$ (dashed green) and $r_D = 1000$ (dotted blue) in the bottom panel.

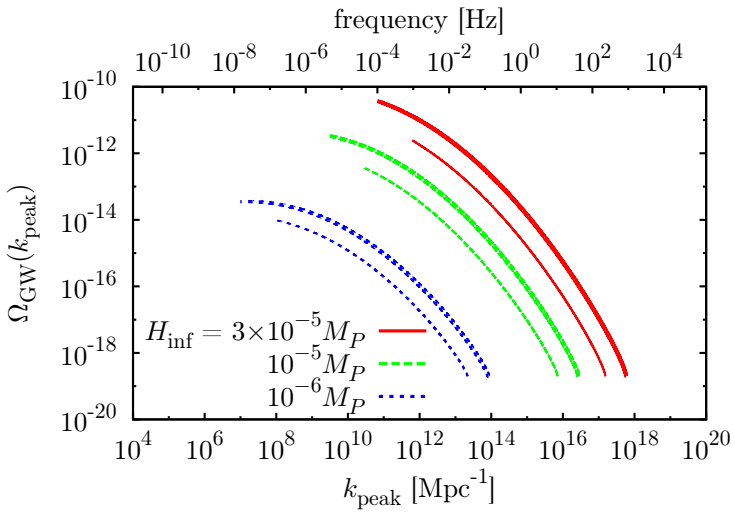

(a)

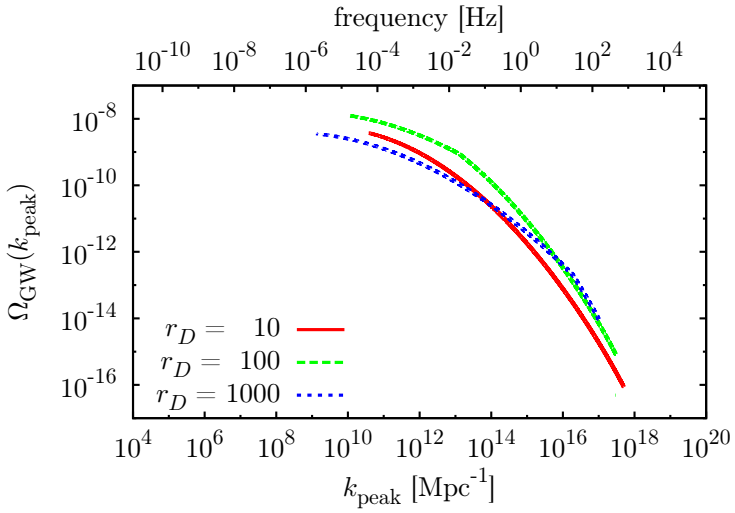

(b)

Figure 4.3: The peak values of $\Omega_{\rm GW}$ in quadratic curvaton model are shown. The horizontal axises is the wave number at peak $k_{\rm peak}$ or corresponding frequency. We have taken $H_{\rm inf} = 3 \times 10^{-5} M_P$ (solid red), $10^{-5} M_P$ (dashed green) and $10^{-6} M_P$ (dotted blue), $r_D = 1$ (thick lines) and $r_D = 0.1$ (thin lines) in the top panel and $H_{\rm inf} = 3 \times 10^{-5} M_P$, $r_D = 10$ (solid red), $r_D = 100$ (dashed green) and $r_D = 1000$ (dotted blue) in the bottom panel.

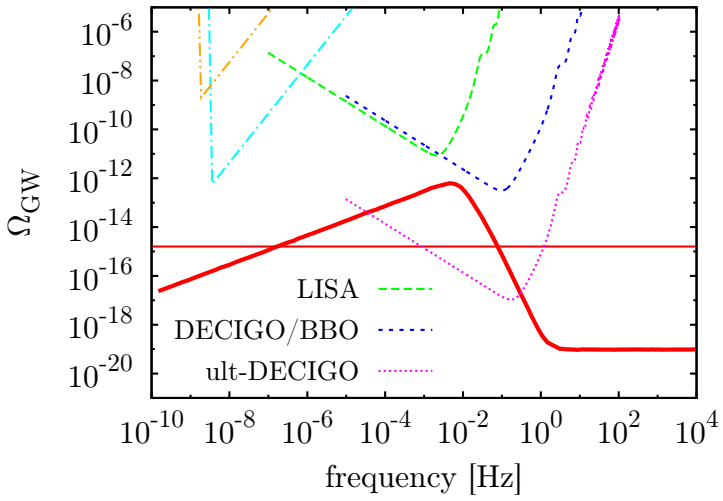

(a)

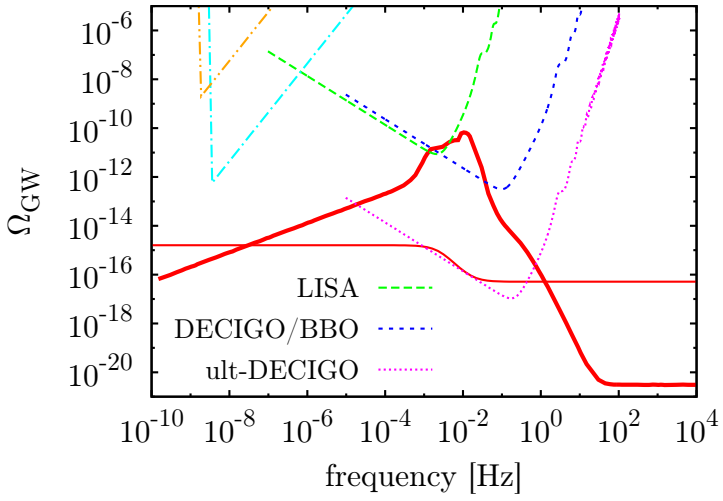

(b)

Figure 4.4: The spectrum of $\Omega_{\rm GW}$ in the quadratic curvaton model is shown as the thick solid red line. We have taken $H_{\rm inf} = 3 \times 10^{-5} M_P$, $n_\sigma = 1.3$, $r_D = 1$ (top panel) and $r_D = 10$ (bottom panel). The thin solid red line represents the contribution from the primordial tensor metric perturbation. We also show the sensitivity curves of LISA (dashed green), DECIGO/BBO (dotted blue), ultimate-DECIGO (small dotted magenta) and the pulsar timing observation by SKA (dash dotted cyan). The dash double-dotted orange line correspond to the current upper limit from the pulsar timing.

taken $k_f = 10^{10}$ (10^7) Mpc^{-1} in the top (bottom) panel and the same value of $H_{\rm inf}$ for each line as in the quadratic case. The dash dotted cyan lines corresponds to the upper bound from the PBH overproduction. Note that the large number of PBHs can be formed for $k_f = 10^7$ Mpc^{-1}, which may explain the observed dark matter [90]. Since we have fixed r_D, $H_{\rm inf}$ and k_f as well as k_c and $\mathcal{P}_{\zeta,\rm curv}(k_c)$ on each line in Fig. 4.5 and Fig. 4.6, we can see that $k_{\rm dec}$ decreases as n_σ increases from Eqs. (2.12), (2.38), (2.45) and (4.71). Thus, the maximum of each line corresponds to $k_{\rm dec} = k_f$ because $\mathcal{P}_{\zeta,\rm curv}(k_{\rm dec}) = \mathcal{P}_{\zeta,\rm curv}(k_c)(k_f/k_c)^{n_\sigma - 1}$ for $k_{\rm dec} > k_f$ and $\mathcal{P}_{\zeta,\rm curv}(k_{\rm dec}) = \mathcal{P}_{\zeta,\rm curv}(k_c)(k_{\rm dec}/k_c)^{n_\sigma - 1}$ for $k_{\rm dec} < k_f$. In addition, Fig. 4.6 shows the maximal amount of gravitational waves increases for small κ. It is because the decay rate of the curvaton is inversely proportional to κ as we can see by fixing r_D, $H_{\rm inf}$, k_f and n_σ.

Fig. 4.7 shows the resultant spectrum of gravitational waves. In this figure, we have taken $H_{\rm inf} = 3\times 10^{-5} M_P$, $n_\sigma = 1.5$ (1.8), $\kappa = 10^{-4}$ (1), $r_D = 1$ and $k_f = 10^{10}$ Mpc^{-1} in the top (bottom) panel. Model parameters are derived to be $f \simeq 2\times 10^{14}$ GeV (4×10^{13} GeV) and $m_\sigma \simeq 3\times 10^{10}$ GeV (9×10^{3} GeV) in the top (bottom) panel. From this result, we can find that the induced gravitational waves in an axion-like curvaton model can be detectable by the future observations such as LISA, DECIGO/BBO or SKA. In addition, the spectrum has a plateau near the peak, which can be a characteristic signature of the axion-like curvaton model. Note also that an enhancement due to the curvaton domination can occur in this model if $r_D > 1$ is chosen and the spectrum is raised similar to Fig. 4.4(b).

4.3.2 Contribution from $\mathcal{S}_{ij}^{\rm kin}$

Next, we focus on the contribution from $\mathcal{S}_{ij}^{\rm kin}$ given by Eq. (4.58). According to [41], the maximal amount of gravitational waves is estimated as

$$\Omega_{\rm GW} \sim 10^{-19} \frac{\Gamma_\sigma}{r_D^2 m_\sigma} \left(\frac{\mathcal{P}_\zeta}{2\times 10^{-9}} \right)^2 . \tag{4.73}$$

Although in [41] the authors have considered a curvaton scenario where the adiabatic curvature perturbation is generated only from the fluctuation of the curvaton and assumed the almost scale-invariant power spectrum of the curvature perturbations, by performing the numerical calculation we confirm that this estimation is also valid in the blue-tilted curvaton scenario. As mentioned in Ref. [41], the above expression indicates that it could be possible to generate the detectable amplitude of the gravitational waves in the curvaton scenario by tuning model parameters (e.g., r_D and Γ_σ/m_σ) properly. However, we show that this contribution is negligible once we take into account the upper bound on the Hubble parameter during inflation. Defining $X = \min(m_\sigma, \Gamma_\phi)$, from (2.12) and (2.13), we get

$$\frac{\Gamma_\sigma}{r_D^2 m_\sigma} = \frac{1}{36 r_D^4} \left(\frac{\sigma_{\rm osc}}{M_P} \right)^4 \left(\frac{X}{m_\sigma} \right) \tag{4.74}$$

which indicates that we need $\sigma_{\rm osc} \gtrsim r M_P$ to enhance the amount of gravitational waves. Substituting (2.20) and (4.74) into (4.73), we obtain

$$\Omega_{\rm GW} \sim 10^{-25} \left(\frac{4}{4+3r_D} \right)^4 \left(\frac{\sigma_{\rm osc}}{\sigma(k)} \right)^4 \left(\frac{X}{m_\sigma} \right) \left(\frac{H_{\rm inf}}{10^{14}\ {\rm GeV}} \right)^4 , \tag{4.75}$$

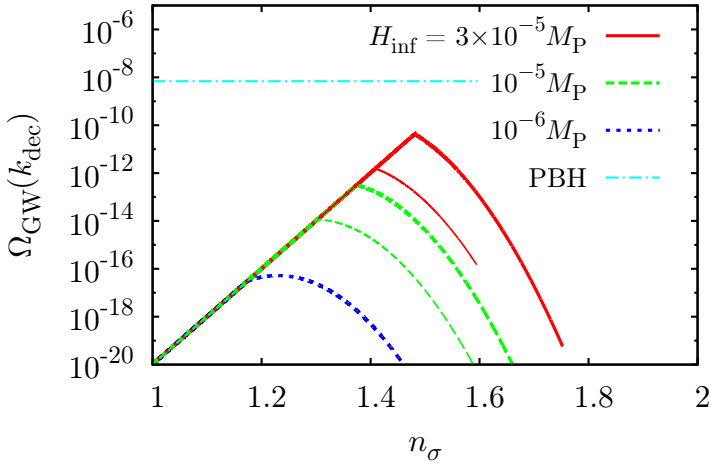

(a)

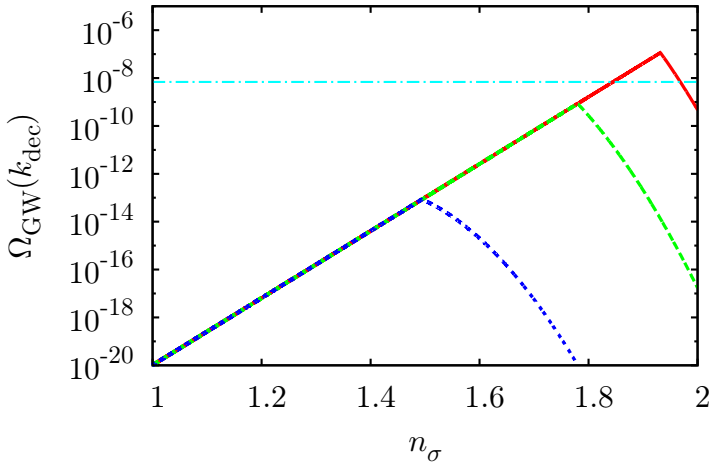

(b)

Figure 4.5: The peak values of $\Omega_{\rm GW}$ in terms of the spectral index n_σ in axion-like curvaton model are shown. We have taken $k_f = 10^{10}$ (10^7) Mpc^{-1} for top (bottom) panel, $\kappa = 1$, $H_{\rm inf} = 3 \times 10^{-5}\ M_P$ (solid red), $10^{-5}\ M_P$ (dashed green) and $10^{-6}\ M_P$ (dotted blue), $r_D = 1$ (thick lines) and $r_D = 0.1$ (thin lines). The dash dotted cyan line shows the upper bound from the PBH overproduction.

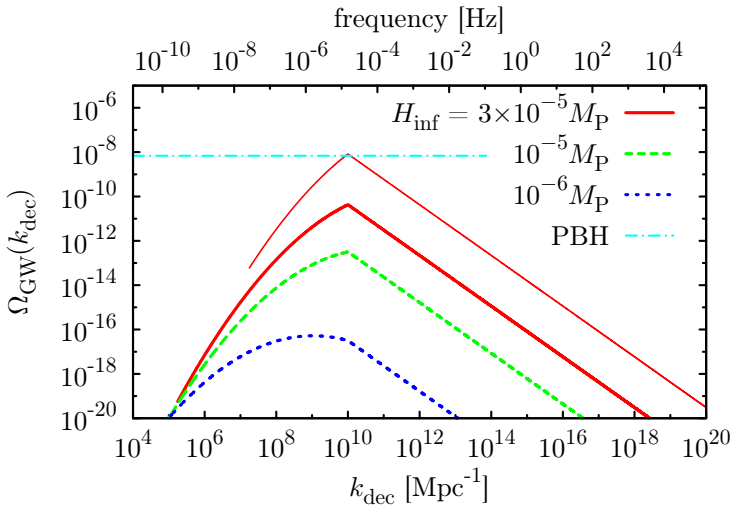

(a)

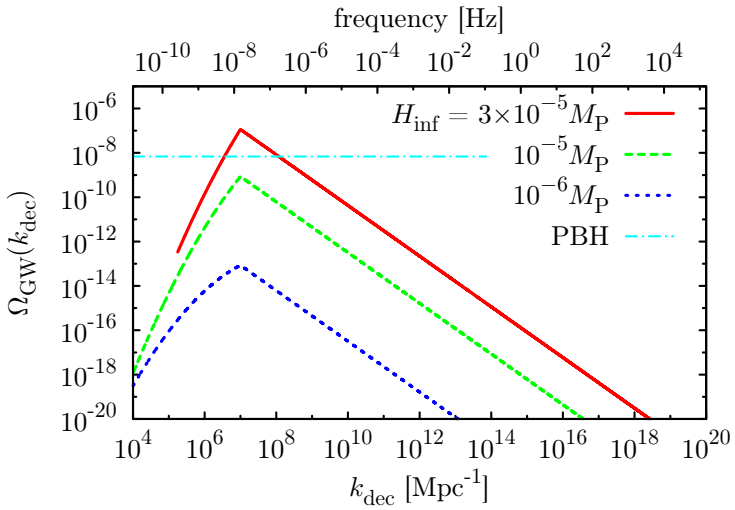

(b)

Figure 4.6: The peak values of $\Omega_{\rm GW}$ in terms of the peak wave number $k_{\rm dec}$ in axion-like curvaton model are shown. We have taken $k_f = 10^{10}$ (10^7) Mpc^{-1} for top (bottom) panel, $r_D = 1$, $H_{\rm inf} = 3 \times 10^{-5}$ M_P (solid red), 10^{-5} M_P (dashed green) and 10^{-6} M_P (dotted blue), $\kappa = 1$ (thick lines) and $\kappa = 10^{-4}$ (thin lines). The dash dotted cyan line shows the upper bound from the PBH overproduction.

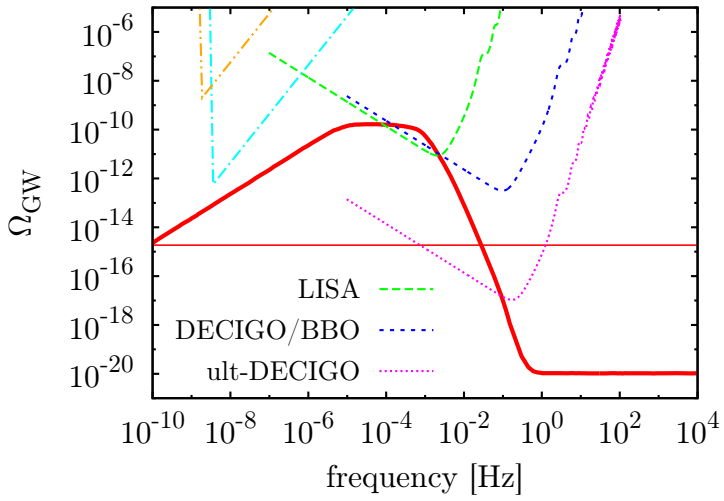

(a)

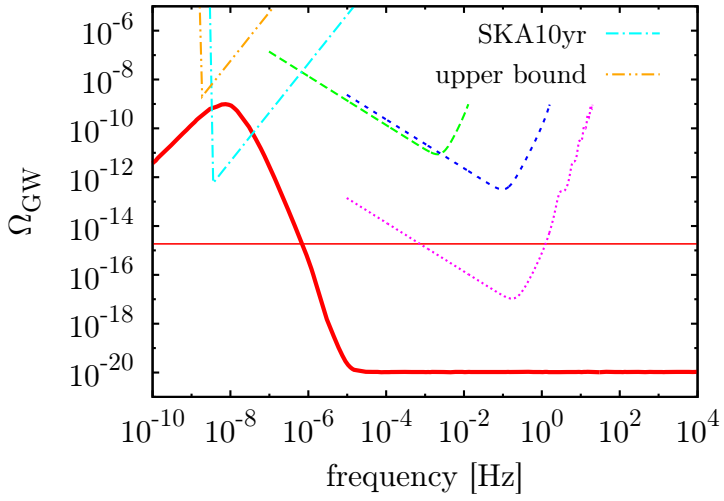

(b)

Figure 4.7: The spectrum of $\Omega_{\rm GW}$ in an axion-like curvaton model is shown as the thick solid red lines. We have taken $H_{\rm inf} = 3 \times 10^{-5} M_P$, $n_\sigma = 1.5$ (1.8), $\kappa = 10^{-4}$ (1), $r_D = 1$ and $k_f = 10^{10}$ (10^7) Mpc^{-1} in the top (bottom) panel. Thin lines shows the contributions from the primordial gravitational waves. We show the same sensitivity curves as in Fig. 4.4.

so the amount of gravitational waves cannot be enhanced as long as $\sigma_{\rm osc} < \sigma(k)$ even if the curvaton has blue-tilted spectrum. We check this argument numerically for the quadratic curvaton model and the axion-like curvaton model which we introduced above.

Note that here we consider the contribution of the adiabatic scalar curvature perturbations and the anisotropic stress due to the kinetic term of the curvaton, separately. Actually, they have the same origin of the fluctuation of the curvaton and hence when we consider these two contributions simultaneously there is a contribution of the cross-term of Φ and $\delta\sigma$ in the power spectrum of the gravitational waves. However, we confirm that the contribution of the anisotropic stress is subdominant compared with that of the adiabatic scalar curvature perturbations and can expect that the contribution of such cross-term is also subdominant. Furthermore, in this paper we evaluate $\delta\sigma$ on flat slicing but Φ in the conformal Newtonian gauge. Thus, there exists the effect of the gauge transformation of $\delta\sigma$ from flat slicing to the conformal Newtonian gauge when the both contributions are simultaneously included. Such an issue to treat the effect of the gauge transformation on second order tensor perturbations explicitly is left as a future work.

Chapter 5

Conclusions

In this thesis, we have investigated the cosmological consequences in the curvaton model, especially focused on the PBH formation and gravitational wave generation. Various observation like CMB temperature anisotropy prove indicate that the present Universe is filled with the dark matter and discovery of QSO at high redshift indicates that the existence of SMBH with mass $\sim 10^9 M_\odot$. We focus on the possibility that the dark matter and the SMBH are explained by non-evaporating PBHs. In order for an enough number of PBHs to be formed, we need a large amplitude of the primordial density perturbation on small scales, that is $\mathcal{P}_\zeta \sim 10^{-3} - 10^{-2}$.. Since the large scale perturbation is strictly constrained by the CMB observation, the power spectrum is required to have rather complex shape; the scale-invariant spectrum is realized on scales $k < 1\ \mathrm{Mpc}^{-1}$ and extremely blue-tilted spectrum on $k > 1\ \mathrm{Mpc}^{-1}$. It is very difficult to realize such spectrum in the single field inflation models, so we are motivated to introduce an additional field without an inflaton, a curvaton. Fortunately, there are many scalar fields within the framework of some high energy physics such as supersymmetric model and some of them may take roles of the curvaton. The required spectrum is easily realized if the large scale scale-invariant perturbations are generated from an inflaton and small scale blue-tilted ones are generated from a curvaton. In addition, since the required amplitude of the curvature perturbations on small scales are large, it is expected that the significant amount of the gravitational waves are generated. This implies the possibility to detect the imprints of the curvaton scenario which realizes the PBH formation.

We have considered the two kind of curvaton models; a quadratic curvaton model and an axion-like curvaton model. A quadratic curvaton model is described by the simple quadratic potential but it cannot predict an extremely blue-tilted spectrum of curvature perturbation, so PBH formation cannot be realized in this model. However, a significant amount of gravitational waves are expected to be generated. An axion-like curvaton model is based on the SUSY, in which the curvaton is identified as the angular direction contained in some complex scalar field. In this model, the power spectrum of the curvature perturbations on small scales can be extremely blue such as $n_\sigma = 2 - 4$. Thus, an enough number of PBHs are expected to formed in this model. The main results of this thesis are written in the following.

PBH formation from curvaton

We have investigated the PBH formation in an axion-like curvaton model. In this model, an extremely blue-tilted power spectrum of curvature perturbation is realized and there is certain parameter space in which the enough PBHs are formed. Parameters are required to be $f \sim H_{\rm inf}$ for an enough number of PBHs. The predicted mass spectrum has a peaked shape and narrow enough to explain the SMBH formation. The peak corresponds to the horizon mass at the curvaton decay. The reheating temperature is required to be high, that is $T_R \gtrsim 10^{13}$ GeV for PBH dark matter and $T_R \gtrsim 10^9$ GeV for SMBH and curvaton energy fraction at decay is required to be $r_D \gtrsim 1$. The model parameter is required to be $f \sim 5 \times 10^{13} - 10^{14}$ GeV, $\Lambda \sim 10^{10} - 10^{11}$ GeV and $m_\sigma \sim 5 \times 10^5 - 10^8$ GeV for PBH dark matter and $f \sim 10^{12}$ GeV, $\Lambda \sim 10^6 - 10^7$ GeV and $m_\sigma \sim 0.5 - 100$ GeV for SMBH. Our main conclusion is that PBHs can be formed under the relatively natural setup without finetuning in an axion-like curvaton model. In addition, it is possible that the PBH dark matter and SMBH can be simultaneously explained if there are multiple axion field during inflation.

GW generation from curvaton

It is known that the gravitational waves can be induced from the scalar perturbations or curvature perturbations because the quadratic terms of scalar perturbation become source terms of gravitational waves in second order perturbation theory. Thus, when we consider the PBH formation from the primordial density perturbations, gravitational waves are automatically generated whose amplitude is expected to be large. In this thesis, we have also calculated the amount of induced gravitational waves in the curvaton models and shown that those models can be testable by the future space-based gravitational wave detectors planned such as LISA, DECIGO and BBO or the pulsar timing observation by SKA. We have also presented the resultant power spectrum of gravitational waves having a characteristic shape, which has a peak at the wave number corresponding to the scale reentering the horizon at the curvaton decay or at the curvaton domination. In addition, a plateau, instead of a peak, can be seen in an axion-like curvaton model, implying that we can see an imprints of this model by the future gravitational wave observations. Furthermore, combining it with the PBH calculation, this blue-tilted curvaton model can simultaneously realize the PBH formation, which account for the cold dark matter or seeds for the supermassive blackholes, and gravitational wave production observable in the future.

Appendix A

Inflation

Inflation is one of the most plausible solution for the horizon problem, monopole problem and the seeds for the structure formation. In addition, the recent CMB observation strongly support that the very early universe have experienced the inflationary epoch. In this appendix, we briefly review the standard slow-roll inflation scenario.

A.1 Background dynamics

A.1.1 Basics on slow-roll inflation

Inflation is the epoch of the accelerated expansion in the very early universe and such a situation is easily realized once the universe is dominated by the vacuum energy, Λ. Actually, the Friedmann equation

$$H^2 = \left(\frac{\dot{a}}{a}\right)^2 = \frac{\Lambda}{3M_P^2} \tag{A.1}$$

yields the solution

$$a(t) = e^{H_{\rm inf}t}, \tag{A.2}$$

with constant $H_{\rm inf}$, which describes the exponentially expanding universe (de Sitter spacetime). One way to realize this situation is the *slow-roll inflation* model. In this model, one introduces the scalar field called inflaton ϕ whose Lagrangian is given by

$$\mathcal{L} = \frac{1}{2}\partial_\mu\phi\partial^\mu\phi - V(\phi). \tag{A.3}$$

Then, by slightly varying the field ϕ in action

$$S = \int d^4\sqrt{-g}\mathcal{L}, \tag{A.4}$$

we obtain the background equation of motion

$$\ddot{\phi} + 3H\dot{\phi} + V'(\phi) = 0, \tag{A.5}$$

where prime denotes the derivative with respect to the inflaton field. On the other hand, the Friedmann equation describing the expansion of the universe is

$$H^2 = \frac{1}{3M_P^2}\left(\frac{1}{2}\dot{\phi}^2 + V(\phi)\right). \tag{A.6}$$

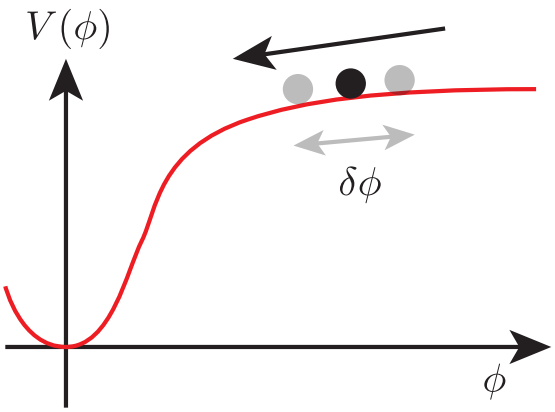

Figure A.1: This figure illustrates the inflaton potential.

Slow-roll inflation requires that the very flat potential of the inflaton and the inflaton slowly rolls down its potential, and then, the equation of motion and Friedmann equation is approximated respectively as

$$\dot{\phi} \simeq -\frac{V'(\phi)}{3H}, \quad H^2 \simeq \frac{V(\phi)}{3M_P^2} \tag{A.7}$$

which is called slow-roll approximations. In other word, the slow-roll inflation occurs if the slow-roll parameters ϵ and η defined as

$$\epsilon \equiv \frac{1}{2}M_P^2\left(\frac{V''}{V}\right), \quad \eta \equiv M_P^2\frac{V''}{V}, \tag{A.8}$$

satisfy $\epsilon \ll 1$ and $|\eta| \ll 1$.

A.1.2 e-folding number

e-folding number, N, is an important quantity during inflation which is defined in terms of the scale factor via

$$e^N = \frac{a(t_f)}{a(t_e)}, \tag{A.9}$$

where t_e is the cosmic time corresponding to the last e-folding number from the end of the inflation and t_f is the time at the end of the infation. N is also expressed in the integral form as

$$N = \int_{t_f}^{t_e}(-H)dt = \frac{1}{M_P^2}\int_{\phi_f}^{\phi_e}\frac{V}{V'}d\phi, \tag{A.10}$$

where we have used the slow-roll approximation.

Next, let us derive the last e-folding number corresponding to the time when the scale of our observable universe (observable scale) exit the horizon. At the end of the inflation, the observable scale, L, becomes e^N times larger than the Hubble horizon during inflation, $L(t_f) = e^N H_{\rm inf}^{-1}$. Then, after inflation, the inflaton field starts to oscillate coherently until the inflaton decays into radiation (reheating). Taking into account that the oscillating

inflaton behaves like a matter, the energy density of universe at the reheating, t_R, is given by

$$\rho(t_R) = \rho_\phi(t_f)\left(\frac{a(t_R)}{a(t_f)}\right)^{-3} \tag{A.11}$$

where $\rho(t_R) = \pi^2/30 g_* T_R^4$ and $\rho_\phi(t_f) = 3H_{\rm inf}^2 M_P^2$ and observable scale becomes

$$L(t_R) = e^N H_{\rm inf}^{-1}\left(\frac{a(t_R)}{a(t_f)}\right). \tag{A.12}$$

Thus, the entropy within the volume of the observable scale, S_N, is calculated as

$$S_N = e^{3N} H_{\rm inf}^{-3}\left(\frac{\rho_\phi(t_f)}{\rho(t_R)}\right) s(T_R) \simeq e^{3N}\frac{4M_P^2}{H_{\rm inf} T_R} \tag{A.13}$$

where $s(T)$ is the entropy density given by

$$s(T) = \frac{2\pi^2}{45} g_* T^3. \tag{A.14}$$

The observed CMB temperature $T_0 = 2.725$ K implies the entropy within the observable scale in our present universe to be $S_L \simeq 10^{87}(L/4000\ {\rm Mpc})^3$, so, taking into account the entropy conservation, e-folding number is related to the observable scale as

$$N = 56 + \ln\left(\frac{L}{4000\ {\rm Mpc}}\right) + \frac{1}{3}\ln\left(\frac{T_R}{10^{10}\ {\rm GeV}}\right) + \frac{1}{3}\left(\frac{H_{\rm inf}}{10^{13}\ {\rm GeV}}\right). \tag{A.15}$$

This means that our observable scale exit the horizon during inflation when the last e-folding number is roughly 50 – 60.

A.2 Generating primordial curvature perturbation

A.2.1 Scalar field fluctuation

Massless scalar field

Let us consider the scalar field which can be decomposed into the homogeneous and perturbation part;

$$\phi(\mathbf{x}, \eta) = \bar{\phi}(\eta) + \delta\phi(\mathbf{x}, \eta). \tag{A.16}$$

Fourier transforming the scalar field fluctuation as

$$\delta\phi(\mathbf{x}, \eta) = \int \frac{d^3k}{(2\pi)^{3/2}} \delta\phi_{\mathbf{k}}(\eta) e^{i\mathbf{k}\mathbf{x}}, \tag{A.17}$$

and redefining the field as $\varphi = a\delta\phi$, the perturbed action for the scalar field fluctuation is rewritten as

$$\int d^4x\sqrt{-g}\left(\frac{1}{2}\partial_\mu\delta\phi\partial^\mu\delta\phi\right) = \int d\eta d^3k \frac{1}{2}\left[\varphi'_{\mathbf{k}}\varphi'_{-\mathbf{k}} - \left(k^2 + \frac{a''}{a}\right)\varphi_{\mathbf{k}}\varphi_{-\mathbf{k}}\right], \tag{A.18}$$

which is known as the Mukhanov action. Further, we express each Fourier mode as

$$\varphi_{\mathbf{k}}(\eta) = v_k(\eta) a_{\mathbf{k}} + v_k^*(\eta) a_{-\mathbf{k}}^\dagger, \tag{A.19}$$

where v_k is a c-number mode function and $a_{\mathbf{k}}$ and $a^\dagger_{\mathbf{k}}$ are respectively the annihilation and creation operators satisfying $a_{\mathbf{k}}|0\rangle = \langle 0|a^\dagger_{\mathbf{k}} = 0$ and the commutation relation;

$$[a_{\mathbf{k}}, a^\dagger_{\mathbf{k}'}] = \delta^{(3)}(\mathbf{k}-\mathbf{k}') \quad \text{and} \quad [a_{\mathbf{k}}, a_{\mathbf{k}'}] = [a^\dagger_{\mathbf{k}}, a^\dagger_{\mathbf{k}'}] = 0. \tag{A.20}$$

Then, from the Mukhanov action, we obtain the equation of motion for each mode function as

$$v_k'' + \left(k^2 - \frac{2}{\eta^2}\right) v_k = 0, \tag{A.21}$$

where we have used the relation $a'/a = -1/\eta$. Because this equation reduces to the mode equation in Minkowski spacetime in the limit $\eta \to -\infty$, we impose the following initial condition

$$\lim_{\eta\to-\infty} v_k(\eta) \to \frac{e^{-ik\eta}}{\sqrt{2k}}, \tag{A.22}$$

and, under this initial condition, we obtain the subhorizon solution as

$$v_k(\eta) = \frac{e^{-ik\eta}}{\sqrt{2k}}\left(1 - \frac{i}{k\eta}\right) \quad \text{for} \quad |k\eta| \ll 1. \tag{A.23}$$

Then we derive the power spectrum of the scalar field fluctuations, $P_\phi(k)$which is defined via

$$\langle \delta\phi_{\mathbf{k}} \delta\phi_{\mathbf{k}'} \rangle = \frac{2\pi^2}{k^3} \mathcal{P}_\phi(k) \delta^{(3)}(\mathbf{k}+\mathbf{k}') \tag{A.24}$$

where angular bracket represents the ensemble average which can be replaced with the vacuum expectation value of the quantum field, $\langle 0|\delta\phi_{\mathbf{k}}\delta\phi_{\mathbf{k}'}|0\rangle$. On subhorizon scales, (A.19) and (A.23) yield

$$\mathcal{P}_{\delta\phi}(k) = \left(\frac{H_{\rm inf}}{2\pi}\right)^2. \tag{A.25}$$

Massive scalar field

The action for the massive scalar field is given by

$$S = \int d^4x\sqrt{-g}\left(\frac{1}{2}\partial_\mu\phi\partial^\mu\phi - \frac{1}{2}m^2\phi^2\right), \tag{A.26}$$

and Mukhanov action for the scalar filed fluctuation is rewritten as

$$\int d\eta d^3k \frac{1}{2}\left[\varphi'_{\mathbf{k}}\varphi'_{-\mathbf{k}} - \left(a^2m^2 + k^2 + \frac{a''}{a}\right)\varphi_{\mathbf{k}}\varphi_{-\mathbf{k}}\right], \tag{A.27}$$

which leads to the evolution equation for the mode function

$$v_k'' + \left(a^2m^2 + k^2 - \frac{2}{\eta^2}\right) v_k = 0. \tag{A.28}$$

Under the initial condition (A.22), the solution is calculated as

$$v_k = e^{i(\nu+1/2)\pi/2}\sqrt{\frac{\pi}{4k}}\sqrt{k\eta}H^{(1)}_\nu(k\eta), \tag{A.29}$$

where $H_\nu^{(1)}$ is the Hankel function and

$$\nu = \sqrt{\frac{9}{4} - \frac{m^2}{H^2}} \simeq \frac{3}{2} - \frac{m^2}{3H^2} \tag{A.30}$$

On superhorizon scales, the mode function becomes

$$v_k = e^{i(\nu-1/2)/\pi/2} \frac{2^\nu \Gamma(\nu)}{2^{3/2}\Gamma(3/2)} \frac{1}{\sqrt{2k}} (k\eta)^{1/2-\nu}, \tag{A.31}$$

and then, the power spectrum is calculated as

$$\mathcal{P}_{\delta\phi}(k,\eta) = \left(\frac{H}{2\pi}\right)^2 \left(\frac{k}{aH}\right)^{2m^2/3H^2} \tag{A.32}$$

Axion-like curvaton

An axion-like curvaton model is described by a complex scalar field Φ which is decomposed as $\Phi = \varphi e^{i\theta}/\sqrt{2}$. A curvaton lives in the angular component and written as $\sigma = f\theta$, where f is the minimum of φ. The Lagrangian is given by

$$\mathcal{L} = -\partial_\mu \Phi \partial^\mu \Phi - m^2 |\Phi|^2. \tag{A.33}$$

Note that the angular direction θ is not canonically normalized variable, so we should decompose the complex scalar field by another way. According to the multi-field inflation model, we decompose the field into the direction parallel and perpendicular to the classical trajectory. Because the potential depends only on the redial direction, φ, we choose the direction perpendicular to φ, χ as another canonically normalized variable. The Lagrangian is rewritten as

$$\mathcal{L} = -\frac{1}{2}\partial_\mu \varphi \partial^\mu \varphi - \frac{1}{2}\partial_\mu \chi \partial^\mu \chi - \frac{1}{2} m \varphi^2. \tag{A.34}$$

The power spectrum of these scalar fields on superhorizon scales are calculated as above,

$$\mathcal{P}_{\delta\varphi} = \left(\frac{H}{2\pi}\right)^2 \left(\frac{k}{ah}\right)^{2m^2/3H^2}, \quad \mathcal{P}_{\delta\chi} = \left(\frac{H}{2\pi}\right)^2. \tag{A.35}$$

Well after the horizon exiting, the fluctuation becomes classical and then, the angular fluctuation is easily calculated in terms of $\delta\chi$,

$$\delta\theta = \tan^{-1}\left(\frac{\delta\chi}{\varphi_*(k)}\right) \simeq \frac{H_{\rm inf}}{2\pi\varphi_*(k)}, \tag{A.36}$$

where φ_* is the value of φ at the scale of interest leaves the horizon. Therefore, the fluctuation of the curvaton is derived as

$$\frac{\delta\sigma}{\sigma} = \frac{\delta\theta}{\theta_i} = \frac{H_{\rm inf}}{2\pi\varphi_*(k)\theta_i}, \tag{A.37}$$

where θ_i is the initial misalignment angle.

A.2.2 Curvature perturbation

The gauge-invariant curvature perturbation, ζ, is calculated on the spatially flat hypersurface, in which any fluctuation is related to the primordial scalar field fluctuations;

$$\zeta = -\frac{H}{\dot{\phi}}\delta\phi_{\mathbf{k}}, \tag{A.38}$$

then, the power spectrum of curvature perturbation, which is fixed at the horizon exiting during inflation, is calculated as

$$\mathcal{P}_\zeta = \left(\frac{H}{2\pi}\right)^2\left(\frac{H^2}{\dot{\phi}}\right)^2\Bigg|_{aH=k}. \tag{A.39}$$

Using the slow-roll approximation (A.7), we obtain the well-known formula,

$$\mathcal{P}_\zeta(k) = \frac{V}{24\pi^2 M_P^4\epsilon}\Bigg|_{aH=k} = \frac{H^2}{8\pi^2 M_P^2\epsilon}\Bigg|_{aH=k}. \tag{A.40}$$

A.2.3 Spectral index

From the above discussion, the power spectrum of the curvature perturbation looks scale-invariant because the Hubble parameter during inflation is assumed to be unchanged. But, actually, the Hubble parameter slightly changes, which causes the scale dependence of the power spectrum. The scale dependence is characterized by the spectral index, n_s, which is defined via

$$n_s - 1 = \frac{d\ln\mathcal{P}_\zeta(k)}{d\ln k}. \tag{A.41}$$

Because $d\ln k = Hdt$ at the horizon exiting, the spectral index can be expressed as

$$n_s - 1 = \frac{2\dot{H}}{H^2} - \frac{\dot{\epsilon}}{H\epsilon} = 2\eta - 6\epsilon. \tag{A.42}$$

Planck observation have severely constrained n_s to be $n_s = 0.9603 \pm 0.0073$ and some inflation models are ruled out from this constraint [102].

Appendix B

A brief review on the cosmological perturbations

In this appendix, we briefly review the cosmological perturbation theory. More detailed discussion is written in [103].

B.1 The gauge-invariant perturbations

B.1.1 Perturbed quantities

The general first order metric perturbation from a flat FRW metric is expressed as

$$ds^2 = a^2\Big[-(1+2\Phi)d\eta^2 + 2B_i dx^i d\eta + [(1-2\Psi)\delta_{ij} + 2E_{ij}]dc^i dx^j\Big], \tag{B.1}$$

where Φ is a 3-scalar called the *lapse*, B_i is a 3-vector called *shift*, Ψ is a 3-scalar called the spatial *curvature* perturbation, and E_{ij} is a spatial 3-tensor called *shear* which is symmetric and traceless. Furthermore, B_i and E_{ij} are decomposed into the scalar, transverse vector, and transverse and traceless tensor as

$$B_i = \partial_i B + S_i \quad \text{with} \quad \partial^i S_i = 0 \tag{B.2}$$

and

$$E_{ij} = 2D_{ij}E + 2(\partial_i F_j + \partial_j F_i) + h_{ij} \quad \text{with} \quad \partial^i F_i = \partial^i h_{ij} = h^i_i = 0, \tag{B.3}$$

where $D_{ij} = \partial_i\partial_j - \delta_{ij}\Delta/3$. The perturbed energy-momentum tensor is described by a energy density ρ, a pressure p, a 4-velocity u^μ, and an anisotropic stress $\Sigma^{\mu\nu}$. The density and pressure perturbation are given straightforwardly as

$$\delta\rho(\eta,\mathbf{x}) = \rho(\eta,\mathbf{x}) - \bar{\rho}(\eta) \quad \text{and} \quad \delta p(\eta,\mathbf{x}) = p(\eta,\mathbf{x}) - \bar{p}(\eta). \tag{B.4}$$

The 4-velocity perturbation has only 3 degrees of freedom because it should satisfy the constraint $g_{\mu\nu}u^\mu u^\nu = -1$ and expressed as

$$u_\mu = (-1-\Phi, v_i), \quad u^\mu = (1-\Phi, v^i + B^i) \tag{B.5}$$

up to first order. Then, the perturbed energy momentum tensor is given by

$$T_0^0 = -(\bar{\rho} + \delta\rho) \tag{B.6}$$

$$T_i^0 = (\bar{\rho} + \bar{p})v_i \tag{B.7}$$

$$T_0^i = -(\bar{\rho} + \bar{p})(v^i + B^i) \tag{B.8}$$

$$T_j^i = (\bar{p} + \delta p)\delta_j^i + \Sigma_j^i. \tag{B.9}$$

Conventionally, we often decompose the velocity perturbations as

$$v_i = \partial_i v + v_i^\perp \quad \text{with} \quad \partial^i v_i^\perp = 0, \tag{B.10}$$

and define the 3-momentum density, δq via $\partial_i \delta q = (\bar{\rho} + \bar{p})\partial_i v$. Similarly, the shear can be decomposed as

$$\Sigma_{ij} = D_{ij}\Sigma + \frac{1}{2}(\partial_i \Sigma_j^{(V)} + \partial_j \Sigma_i^{(V)}) + \Sigma_{ij}^{(T)} \quad \text{with} \quad \partial^i \Sigma_i^{(V)} = \partial^i \Sigma_{ij}^{(T)} = 0. \tag{B.11}$$

B.1.2 Gauge transformation and gauge-invariant variables

Let us consider the general coordinate transformation

$$x^\mu \to \tilde{x}^\mu + \xi^\mu, \tag{B.12}$$

where ξ^μ are infinitesimal function of spacetime. Under these transformations and taking into account the invariance of the line element, $ds^2 = g_{\mu\nu}dx^\mu dx^\nu = \tilde{g}_{\mu\nu}d\tilde{x}^\mu d\tilde{x}^\nu$, the scalar metric perturbations are transformed as

$$\Phi \to \Phi - \frac{1}{a}(a\alpha)' \tag{B.13}$$

$$B \to B + \xi' - \alpha \tag{B.14}$$

$$\Psi \to \Psi + \frac{a'}{a}\alpha \tag{B.15}$$

$$E \to E + \xi, \tag{B.16}$$

where we rewrote ξ^μ as

$$\xi^0 = \alpha, \quad \xi^i = \xi_\perp^i + \partial^i \xi \quad \text{with} \quad \partial_i \xi_\perp^i = 0. \tag{B.17}$$

Similarly, the scalar components of matter perturbations are transformed as

$$\delta\rho \to \delta\rho - \bar{\rho}'\alpha \tag{B.18}$$

$$\delta p \to \delta p - \bar{p}'\alpha \tag{B.19}$$

$$\delta q \to \delta q + (\bar{\rho} + \bar{p})\alpha. \tag{B.20}$$

From the above transformation rules, we can construct the gauge-invariant variables. First of all, there are two important variables constructed from metric perturbations;

$$\Phi_B = \Phi - \frac{1}{a}[a(B - E')]', \quad \Psi_B = \Psi + \frac{a'}{a}(B - E') \tag{B.21}$$

which are called Bardeen potential. In addition, we can construct the gauge-invariant variables by combinations of matter and metric perturbations. Two well known examples are the curvature perturbation on uniform density hypersurface and the comoving curvature perturbation defined respectively as

$$-\zeta = \Psi + \frac{\mathcal{H}}{\bar{\rho}'}\delta\rho \tag{B.22}$$

and

$$\mathcal{R} = \Psi - \frac{\mathcal{H}}{\bar{\rho}+\bar{p}}\delta q, \tag{B.23}$$

where we have used the conformal Hubble parameter defied as $\mathcal{H} = a'/a$.

B.2 The evolution of perturbations

The evolution equations for perturbed variables are derived from the perturbed Einstein equations

$$\delta G_{\mu\nu} = 8\pi G \delta T_{\mu\nu}. \tag{B.24}$$

Here we adopt the conformal-Newtonian gauge on which we set $B = E = 0$. Note that metric perturbations in this gauge, Φ, Ψ coincide with the gauge-invariant Bardeen potentials, Φ_B and Ψ_B. After a complicated calculation for the perturbed Einstein tensor, we obtain the evolution equations as

$$\Delta\Psi - 3\mathcal{H}(\Psi' + \mathcal{H}\Phi) = -4\pi G a^2 \delta T^0_0 \tag{B.25}$$

$$\partial_i(\Psi' + \mathcal{H}\Phi) = 4\pi G a^2 \delta T^0_i \tag{B.26}$$

$$\begin{aligned}&[\Psi'' + \mathcal{H}(2\Psi+\Phi)' + (2\mathcal{H}' + \mathcal{H}^2)\Phi + \frac{1}{2}\Delta(\Phi-\Psi)]\delta^i_j \\ &\quad - \frac{1}{2}\partial^i\partial_j(\Phi-\Psi) = 4\pi G a^2 \delta T^i_j.\end{aligned} \tag{B.27}$$

Fourier transforming the perturbations and extracting only the scalar component, these equations are rewritten as

$$3\mathcal{H}(\Psi' + \mathcal{H}\Phi) + k^2\Psi = -4\pi G a^2 \delta\rho \tag{B.28}$$

$$\Psi' + \mathcal{H}\Phi = -4\pi G a^2 \delta q \tag{B.29}$$

$$\Psi'' + \mathcal{H}(2\Psi+\Phi)' + (2\mathcal{H}' + \mathcal{H}^2)\Phi = 4\pi G a^2 \left(\delta p - \frac{2}{3}k^2\delta\Sigma\right) \tag{B.30}$$

$$\Psi - \Phi = 8\pi G a^2 \delta\Sigma, \tag{B.31}$$

which implies the absence of the anisotropic stress, $\delta\Sigma = 0$, means $\Psi = \Phi$ and we assume it hereafter. Combining these equations with energy-momentum conservation given by

$$\delta\rho' + 3\mathcal{H}(\delta\rho + \delta p) = k^2\delta q + 3(\bar{\rho}+\bar{p})\Phi' \tag{B.32}$$

$$\delta q' + 3\mathcal{H}\delta q = -\delta p - (\bar{\rho}+\bar{p})\Phi, \tag{B.33}$$

and assuming the radiation dominated universe, $p = \rho/3$, we obtain the evolution equation for Φ as

$$\Phi'' + \frac{2}{\eta}\Phi' + \frac{k^2}{3}\Phi = 0. \tag{B.34}$$

The solution of this differential equation is given by the spherical Bessel functions of order 1, which is explicitly expressed as

$$\Phi = 3\Phi_p\left(\frac{\sin(k\eta/\sqrt{3}) - (k\eta)\cos(k\eta/\sqrt{3})}{(k\eta/\sqrt{3})^3}\right), \tag{B.35}$$

where Φ_p is the primordial value of Φ. The behavior of this solution can be easily understood as following. Before the horizon entry, $k\eta < 1$, Φ remains the primordial value and after the horizon entry, Φ begins damping oscillation. Because Φ remains unchanged on superhorizon scales, the density perturbation, comoving curvature perturbation and curvature perturbation on uniform density slicing can be related as

$$\mathcal{R} = -\zeta = -\frac{5+3w}{6(1+w)}\frac{\delta\rho}{\bar{\rho}} \quad \text{for} \quad k\eta \ll 1. \tag{B.36}$$

Appendix C

The Press-Schechter theory

In order to count the number of the non-linear objects like PBHs with some given masses, one often invokes the Press-Schechter theory [104]. It is believed that the collapse occurs in the region at which the density contrast exceeds some threshold value, δ_c, which is estimated as $\delta_c = 1.69$ in the spherical collapse model. In the Press-Schechter theory, the fraction of the volume of the whole universe with the smoothed density field on some scale R satisfying the condition $\delta(R) > \delta_c$ can be regarded as rough estimate for the mass fraction of the universe which collapses into nonlinear objects with mass, $M(R)$, in a volume corresponding to the scale R. Then, let us estimate the mass function, i.e. the comoving number density of nonlinear object with a given mass, in the Press-Schechter theory.

For the Gaussian density perturbation, the probability distribution function for $\delta(\mathbf{k})$ is given by

$$p(\delta)d\delta = \frac{1}{\sqrt{2\pi\sigma^2}} \exp\left(- \frac{\delta^2}{2\sigma^2} \right) d\delta \tag{C.1}$$

where σ^2 is the variance of the density perturbation. Similarly, the density perturbation smoothed over some mass scale $\delta(M)$ is also given by the Gaussian distribution;

$$p(\delta(M))d\delta(M) = \frac{1}{\sqrt{2\pi\sigma^2(M)}} \exp\left(- \frac{\delta^2(M)}{2\sigma^2(M)} \right) d\delta(M) \tag{C.2}$$

where $\sigma^2(M)$ is the variance of $\delta(M)$. In the Press-Schechter formalism, the non-linear object whose mass is larger than M is formed in those regions where the smoothed density perturbation, $\delta(M)$, is larger than some critical density δ_c, The probability of forming such objects is given by

$$p_{>\delta_c}(M) = \int_{\delta_c}^{\infty} p(\delta(M))d\delta(M) = \frac{1}{\sqrt{2\pi}} \int_{\delta_c/\sigma(M)}^{\infty} e^{-x^2/2} dx, \tag{C.3}$$

where $\sigma(M) = \sqrt{\sigma^2(M)}$. Expressing the comoving number density of those nonlinear objects whose masses are between M and dM as $n(M)dM$, all masses contained in these objects is written as $n(M)MdM$, which is calculated as

$$n(M)MdM = 2\bar{\rho}_{\rm com} \left| p_{>\delta_c}(M) - p_{>\delta_c}(M + dM) \right| = 2\bar{\rho}_{\rm com} \left| \frac{dp_{>\delta_c}}{d\sigma(M)} \right| \left| \frac{d\sigma(M)}{dM} \right| dM. \tag{C.4}$$

Then, substituting (C.3) into it, we obtain

$$n(M) = \sqrt{\frac{2}{\pi}} \frac{\bar{\rho}_{\rm com}}{M^2} \left| \frac{d\ln\sigma(M)}{d\ln M} \right| \frac{\delta_c}{\sigma(M)} \exp\left(-\frac{\delta_c^2}{2\sigma^2(M)} \right), \tag{C.5}$$

which is known as the Press-Schechter mass function.

Then, we apply it to the PBH mass function. Because the comoving energy density is redshifted obeying $\rho_{\rm com} \propto a^{-1}$ with $a \propto T^{-1}$ in radiation dominated universe, we get

$$\rho_{\rm com}(T_f) = \rho_{\rm com}(T_*) \left(\frac{M_{\rm BH}}{M_*} \right)^{1/2}, \tag{C.6}$$

where T_f and T_* are PBH formation temperature with mass $M_{\rm BH}$ and M_* respectively. So, we obtain the PBH mass function as

$$\frac{dn_{\rm PBH}}{dM_{\rm BH}} = \sqrt{\frac{1}{18\pi}} \frac{\rho_{\rm com}(T_*)}{M_{\rm BH}^2} \left(\frac{M_*}{M_{\rm BH}} \right)^{1/2} \left| \frac{d\ln\sigma^2(M_{\rm BH})}{d\ln M_{\rm BH}} \right| \frac{\beta(M_{\rm BH})}{\sigma^2(M_{\rm BH})}. \tag{C.7}$$

Appendix D

Second order gravity

In this appendix, we derive the second order Einstein equation as an evolution equation for the stochastic gravitational waves. We consider the perturbed metric in conformal-Newtonian gauge given by

$$ds^2 = a^2(\eta)\bigg[-(1+2\Phi)d\eta^2 + \bigg\{(1-2\Psi)\delta_{ij} + \frac{1}{2}h_{ij}\bigg\}dx^i dx^j\bigg], \tag{D.1}$$

where Φ and Ψ are scalar metric perturbations and h_{ij} is a tensor metric perturbation. Conventionally, we rewrite them as following,

$$g_{00} = -a^2(1+2\Phi),\ g_{0i} = 0,\ g_{ij} = a^2\bigg[(1-2\Psi)\delta_{ij} + \frac{1}{2}h_{ij}\bigg]. \tag{D.2}$$

The inverse metric tensor is obtained through $g^{\mu\lambda}g^{\nu\lambda} = \delta^{\mu}_{\nu}$, which is written as

$$g^{00} = -a^{-2}(1-2\Phi+4\Phi^2),\ g^{0i} = 0,\ g^{ij} = a^{-2}\bigg[(1+2\Psi+4\Psi^2)\delta^{ij} - \frac{1}{2}h^{ij}\bigg] \tag{D.3}$$

up to second order perturbation. Note that we assume that the tensor mode metric perturbation h_{ij} is second order quantity. The Christoffel symbol is defined as

$$\Gamma^{\alpha}_{\beta\gamma} = \frac{1}{2}g^{\alpha\lambda}\bigg(\frac{\partial g_{\beta\lambda}}{\partial x^{\gamma}} + \frac{\partial g_{\gamma\lambda}}{\partial x^{\beta}} - \frac{\partial g_{\beta\gamma}}{\partial x^{\lambda}}\bigg), \tag{D.4}$$

and up to second order, we get

$$\Gamma^0_{00} = \mathcal{H} + \Phi' - 2\Phi\Phi' \tag{D.5}$$

$$\Gamma^0_{0i} = \partial_i\Phi - 2\Phi\partial_i\Phi \tag{D.6}$$

$$\Gamma^0_{ij} = \mathcal{H}\delta_{ij} - (2\mathcal{H}\Phi + 2\mathcal{H}\Psi + \Psi')\delta_{ij} + (4\mathcal{H}\Phi^2 + 2\Phi\Psi' + 4\mathcal{H}\Phi\Psi)\delta_{ij} + \frac{1}{2}\mathcal{H}h_{ij} \tag{D.7}$$

$$\Gamma^i_{00} = \partial^i\Phi + 2\Psi\partial^i\Phi \tag{D.8}$$

$$\Gamma^i_{0j} = \mathcal{H}\delta^i_j - \Psi\delta^i_j - 2\Psi\Psi'\delta^i_j \tag{D.9}$$

$$\Gamma^i_{jk} = \partial_j\Psi\delta^i_k - \partial_k\Psi\delta^i_j + \partial^i\Psi\delta_{jk} + 2\Psi(-\partial_j\Psi\delta^i_k - \partial_k\Psi\delta^i_j + \partial^i\Psi\delta_{jk}) - \frac{1}{4}\partial^i h_{jk}. \tag{D.10}$$

The Riemann tensor is defined as

$$R^{\alpha}_{\beta\mu\nu} = \partial_\mu \Gamma^{\alpha}_{\beta\nu} - \partial_\nu \Gamma^{\alpha}_{\beta\mu} + \Gamma^{\alpha}_{\lambda\mu}\Gamma^{\lambda}_{\beta\nu} - \Gamma^{\alpha}_{\lambda\nu}\Gamma^{\lambda}_{\beta\mu}, \tag{D.11}$$

and the Ricci tensor is defined by contracting the Riemann tensor:

$$R_{\mu\nu} = \partial_\alpha \Gamma^{\alpha}_{\mu\nu} - \partial_\mu \Gamma^{\alpha}_{\nu\alpha} + \Gamma^{\alpha}_{\sigma\alpha}\Gamma^{\sigma}_{\mu\nu} - \Gamma^{\alpha}_{\sigma\nu}\Gamma^{\sigma}_{\mu\alpha}, \tag{D.12}$$

and up to second order we obtain

$$\begin{aligned} R_{00} = {} & -3\mathcal{H}' + \partial^i\partial_i\Phi + 3\Psi'' + 3\mathcal{H}\Psi' + 3\mathcal{H}\Phi' - 6\mathcal{H}\Phi\Phi' - \partial^k\Phi\partial_k\Phi \\ & - 3\Phi'\Psi' + 2\Psi\partial^i\partial_i\Phi - \partial_k\Psi\partial^k\Phi + 6\mathcal{H}\Psi\Psi' + 6\Psi\Psi'' + 3(\Psi')^2 \end{aligned} \tag{D.13}$$

$$R_{0i} = 2\partial_i\Psi' + 2\mathcal{H}\partial_i\Phi - 4\mathcal{H}\Phi\partial_i\Phi - 2\Psi'\partial\Phi + 4\Psi'\partial_i\Psi + 4\Psi\partial_i\Psi' \tag{D.14}$$

$$\begin{aligned} R^{(\mathrm{d})}_{ij} = {} & (\mathcal{H}' + 2\mathcal{H}^2)\delta_{ij} + \big[- \mathcal{H}\Phi' - 5\mathcal{H}\Psi' - 2\mathcal{H}^2\Phi \\ & - 2(\mathcal{H}' + \mathcal{H}^2)\Psi - 2\mathcal{H}^2\Psi - \Psi'' + \partial^k\partial_k\Psi\big]\delta_{ij} \\ & + \big[4(\mathcal{H}' + 2\mathcal{H}^2)\Phi^2 + 4\mathcal{H}\Phi\Phi' + 10\mathcal{H}\Phi\Psi' + 2\mathcal{H}\Phi'\Psi + \Phi'\Psi' + 2\Phi\Psi'' \\ & + 4(\mathcal{H}' + 2\mathcal{H}^2)\Phi\Psi + \partial_k\Psi\partial^k\Phi + (\Psi')^2 + \partial_k\Psi\partial^k\Psi + 2\Psi\partial_k\partial^k\Psi\big]\delta_{ij} \end{aligned} \tag{D.15}$$

$$\begin{aligned} R^{(\mathrm{nd})}_{ij} = {} & \frac{1}{2}(\mathcal{H}' + \mathcal{H}^2)h_{ij} + \frac{1}{2}\mathcal{H}h'_{ij} - \frac{1}{4}\partial_i\partial^i h_{ij} + \frac{1}{4}h''_{ij} \\ & + \partial_i\Phi\partial_j\Phi + 2\Phi\partial_i\partial_j\Phi - \partial_j\Phi\partial_i\Psi - \partial_i\Phi\partial_j\Psi + 3\partial_i\Psi\partial_j\Psi + 2\Psi\partial_i\partial_j\Psi, \end{aligned} \tag{D.16}$$

where the superscripts (d) and (nd) denote the diagonal and non-diagonal respectively. The Ricci scalar is defined by contracting the Ricci tensor given by

$$\begin{aligned} R = R^{\mu}_{\mu} = {} & \frac{6}{a^2}(\mathcal{H}' + \mathcal{H}^2) \\ & + \frac{1}{a^2}\Big[- 2\Delta\Phi - 6\Psi'' - 6\mathcal{H}\Phi' - 18\mathcal{H}\Psi' - 12(\mathcal{H}' + \mathcal{H}^2)\Psi + 4\Delta\Psi \\ & + 24(\mathcal{H}' + \mathcal{H}^2)\Phi^2 + 2\partial_k\Phi\partial^k\Phi + 4\Phi\Delta\Phi + 24\mathcal{H}\Phi\Phi' + 6\Phi'\Psi' + 36\mathcal{H}\Phi\Psi' \\ & + 2\partial_k\Psi\partial^k\Phi - 4\Psi\Delta\Phi + 12\Phi\Psi'' - 12\Psi\Psi'' - 36\mathcal{H}\Psi'\Psi + 6\partial_k\Psi\partial^k\Psi + 16\Psi\Delta\Psi\Big]. \end{aligned} \tag{D.17}$$

Then, Einstein tensors up to second order are calculated as

$$G_0^0 = -\frac{3}{a^2}\mathcal{H}^2 + \frac{1}{a^2}\Big[6\mathcal{H}\Phi + 6\mathcal{H}\Psi - 2\Delta\Psi \\ - 12\mathcal{H}^2\Phi^2 - 12\mathcal{H}\Phi\Psi' - 3\partial_i\Psi\partial^i\Psi - 8\Psi\Delta\Psi + 12\mathcal{H}\Psi\Psi' - 3(\Psi')^2\Big] \tag{D.18}$$

$$G_0^i = \frac{1}{a^2}\Big(- 2\mathcal{H}\partial^i\Phi - 2\partial^i\Psi - 4\mathcal{H}\Phi\partial^i\Phi + 4\mathcal{H}\Psi\partial^i\Phi - 2\Psi'\partial^i\Phi + 4\Psi'\partial^i\Psi + 8\Psi\partial^i\Psi'\Big) \tag{D.19}$$

$$G_j^{(\mathrm{d})i} = \frac{1}{a^2}\Big[- 2\mathcal{H}' + \mathcal{H}^2 + 2\mathcal{H}\Phi' + (4\mathcal{H}' + 2\mathcal{H}^2)\Phi + \Delta\Phi + 4\mathcal{H}\Psi' + 2\Psi'' - \Delta\Psi \\ - (4\mathcal{H}^2\Phi^2 + 8\mathcal{H}')\Phi^2 - 8\mathcal{H}\Phi\Phi' - \partial_k\Phi\partial^k\Phi - 2\Phi\Delta\Phi - 4\Phi\Psi'' - 2\Phi'\Psi' \\ - 8\mathcal{H}\Phi\Psi' - 2\partial_k\Psi\partial^k\Psi - 4\Psi\Delta\Psi + (\Psi')^2 + 8\mathcal{H}\Psi\Psi' + 4\Psi\Psi'' + 2\Psi\Delta\Phi\Big] \tag{D.20}$$

$$G_j^{(\mathrm{nd})i} = \frac{1}{a^2}\Big[- \partial^i\partial_j\Phi + \partial^i\partial_j\Psi + \frac{1}{2}\mathcal{H}h_j^i - \frac{1}{4}\Delta h_j^i + \frac{1}{4}(h_j^i)'' + \partial^i\Phi\partial_j\Phi \\ + 2\Phi\partial^i\partial_j\Phi - 2\Psi\partial^i\partial_j\Phi - \partial^i\Psi\partial_j\Phi - \partial^i\Phi\partial_j\Psi + 3\partial^i\Psi\partial_j\Psi + 4\Psi\partial^i\partial_j\Psi\Big]. \tag{D.21}$$

Now, let us derive the evolution equation for the tensor mode up to second order. Assuming that the first order anisotropic stress is zero, which implies $\Phi = \Phi$, and taking into account the second order energy momentum tensor,

$$T_j^i = (\bar{\rho} + \bar{p})v^i v_j \quad \text{with} \quad v_i = -\frac{1}{4\pi G a^2(\bar{\rho} + \bar{p})}\partial_i(\Phi' + \mathcal{H}\Phi), \tag{D.22}$$

the Einstein equation $G_j^{(\mathrm{nd}i} = 8\pi G T_j^{(\mathrm{nd})i}$ yields

$$h_{ij}'' + 2\mathcal{H}h_{ij} - \Delta h_{ij} = -4\hat{\mathcal{T}}_{ij}^{lm}\mathcal{S}_{lm}, \tag{D.23}$$

where $\hat{\mathcal{T}}_{ij}^{lm}$ is the projection tensor which projects any tensor into the transverse traceless one and $\mathcal{S}_{ij}$ is defined as

$$\mathcal{S}_{ij} = 4\Phi\partial_i\partial_j\Phi + 2\partial_i\Phi\partial_j\Phi - \mathcal{H}^{-2}\partial_i(\Phi' + \mathcal{H}\Phi)\partial_j(\Phi' + \mathcal{H}\Phi). \tag{D.24}$$

Bibliography

[1] **Planck Collaboration** Collaboration, P. Ade *et al.*, "Planck 2013 results. XVI. Cosmological parameters," arXiv:1303.5076 [astro-ph.CO].

[2] G. Hinshaw, D. Larson, E. Komatsu, D. Spergel, C. Bennett, *et al.*, "Nine-Year Wilkinson Microwave Anisotropy Probe (WMAP) Observations: Cosmological Parameter Results," arXiv:1212.5226 [astro-ph.CO].

[3] **Planck Collaboration** Collaboration, P. Ade *et al.*, "Planck 2013 Results. XXIV. Constraints on primordial non-Gaussianity," arXiv:1303.5084 [astro-ph.CO].

[4] S. P. Martin, "A Supersymmetry primer," arXiv:hep-ph/9709356 [hep-ph].

[5] R. Peccei and H. R. Quinn, "CP Conservation in the Presence of Instantons," *Phys.Rev.Lett.* **38** (1977) 1440–1443.

[6] Y. B. Zel'dovich and I. D. Novikov, "The Hypothesis of Cores Retarded during Expansion and the Hot Cosmological Model," *sovast* **10** (Feb., 1967) 602.

[7] B. J. Carr and S. Hawking, "Black holes in the early Universe," *Mon.Not.Roy.Astron.Soc.* **168** (1974) 399–415.

[8] B. J. Carr, "The Primordial black hole mass spectrum," *Astrophys.J.* **201** (1975) 1–19.

[9] S. Hawking, "Particle Creation by Black Holes," *Commun.Math.Phys.* **43** (1975) 199–220.

[10] B. Carr, K. Kohri, Y. Sendouda, and J. Yokoyama, "New cosmological constraints on primordial black holes," *Phys.Rev.* **D81** (2010) 104019, arXiv:0912.5297 [astro-ph.CO].

[11] M. Kawasaki, N. Sugiyama, and T. Yanagida, "Primordial black hole formation in a double inflation model in supergravity," *Phys.Rev.* **D57** (1998) 6050–6056, arXiv:hep-ph/9710259 [hep-ph].

[12] M. Kawasaki and T. Yanagida, "Primordial black hole formation in supergravity," *Phys.Rev.* **D59** (1999) 043512, arXiv:hep-ph/9807544 [hep-ph].

[13] J. Yokoyama, "Chaotic new inflation and formation of primordial black holes," *Phys.Rev.* **D58** (1998) 083510, arXiv:astro-ph/9802357 [astro-ph].

[14] T. Kawaguchi, M. Kawasaki, T. Takayama, M. Yamaguchi, and J. Yokoyama, "Formation of intermediate-mass black holes as primordial black holes in the inflationary cosmology with running spectral index," *Mon.Not.Roy.Astron.Soc.* **388** (2008) 1426–1432, arXiv:0711.3886 [astro-ph].

[15] P. H. Frampton, M. Kawasaki, F. Takahashi, and T. T. Yanagida, "Primordial Black Holes as All Dark Matter," *JCAP* **1004** (2010) 023, arXiv:1001.2308 [hep-ph].

[16] K. Kohri, D. H. Lyth, and A. Melchiorri, "Black hole formation and slow-roll inflation," *JCAP* **0804** (2008) 038, arXiv:0711.5006 [hep-ph].

[17] M. Drees and E. Erfani, "Running-Mass Inflation Model and Primordial Black Holes," *JCAP* **1104** (2011) 005, arXiv:1102.2340 [hep-ph].

[18] D. H. Lyth and D. Wands, "Generating the curvature perturbation without an inflaton," *Phys.Lett.* **B524** (2002) 5–14, arXiv:hep-ph/0110002 [hep-ph].

[19] K. Enqvist and M. S. Sloth, "Adiabatic CMB perturbations in pre - big bang string cosmology," *Nucl.Phys.* **B626** (2002) 395–409, arXiv:hep-ph/0109214 [hep-ph].

[20] T. Moroi and T. Takahashi, "Cosmic density perturbations from late decaying scalar condensations," *Phys.Rev.* **D66** (2002) 063501, arXiv:hep-ph/0206026 [hep-ph].

[21] J. Yokoyama, "Formation of MACHO primordial black holes in inflationary cosmology," *Astron.Astrophys.* **318** (1997) 673, arXiv:astro-ph/9509027 [astro-ph].

[22] U. Seljak and M. Zaldarriaga, "Signature of gravity waves in polarization of the microwave background," *Phys.Rev.Lett.* **78** (1997) 2054–2057, arXiv:astro-ph/9609169 [astro-ph].

[23] M. Kamionkowski, A. Kosowsky, and A. Stebbins, "A Probe of primordial gravity waves and vorticity," *Phys.Rev.Lett.* **78** (1997) 2058–2061, arXiv:astro-ph/9609132 [astro-ph].

[24] M. Kamionkowski, A. Kosowsky, and A. Stebbins, "Statistics of cosmic microwave background polarization," *Phys.Rev.* **D55** (1997) 7368–7388, arXiv:astro-ph/9611125 [astro-ph].

[25] T. L. Smith, M. Kamionkowski, and A. Cooray, "Direct detection of the inflationary gravitational wave background," *Phys.Rev.* **D73** (2006) 023504, arXiv:astro-ph/0506422 [astro-ph].

[26] S. Matarrese, O. Pantano, and D. Saez, "A General relativistic approach to the nonlinear evolution of collisionless matter," *Phys.Rev.* **D47** (1993) 1311–1323.

[27] S. Matarrese, O. Pantano, and D. Saez, "General relativistic dynamics of irrotational dust: Cosmological implications," *Phys.Rev.Lett.* **72** (1994) 320–323, arXiv:astro-ph/9310036 [astro-ph].

[28] S. Matarrese, S. Mollerach, and M. Bruni, "Second order perturbations of the Einstein-de Sitter universe," *Phys.Rev.* **D58** (1998) 043504, arXiv:astro-ph/9707278 [astro-ph].

[29] H. Noh and J.-c. Hwang, "Second-order perturbations of the Friedmann world model," *Phys.Rev.* **D69** (2004) 104011.

[30] C. Carbone and S. Matarrese, "A Unified treatment of cosmological perturbations from super-horizon to small scales," *Phys.Rev.* **D71** (2005) 043508, arXiv:astro-ph/0407611 [astro-ph].

[31] K. Nakamura, "Second-order gauge invariant cosmological perturbation theory: Einstein equations in terms of gauge invariant variables," *Prog.Theor.Phys.* **117** (2007) 17–74, arXiv:gr-qc/0605108 [gr-qc].

[32] S. Mollerach, D. Harari, and S. Matarrese, "CMB polarization from secondary vector and tensor modes," *Phys.Rev.* **D69** (2004) 063002, arXiv:astro-ph/0310711 [astro-ph].

[33] K. N. Ananda, C. Clarkson, and D. Wands, "The Cosmological gravitational wave background from primordial density perturbations," *Phys.Rev.* **D75** (2007) 123518, arXiv:gr-qc/0612013 [gr-qc].

[34] D. Baumann, P. J. Steinhardt, K. Takahashi, and K. Ichiki, "Gravitational Wave Spectrum Induced by Primordial Scalar Perturbations," *Phys.Rev.* **D76** (2007) 084019, arXiv:hep-th/0703290 [hep-th].

[35] H. Assadullahi and D. Wands, "Constraints on primordial density perturbations from induced gravitational waves," *Phys.Rev.* **D81** (2010) 023527, arXiv:0907.4073 [astro-ph.CO].

[36] L. Alabidi, K. Kohri, M. Sasaki, and Y. Sendouda, "Observable Spectra of Induced Gravitational Waves from Inflation," *JCAP* **1209** (2012) 017, arXiv:1203.4663 [astro-ph.CO].

[37] L. Alabidi, K. Kohri, M. Sasaki, and Y. Sendouda, "Observable induced gravitational waves from an early matter phase," *JCAP* **1305** (2013) 033, arXiv:1303.4519 [astro-ph.CO].

[38] R. Saito and J. Yokoyama, "Gravitational wave background as a probe of the primordial black hole abundance," *Phys.Rev.Lett.* **102** (2009) 161101, arXiv:0812.4339 [astro-ph].

[39] E. Bugaev and P. Klimai, "Induced gravitational wave background and primordial black holes," *Phys.Rev.* **D81** (2010) 023517, arXiv:0908.0664 [astro-ph.CO].

[40] E. Bugaev and P. Klimai, "Constraints on the induced gravitational wave background from primordial black holes," *Phys.Rev.* **D83** (2011) 083521, arXiv:1012.4697 [astro-ph.CO].

[41] N. Bartolo, S. Matarrese, A. Riotto, and A. Vaihkonen, "The Maximal Amount of Gravitational Waves in the Curvaton Scenario," *Phys.Rev.* **D76** (2007) 061302, arXiv:0705.4240 [astro-ph].

[42] K. Enqvist, S. Nurmi, and G. Rigopoulos, "Parametric Decay of the Curvaton," *JCAP* **0810** (2008) 013, arXiv:0807.0382 [astro-ph].

[43] H. Assadullahi and D. Wands, "Gravitational waves from an early matter era," *Phys.Rev.* **D79** (2009) 083511, arXiv:0901.0989 [astro-ph.CO].

[44] T. Suyama and J. Yokoyama, "Temporal enhancement of super-horizon curvature perturbations from decays of two curvatons and its cosmological consequences," *Phys.Rev.* **D84** (2011) 083511, arXiv:1106.5983 [astro-ph.CO].

[45] "LISA; Laser Interferometer Space Antenna webpage." http://sci.esa.int/lisa/.

[46] S. Kawamura, T. Nakamura, M. Ando, N. Seto, K. Tsubono, *et al.*, "The Japanese space gravitational wave antenna DECIGO," *Class.Quant.Grav.* **23** (2006) S125–S132.

[47] "DECIGO: space gravitational wave antenna webpage." http://tamago.mtk.nao.ac.jp/decigo/.

[48] V. Corbin and N. J. Cornish, "Detecting the cosmic gravitational wave background with the big bang observer," *Class.Quant.Grav.* **23** (2006) 2435–2446, arXiv:gr-qc/0512039 [gr-qc].

[49] A. Lommen, "New limits on gravitational radiation using pulsars," arXiv:astro-ph/0208572 [astro-ph].

[50] "The Square Kilometre Array webpage." http://www.skatelescope.org.

[51] A. A. Starobinsky, "Multicomponent de Sitter (Inflationary) Stages and the Generation of Perturbations," *JETP Lett.* **42** (1985) 152–155.

[52] M. Sasaki and E. D. Stewart, "A General analytic formula for the spectral index of the density perturbations produced during inflation," *Prog.Theor.Phys.* **95** (1996) 71–78, arXiv:astro-ph/9507001 [astro-ph].

[53] D. Wands, K. A. Malik, D. H. Lyth, and A. R. Liddle, "A New approach to the evolution of cosmological perturbations on large scales," *Phys.Rev.* **D62** (2000) 043527, arXiv:astro-ph/0003278 [astro-ph].

[54] D. H. Lyth, K. A. Malik, and M. Sasaki, "A General proof of the conservation of the curvature perturbation," *JCAP* **0505** (2005) 004, arXiv:astro-ph/0411220 [astro-ph].

[55] A. S. Josan, A. M. Green, and K. A. Malik, "Generalised constraints on the curvature perturbation from primordial black holes," *Phys.Rev.* **D79** (2009) 103520, arXiv:0903.3184 [astro-ph.CO].

[56] A. S. Josan and A. M. Green, "Gamma-rays from ultracompact minihalos: potential constraints on the primordial curvature perturbation," *Phys.Rev.* **D82** (2010) 083527, arXiv:1006.4970 [astro-ph.CO].

[57] T. Bringmann, P. Scott, and Y. Akrami, "Improved constraints on the primordial power spectrum at small scales from ultracompact minihalos," *Phys.Rev.* **D85** (2012) 125027, arXiv:1110.2484 [astro-ph.CO].

[58] J. Chluba, A. L. Erickcek, and I. Ben-Dayan, "Probing the inflaton: Small-scale power spectrum constraints from measurements of the CMB energy spectrum," *Astrophys.J.* **758** (2012) 76, arXiv:1203.2681 [astro-ph.CO].

[59] S. Kasuya and M. Kawasaki, "Axion isocurvature fluctuations with extremely blue spectrum," *Phys.Rev.* **D80** (2009) 023516, arXiv:0904.3800 [astro-ph.CO].

[60] S. Kasuya, M. Kawasaki, and T. Yanagida, "Cosmological axion problem in chaotic inflationary universe," *Phys.Lett.* **B409** (1997) 94–100, arXiv:hep-ph/9608405 [hep-ph].

[61] M. Dine, L. Randall, and S. D. Thomas, "Baryogenesis from flat directions of the supersymmetric standard model," *Nucl.Phys.* **B458** (1996) 291–326, arXiv:hep-ph/9507453 [hep-ph].

[62] J. C. Niemeyer and K. Jedamzik, "Near-critical gravitational collapse and the initial mass function of primordial black holes," *Phys.Rev.Lett.* **80** (1998) 5481–5484, arXiv:astro-ph/9709072 [astro-ph].

[63] A. M. Green and A. R. Liddle, "Critical collapse and the primordial black hole initial mass function," *Phys.Rev.* **D60** (1999) 063509, arXiv:astro-ph/9901268 [astro-ph].

[64] M. Shibata and M. Sasaki, "Black hole formation in the Friedmann universe: Formulation and computation in numerical relativity," *Phys.Rev.* **D60** (1999) 084002, arXiv:gr-qc/9905064 [gr-qc].

[65] A. R. Liddle and D. H. Lyth, *Cosmological Inflation and Large-Scale Structure*. Cambridge Univ. Press, Cambridge, 2000.

[66] B. Paczynski, "Gravitational microlensing by the galactic halo," *Astrophys.J.* **304** (1986) 1–5.

[67] **MACHO Collaboration** Collaboration, C. Alcock *et al.*, "The MACHO project: limits on planetary mass dark matter in the galactic halo from gravitational microlensing," *Astrophys.J.* **471** (1996) 774, arXiv:astro-ph/9604176 [astro-ph].

[68] **MACHO Collaboration, EROS Collaboration** Collaboration, C. Alcock *et al.*, "EROS and MACHO combined limits on planetary mass dark matter in the galactic halo," *Astrophys.J.Lett.* (1998) , arXiv:astro-ph/9803082 [astro-ph].

[69] **EROS-2 Collaboration** Collaboration, P. Tisserand *et al.*, "Limits on the Macho Content of the Galactic Halo from the EROS-2 Survey of the Magellanic Clouds," *Astron.Astrophys.* **469** (2007) 387–404, arXiv:astro-ph/0607207 [astro-ph].

[70] L. Wyrzykowski, S. Kozlowski, J. Skowron, A. Udalski, M. Szymanski, *et al.*, "The OGLE View of Microlensing towards the Magellanic Clouds. III. Ruling out sub-solar MACHOs with the OGLE-III LMC data," arXiv:1012.1154 [astro-ph.GA].

[71] L. Wyrzykowski, J. Skowron, S. Kozlowski, A. Udalski, M. Szymanski, *et al.*, "The OGLE View of Microlensing towards the Magellanic Clouds. IV. OGLE-III SMC Data and Final Conclusions on MACHOs," arXiv:1106.2925 [astro-ph.GA].

[72] **Kepler Collaboration** Collaboration, W. J. Borucki *et al.*, "Kepler Planet-Detection Mission: Introduction and First Results," *Science* **327** (2010) 977–980.

[73] D. G. Koch, W. J. Borucki, G. Basri, N. M. Batalha, T. M. Brown, *et al.*, "Kepler Mission Design, Realized Photometric Performance, and Early Science," *Astrophys.J.* **713** (2010) L79–L86, arXiv:1001.0268 [astro-ph.EP].

[74] K. Griest, M. J. Lehner, A. M. Cieplak, and B. Jain, "Microlensing of Kepler Stars as a Method of Detecting Primordial Black Hole Dark Matter," *Phys.Rev.Lett.* **107** (2011) 231101, arXiv:1109.4975 [astro-ph.CO].

[75] A. M. Cieplak and K. Griest, "Improved Theoretical Predictions of Microlensing Rates for the Detection of Primordial Black Hole Dark Matter," *Astrophys.J.* **767** (2013) 145, arXiv:1210.7729 [astro-ph.CO].

[76] K. Griest, A. M. Cieplak, and M. J. Lehner, "New Limits on Primordial Black Hole Dark Matter from an Analysis of Kepler Source Microlensing Data," *Phys.Rev.Lett.* **111** (2013) 181302, arXiv:1307.5798 [astro-ph.CO].

[77] M. Ricotti, J. P. Ostriker, and K. J. Mack, "Effect of Primordial Black Holes on the Cosmic Microwave Background and Cosmological Parameter Estimates," *Astrophys.J.* **680** (2008) 829, arXiv:0709.0524 [astro-ph].

[78] J. C. Mather, E. Cheng, D. Cottingham, R. Eplee, D. Fixsen, *et al.*, "Measurement of the Cosmic Microwave Background spectrum by the COBE FIRAS instrument," *Astrophys.J.* **420** (1994) 439–444.

[79] D. Fixsen, E. Cheng, J. Gales, J. C. Mather, R. Shafer, *et al.*, "The Cosmic Microwave Background spectrum from the full COBE FIRAS data set," *Astrophys.J.* **473** (1996) 576, arXiv:astro-ph/9605054 [astro-ph].

[80] F. Capela, M. Pshirkov, and P. Tinyakov, "Constraints on Primordial Black Holes as Dark Matter Candidates from Star Formation," *Phys.Rev.* **D87** (2013) 023507, arXiv:1209.6021 [astro-ph.CO].

[81] F. Capela, M. Pshirkov, and P. Tinyakov, "Constraints on primordial black holes as dark matter candidates from capture by neutron stars," arXiv:1301.4984 [astro-ph.CO].

[82] P. Pani and A. Loeb, "Exclusion of the remaining mass window for primordial black holes as the dominant constituent of dark matter," 1401.3025. http://arxiv.org/abs/1401.3025.

[83] J. Kormendy and D. Richstone, "Inward bound: The Search for supermassive black holes in galactic nuclei," *Ann.Rev.Astron.Astrophys.* **33** (1995) 581.

[84] J. Magorrian, S. Tremaine, D. Richstone, R. Bender, G. Bower, *et al.*, "The Demography of massive dark objects in galaxy centers," *Astron.J.* **115** (1998) 2285, arXiv:astro-ph/9708072 [astro-ph].

[85] C. J. Willott, R. J. McLure, and M. J. Jarvis, "A 3x10**9 solar mass black hole in the quasar SDSS J1148+5251 at z=6.41," *Astrophys.J.* **587** (2003) L15–L18, arXiv:astro-ph/0303062 [astro-ph].

[86] W. Hu, D. Scott, and J. Silk, "Power spectrum constraints from spectral distortions in the cosmic microwave background," *Astrophys.J.* **430** (1994) L5–L8, arXiv:astro-ph/9402045 [astro-ph].

[87] T. Harada, H. Maeda, and B. J. Carr, "Self-similar cosmological solutions with dark energy. I. Formulation and asymptotic analysis," *Phys.Rev.* **D77** (2008) 024022, arXiv:0707.0528 [gr-qc].

[88] H. Maeda, T. Harada, and B. J. Carr, "Self-similar cosmological solutions with dark energy. II. Black holes, naked singularities and wormholes," *Phys.Rev.* **D77** (2008) 024023, arXiv:0707.0530 [gr-qc].

[89] R. Bean and J. Magueijo, "Could supermassive black holes be quintessential primordial black holes?," *Phys.Rev.* **D66** (2002) 063505, arXiv:astro-ph/0204486 [astro-ph].

[90] M. Kawasaki, N. Kitajima, and T. T. Yanagida, "Primordial black hole formation from an axion-like curvaton model," *Phys. Rev.* **D87** (2013) 063519, arXiv:1207.2550 [hep-ph].

[91] M. Y. Khlopov and A. Polnarev, "PRIMORDIAL BLACK HOLES AS A COSMOLOGICAL TEST OF GRAND UNIFICATION," *Phys.Lett.* **B97** (1980) 383–387.

[92] A. Polnarev and M. Y. Khlopov, "COSMOLOGY, PRIMORDIAL BLACK HOLES, AND SUPERMASSIVE PARTICLES," *Sov.Phys.Usp.* **28** (1985) 213–232.

[93] C. T. Byrnes, E. J. Copeland, and A. M. Green, "Primordial black holes as a tool for constraining non-Gaussianity," *Phys.Rev.* **D86** (2012) 043512, arXiv:1206.4188 [astro-ph.CO].

[94] H. I. Kim and C. H. Lee, "Constraints on the spectral index from primordial black holes," *Phys.Rev.* **D54** (1996) 6001–6007.

[95] J. Yokoyama, "Cosmological constraints on primordial black holes produced in the near critical gravitational collapse," *Phys.Rev.* **D58** (1998) 107502, arXiv:gr-qc/9804041 [gr-qc].

[96] **WMAP Collaboration** Collaboration, E. Komatsu *et al.*, "Seven-Year Wilkinson Microwave Anisotropy Probe (WMAP) Observations: Cosmological Interpretation," *Astrophys.J.Suppl.* **192** (2011) 18, arXiv:1001.4538 [astro-ph.CO].

[97] V. Acquaviva, N. Bartolo, S. Matarrese, and A. Riotto, "Second order cosmological perturbations from inflation," *Nucl.Phys.* **B667** (2003) 119–148, arXiv:astro-ph/0209156 [astro-ph].

[98] H. Kodama and M. Sasaki, "Cosmological Perturbation Theory," *Prog.Theor.Phys.Suppl.* **78** (1984) 1–166.

[99] V. F. Mukhanov, H. Feldman, and R. H. Brandenberger, "Theory of cosmological perturbations. Part 1. Classical perturbations. Part 2. Quantum theory of perturbations. Part 3. Extensions," *Phys.Rept.* **215** (1992) 203–333.

[100] S. Dodelson, *Modern cosmology*. Academic Press, San Diego, CA, 2003.

[101] M. Kawasaki, N. Kitajima, and S. Yokoyama, "Gravitational waves from a curvaton model with blue spectrum," *JCAP* **1308** (2013) 042, arXiv:1305.4464 [astro-ph.CO].

[102] **Planck Collaboration** Collaboration, P. Ade *et al.*, "Planck 2013 results. XXII. Constraints on inflation," arXiv:1303.5082 [astro-ph.CO].

[103] K. A. Malik and D. Wands, "Cosmological perturbations," *Phys.Rept.* **475** (2009) 1–51, arXiv:0809.4944 [astro-ph].

[104] W. H. Press and P. Schechter, "Formation of galaxies and clusters of galaxies by selfsimilar gravitational condensation," *Astrophys.J.* **187** (1974) 425–438.